NTNU – Trondheim
Norwegian University of
Science and Technology

The Breaking Process of an Idealized Polymeric Bundle under Applied Tensile Stress

Gaute Linga

Master of Science in Physics and Mathematics
Submission date: June 2014
Supervisor: Alex Hansen, IFY
Co-supervisor: Pietro Ballone, IFY

Norwegian University of Science and Technology
Department of Physics

NTNU – Trondheim
Norwegian University of
Science and Technology

The Breaking Process of an Idealized Polymeric Bundle under Applied Tensile Stress

Gaute Linga

June 2014

MASTER'S THESIS IN APPLIED PHYSICS
Department of Physics
Norwegian University of Science and Technology

Supervisor: Prof. Alex Hansen
Co-supervisor: Adj. Prof. Pietro Ballone

Abstract

We introduce a particle-based model of an idealized polymeric bundle, whose properties are investigated by means of molecular dynamics simulations. We analyse in particular the effect of applying a tensile stress, stretching and eventually breaking the bundle.

The simulation results show that, despite its simplicity, the model captures characteristic features of polymeric materials, e.g. a multistage creep and creep ringing. The results indicate that the system evolves in a near-equilibrium state during almost the entire creep process, reflected in the data collapse of the *effective stress–strain* curve.

Two distinct variants of the basic model are studied, the first one allowing and the second one disallowing recombination of broken bonds. The former model is observed to undergo a phase transition, taking place at a critical tensile force F_c. Below this threshold, the bundle is observed to stabilize, and above the threshold, the bundle breaks down. In both model assumptions, the bundle lifetime t_f seems to exhibit Basquin-like power-law dependence upon the applied force F; for the former this is estimated to be $t_f \sim F^{-\gamma}$, with $\gamma = 4 \pm 0.1$. Simulation results follow the same power law over the accessible range in F, spanning about half a decade.

The elongation difference as a function of normalized time also shows a remarkable data collapse for a range in F, hinting to universality in the creep process. Moreover, at imminent failure, the strain rate is shown to grow as $\dot{L} \sim \tau_{\text{ttf}}^{-1}$, where τ_{ttf} is the normalized time-to-failure. This is in excellent agreement with recent experimental findings for a protein gel [32].

New theoretical approaches are also made to understand the breaking process of a bundle of polymers. In particular, a simple one-step fiber bundle model is proposed. The model may serve to explain the phase transition that was observed for the simulation model that allowed for recombination.

Sammendrag

Vi introduserer en partikkelbasert modell for en idealisert polymerbunt, som vi utforsker ved hjelp av molekulærdynamikksimuleringer. Spesielt undersøkes effekten av å pålegge en konstant kraft på bunten, som strekkes og brytes.

Simuleringsresultatene viser at på tross av sin enkelhet fanger modellen opp karakteristiske trekk ved polymeriske materialer, f.eks. et flertrinns krypregime og krypringing. Resultatene indikerer at systemet er nært likevekt gjennom nesten hele krypprosessen. To ulike varianter av modellen blir studert; henholdsvis med og uten rekombinering av brukne bånd. Den første modellen ser ut til undergå en faseovergang, som skjer ved en viss kritisk strekkraft F_c. Med pfrt strekkraft under F_c ser bunten ut til å stabilisere seg i stedet for å bryte helt sammen, hvilket den gjør over denne terskelen. I begge modellantakelsene ser levetiden t_f ut til å følge en potenslovavhengighet av kraften F; for den første blir denne estimert til $t_f \sim F^{-\gamma}$, med $\gamma = 4 \pm 0.1$, gyldig over det tilgjengelige omrdet av F.

Strekklengdeforskjellen som funksjon av normalisert tid viser et datakollaps for et stort spenn i krefter, og hinter om universalitet i krypprosessen. I tillegg vokser strekkraten som $\dot{L} \sim \tau_{\text{ttf}}^{-1}$, hvor τ_{ttf} er den normaliserte tiden til sammenbrudd for bunten. Dette er i svært god overensstemmelse med nylige eksperimenter for en protein-gel [32].

Nye teoretiske tilnærminger er gjort for å forstå denne prosessen, bl.a. er en enkel ett-stegsmodell foreslått. Modellen kan kvalitativt forklare den observerte faseovergangen i modellen uten rekombinasjon.

Preface

This thesis will be submitted as the final requirement for the degree of Master of Science and Technology (Sivilingeniør) in Applied Physics and Mathematics, and concludes my studies at the Norwegian University of Science and Technology, NTNU. The thesis constitutes one semester of work (TFY4900, 30 credits), and has been carried out at the Department of Physics under the joint supervision of Prof. Alex Hansen and Adj. Prof. Pietro Ballone.

I want to thank Alex for offering such a challenging project, for our weekly meetings, and for generously providing information on the top-down approach to the subject in scope of this thesis. My sincere thanks also go to Pietro for the countless hours he has spent on the bottom-up approach, taking time to discuss both numerics and interpretation of results, either in person, or via email or Skype, when in Rome. I also want to thank the Department of Physics for providing the necessary computational resources.

Personally, I want to thank my parents for their unconditional support during my studies, and my friends, for keeping my spirits up, for at times being sinks of frustration, and for making my years as a student some of my best so far. Finally, I want to thank my girlfriend, Linn, for understanding me.

An electronic version of this document, along with some videos, can be found online at http://folk.ntnu.no/gautelin/master/.

Trondheim, June 16, 2014

Gaute Linga

Contents

1 Introduction

The strength of materials ultimately depends on their microscopic composition, and the chemical compounds constituting them. Since the beginning of modern science, materials' resistance to and failure under an external load has been extensively studied, but the complete description of breaking processes, from the bottom up – from the microscopic constituents to the macroscopic breakdown – remains a challenge still today [17, 21]. Due to advances in polymer engineering, biophysics and in nanotechnology, the need for a precise description and accurate models describing these processes is emergent. In particular, knowledge of the fracture processes of polymeric materials is needed, as they constitute large classes of materials, examples of which span from synthetic textiles, rubber and plastics to biopolymers such as in the DNA molecule and in proteins [45]. Numerous experimental studies [29, 32] have shown that such materials may display highly different behaviour depending on their chemical composition and configuration. Moreover, on the particle level, the interactions between particles are known, to a large extent, but the connection to the macroscopic world is not clear as of today. The exponential increase in computer power has in recent years provided promising results in the unification of the microscopic and macroscopic understanding of material properties [12].

In this thesis we investigate a specific *complex system*. Complex systems may be defined as systems composed of many interacting particles, or objects, not necessary of the same kind, that interact in a nonlinear fashion. Heuristically, it may be easier to understand through some examples of complex systems, as the latter are found at virtually all spatial and temporal scales. A standard large-scale example is the Earth's climate, for which sea flow, air flow, atmospheric conditions, geological processes, tides, solar radiation are effects and mechanisms that interplay to govern the evolution of the climate over time. Another example is granular systems subject of a force. The granular media is composed of many similar particles of similar geometric properties, which move around in an irregular manner – the individual mechanisms controlling the flow may be known, but the collective behaviour is more difficult to describe due to the many variables involved [3, 43]. On the microscopic scale we also find complex systems, such as in a living cell, the formation of proteins or in the duplication of DNA – numerous mechanisms are at work, and quantities change in time and influence each other. Since complex systems are so intrinsically complicated, it is, from a physicist's point of view, important to identify the important, relevant, ones. Complex systems may in this sense often be regarded as many-body problems with non-linear interactions, where the individual interactions may be known, but the collective behaviour is not. The collective behaviour may in fact be much richer than the individual parts of the system alone, as complex systems often are associated with chaos, intermittency and critical phenomena [40].

In the present scope, the complex system we study is a slightly idealized bundle of polymeric chains. The experimental scenario we investigate is the application of external tensile stress to such a bundle. The bundle is stretched, and – if the stretching force is large enough – consequently broken. On the microscopic scale, this problem is classically[1] well-defined, as we know the mechanisms that keep such chains intact: The covalent bonds between neighbouring monomers [46]. Already at a slightly larger spatial scale, namely on considering polymer chains,

[1] Classically in the sense that we neglect quantum effects.

the system becomes complex: The monomers will thermally oscillate in a more or less random fashion, affecting each other. If the separation between two monomers of the chain becomes large enough due to these fluctuations, the chain will break. Once again, increasing the scale, looking at a bundle of many chains, the situation becomes even more complex. Chains interact with each other, and load is distributed differently on the individual chains as more chains are broken, in a stochastic manner, and the force each fiber is subject to fluctuates in time. Several bi-effects are at play: broken bonds may heal, chemical conditions may differ – temperature and acidity may fluctuate locally – and phase transitions may occur. Moreover, single breaking events may trigger new breakings, causing local or global avalanches in the fiber failure process. Generally, there is no reason to assume that such a process takes place at equilibrium, so standard thermodynamics may not be employed carelessly.

At the other end of the scale, such stretching-and-breaking processes have been studied extensively, both experimentally and theoretically [21, 41]. A class of models known as fiber bundle models, which are to be presented, has proven effective in understanding such systems. In a heuristic, but intuitive, manner, these models incorporate many of the quantities that may determine such processes on the macroscopic scale – such as quantizing the fiber strengths according to statistical distributions. This field is by no means complete, as the connection to the microscopic mechanisms are still unclear. Even considering a single such fiber, the scale may be macroscopic. In this sense, we have a macroscopic model, and a microscopic description, but not the connection between these.

The present work is thus to be regarded as a preliminary stage of a larger research program, which aims to connect the two scales of understanding. In this context, some natural questions to ask are:

- What are the important quantities to microscopically describe the breaking dynamics of a polymer bundle?
- How can we connect the microscopic many-body description of a bundle to a macroscopic one?
- What is the microscopic process leading to failure of a material under stress, and how does it depend on the important parameters?

At this stage, we may not find answers to these questions which are valid for all polymeric systems, but we may attempt to do so for the particular system under consideration, in order to carve out the way for further studies.

We describe the many-body problem associated with a bundle of polymers, with a model which is *as simple as possible*. In order to address the basic physics, we need in this sense a model with as few adjustable parameters as possible. The model describes thus an idealized polymeric sample – a bundle of ideal chains wherein the beads interact only with their nearest neighbours in the chains. This interaction must by necessity be anharmonic, on order to allow for chains to break. The model is implemented and simulated numerically by means of molecular dynamics, and we inspect the breaking process qualitatively and quantitatively.

The general aim of this thesis is hence to bridge the gap between the well-documented macroscopic description of a fiber bundle model and the microscopic mechanisms. To this end, we propose a molecular model – a microscopic description – representing such a fiber bundle, and through molecular dynamics simulations the evolution of such a system is simulated.

The thesis is organized as follows: Chapter 1 is the introduction you have been reading up until now. Chapter 2 concerns the theoretical description of polymers, starting with single

chains and extending to a bundle of chains, obtaining an equation-of-state for a bundle in the thermodynamic limit and finally briefly contemporary studies of single-chain rupture. In Chapter 3, a class of macroscopic models describing failure of materials, known as fiber bundle models, are presented. We present the generic model, and an extension for including thermal fluctuations in the model, before we present a new model for thermal failure of a fiber bundle. In this model, the failure process of the fiber bundle is modelled as a continuous-time one-step process, and the model allows for taking explicitly into account the healing of fibers. In Chapter 4 we present the numerical methods that were used for the numerical simulations. In Chapter 6 the main results from the simulations are presented. In Chapter 7 we discuss and interpret the results and attempt to draw lines between the theory that has been developed and the results. We also discuss the limitations and error sources involved in both the model and the method that has been employed. Finally, in Chapter 8, we draw conclusions and point to the future, suggesting a concrete programme for further research into this area.

2 Polymers

In this chapter, we present a basic theoretical framework sufficent to understand and interpret the simulations we present in this thesis. To this end, we introduce two of the simplest models for describing polymeric chains, namely the freely jointed chain (FJC) model and the Gaussian chain. After presenting the description of single-chain systems, we extend to systems of many chains, regarding these systems in the thermodynamic limit. We consider the mean stress-strain relationship for these systems in an equilibrium state.

The basic theory presented in this chapter is limited and fairly concise, intended as a minimal framework for understanding polymer physics. More extensive and thorough introductions to polymer physics can be found in e.g. the classic works of de Gennes [9] and Strobl [46].

2.1 What is a polymer?

Polymers are large molecules comprised by long chains of repeated subunits, known as monomers, linked together by covalent bonds [46]. Polymers usually represent organic compounds, containing carbon, oxygen, nitrogen and halogens. They are formed through the process of *polymerization*, i.e. linking together a large amount of monomers. Due to the potential diversity in chemical composition, the physical properties of polymers may vary extensively between different types [19]. Polymers may compose both synthetic, man-made materials, such as polystyrene and nylon, and natural materials: wool, rubber, cellulose and biological tissue, such as in DNA and proteins [45], to mention just a few.

Polymers are found in a variety of conformations: linear chains, branched chains, and crosslinked chains. In the present scope, we consider only the first, as this is the simplest one.

2.2 The freely jointed chain

The freely jointed chain model, also known as the ideal chain, is the simplest model of a polymer [11]. In this model, we assume a fixed separation b – the *Kuhn length* – between each of the $n+1$ beads in the chain. We assume no excluded volume, i.e. that non-neighbouring beads may overlap, and the bonds to be fully isotropic. Hence, the spatial probability distribution of the beads of the chain will be equivalent to that of a random walk in time. We take the positions of each bead $i = 0, \dots, n$ to be denoted by $\mathbf{r}_i$, and furthermore $\mathbf{b}_i = \mathbf{r}_{i+1} - \mathbf{r}_i$ to be the relative displacement, or the *bond vectors*. Hence, the end-to-end separation vector is given by

$$\mathbf{R} = \mathbf{r}_n - \mathbf{r}_0 = \sum_{i=1}^{n} \mathbf{b}_i, \tag{2.1}$$

and the constraint on the bond vectors is given by $|\mathbf{b}_i| = b$. Hence, one can regard all the bond vectors as having identical, isotropic probability distributions. It can be shown (see Appendix A.1 for a derivation) that the probability distribution of the end-to-end distribution of the freely

jointed chain in the large-n limit is given by

$$p(\mathbf{R}) = \left(\frac{3}{2\pi nb^2}\right)^{3/2} \exp\left(-\frac{3R^2}{2nb^2}\right), \tag{2.2}$$

i.e. a Gaussian distribution in three dimensions. An interesting property of such a free chain is that the mean square end-to-end separation scales as

$$\mathbf{R}^2 \sim n, \tag{2.3}$$

i.e. it prefers to be in a coiled-up conformation in the absence of an applied force.

2.2.1 Applying a tensile force

In the scope of this thesis, it is particularly interesting to consider how this chain behaves when it is stretched. We therefore imagine attaching the two ends of the polymer to a micro-manipulation device exerting a force $\mathbf{F}$ upon it. It can be shown[1] that the mean elongation L of the freely jointed chain can be expressed as

$$L = nb\mathcal{L}(\beta Fb), \tag{2.4}$$

where $\mathcal{L}(x) = \coth x - x^{-1}$ is the Langevin function, and $\beta = 1/k_{\mathrm{B}}T$ is the Boltzmann factor. Equation (2.4) thus effectively yields the stress–strain curve of a single FJC, giving the relation between the applied force and the elongation. The Langevin function has the properties

$$\mathcal{L}(x) = \begin{cases} x/3 & \text{if } x \ll 1, \\ 1 & \text{if } x \gg 1. \end{cases} \tag{2.5}$$

Hence, when the elongation L is small compared to the *contour length* $L_{\mathrm{c}} = nb$, the stress–strain relation is given by

$$F = \frac{3k_{\mathrm{B}}T}{nb^2}L. \tag{2.6}$$

From this it is clear that the chain in this regime can be regarded as a Hookean spring with the spring constant $3k_{\mathrm{B}}T/nb^2$, i.e. an entropic spring with a strength that increases linearly with the thermal motion of the beads. Moreover, from the large x limit in Equation (2.5) one realizes that the chain has a finite extensibility given by the contour length of the chain.

Note that the above expression corresponds to an unconfined FJC in free space. To calculate the effect of confining the chain between two impenetrable plates, we employ a model that is more analytically tractable, namely the Gaussian chain.

2.3 The Gaussian chain

The Gaussian chain can be viewed as a coarse-grained version of the FJC. We may think of the chain as composed of a large number of smaller chains, each of the n segments $\mathbf{b}_i$ distributed as the FJC in the large n limit, namely as the Gaussian

$$p(\mathbf{b}_i) = \left(\frac{3}{2\pi b^2}\right)^{3/2} \exp\left(-\frac{3b_i^2}{2b^2}\right). \tag{2.7}$$

[1] The interested reader is referred to Appendix A.2 for the fairly straightforward derivation.

The Gaussian chain is invariant under the scaling $(n, b) \to (\lambda^{-2}n, \lambda b)$. and thus it has no finite extensibility [46]. This means that it is only representative of real chains that are in a fairly coiled-up state.

We are interested in the thermodynamic properties of a chain that is attached to, and confined between, two parallel plates, separated by a distance L. In this respect, we need to find its partition function. We assume that we have two parallel plates fixed at, respectively, $z = 0$ and $z = L$, and a Gaussian chain with one end fixed at $z = \epsilon$, and one end fixed at $z = L - \epsilon$. In Appendix A.3 we derive the partition function for a Gaussian chain under such conditions, yielding

$$\mathcal{Z}_2(L; n) = \frac{2\pi^2\epsilon^2}{L^3} \sum_{k=1}^{\infty} (-1)^{k+1} k^2 \exp\left(-\frac{b^2\pi^2k^2}{6L^2}n\right), \tag{2.8}$$

valid for small ϵ.

2.4 The Gaussian bundle

As a generalization of the single-chain conformation, we now present a model for a bundle of chains stitched between two plates [50]. The individual chains do not see the other chains, and the force each of the chains exert upon the wall is independent of the conformations of the other chains – it only depends on the plate separation L. Even considering force-controlled conditions on the bundle, this approximation may be valid – in the thermodynamic limit. Assuming that we have so many chains that the fluctuations in the plate positions are small, i.e. the plate separation is constant, we can regard the individual chains to follow strain-controlled conditions – the large number of other chains fixes the length of a single chain.

Since the chains don't interact when the plates are fixed, we may multiply the partition functions (2.8) together to yield the partition function for the entire bundle. For a bundle of N chains[2], we then have that the total partition function becomes

$$\mathcal{Z}(L, N; n) = \mathcal{Z}_2(L; n)^N. \tag{2.10}$$

2.4.1 Stress-strain curve

It is clear that in the macroscopic limit, disregarding fluctuations and assuming equilibrium, the elongation L becomes analogous to the role the volume takes in regular thermodynamics. Similarly, the total force F exerted *on* the bundle by the plates is analogous to the pressure. In the assumption of equilibrium lies the fact that bonds are not allowed to break. In mathematical terms, this yields the work differential

$$\mathrm{d}W = -F\mathrm{d}L, \tag{2.11}$$

[2]Using the partition functions derived in Appendix A.3, we could in principle trivially include the presence of broken chains. For a bundle of initially N chains from which k fibers are broken, the total partition function corresponding to the total chain conformation becomes

$$\mathcal{Z}(L, N, k; n) = \mathcal{Z}_2(L; n)^k \prod_{j=1}^{N-k} \mathcal{Z}_1(L; n - n_j)\mathcal{Z}_1(L; n_j), \tag{2.9}$$

where n_j denotes the bead at which the jth chain has broken. It is clear that the broken chains exert a force on the plates. However, we have not considered this in this thesis.

which means that the thermodynamic identity becomes

$$\mathrm{d}U = \mathrm{d}Q - \mathrm{d}W \tag{2.12}$$
$$= T\mathrm{d}S + F\mathrm{d}L. \tag{2.13}$$

We now assume that the internal energy is dependent only on the temperature T, namely by the relation

$$U = C_L T, \tag{2.14}$$

where C_L is the heat capacity of the bundle at fixed length. Hence, the full thermodynamic identity becomes

$$C_L \mathrm{d}T = T\mathrm{d}S + F\mathrm{d}L. \tag{2.15}$$

To determine the state function $F = F(L,T)$ we integrate along the isothermal ($\mathrm{d}T = 0$), so that (2.15) yields

$$F = -T\left(\frac{\partial S}{\partial L}\right)_T \tag{2.16}$$

According to Boltzmann's principle, the entropy is defined as

$$S = k_\mathrm{B} \ln \Omega, \tag{2.17}$$

where Ω is the number of accessible microstates. Since $\Omega \propto \mathcal{Z}$ in the canonical ensemble, i.e. under isothermal conditions, we have that the force F becomes

$$F = -k_\mathrm{B} T\left(\frac{\partial \ln \mathcal{Z}}{\partial L}\right)_T \tag{2.18}$$

This is the total force the bundle exerts on the plates.

Now, Equation (2.10) yields

$$\ln \mathcal{Z} = N \ln(\mathcal{Z}_2(L; n_b)) \tag{2.19}$$
$$= N\left\{\ln(2\pi^2\epsilon^2) - 3\ln L + \ln\left[\sum_{k=1}^{\infty}(-1)^{k+1}k^2 \exp\left(-\frac{b^2\pi^2k^2}{6L^2}n\right)\right]\right\} \tag{2.20}$$

and hence we have from Equation (2.18) that

$$\sigma = \frac{F}{N} = k_\mathrm{B}T\left[\frac{3}{L} - \frac{nb^2\pi^2}{3L^3}\frac{\sum_{k=1}^{\infty}(-1)^k k^4 \exp\left(-\frac{b^2\pi^2k^2}{6L^2}n\right)}{\sum_{k=1}^{\infty}(-1)^k k^2 \exp\left(-\frac{b^2\pi^2k^2}{6L^2}n\right)}\right], \tag{2.21}$$

where we have introduced the stress $\sigma = F/N$ – i.e. the average force per chain. This formula yields the stress–strain relation for the Gaussian bundle, and may in the thermodynamical sense serve as an equation-of-state for the bundle.

2.5 The FJC bundle

We now move back to the FJC model, for which single-chain conformations were described in Section 2.2. We consider now a bundle of FJCs. Each chain is attached to two parallel plates, but is otherwise unconfined. If we disregard fluctuations, assuming each of the N chains to feel the same force from the plates, $\sigma = F/N$, we may also find an expression for the expected separation, by simply replacing $F \to \sigma$ in Equation 2.4. This yields

$$L = nb\mathcal{L}(\beta\sigma b), \tag{2.22}$$

which gives the stress-strain curve for the FJC bundle. This can be inverted in order to get σ from L:

$$\sigma = \frac{1}{\beta b}\mathcal{L}^{-1}\left(\frac{L}{nb}\right), \tag{2.23}$$

where $\mathcal{L}^{-1}(x)$ is the inverse Langevin function. Note that in this case we have assumed that the effect of confinement between the two plates is negligible, or in other words, that the two plates are fully penetrable, and so this corresponds to a slightly different conditions than those of the Gaussian bundle.

2.6 Comparison, limitations and extensions

The crude assumptions made in the above, such as neglecting fluctuations, expresses the fact that both of the above should be regarded as mean-field approaches to describing a bundle of freely jointed chains. However, in the thermodynamic limit, these approximations may be valid. We note that upon expanding (2.23) for small L/nb – i.e. small plate separations compared to the contour length of the chain – we obtain

$$\sigma = \frac{3L}{\beta n b^2}, \tag{2.24}$$

which is the same as the expression one would obtain from the unconfined Gaussian chain, which is the expression that the confined Gaussian chain tends to in the large L (or small b) limit. This is illustrated in Figure 2.1. It is seen that the three models exhibit distinct behaviours. The FJC bundle incorporates the effect of finite extensibility by converging towards the extension $L = nb$ – the contour length – as $F \to \infty$, but does not incorporate the effect of confinement. The confined Gaussian chain, on the other hand, incorporates the effect of confinement, but due to the continuous nature of the model, it does not account for the finite extensibility of discrete chains and acts like a Hookean spring in the large F limit. The unconfined Gaussian bundle is seen to lie between these two models, by not taking into account any of the effects, but seems to be a fair approximation at intermediate values of the applied stress, and may thus serve as a useful tool in understanding the stretching dynamics of the bundle.

A discrepancy in the models described above is that they apply to different systems. In the FJC bundle we have made no assumptions on the number of beads per chain, but we have neglected fluctuations and the effect of confinement, i.e. beads that constantly hit the walls exerting a pressure on it. This effect may be small at large plate separations, when the freely jointed chains are very stretched (almost rolled out), but at sufficiently small separations, this is certainly not so, as beads will move and contribute to pushing the plates apart.

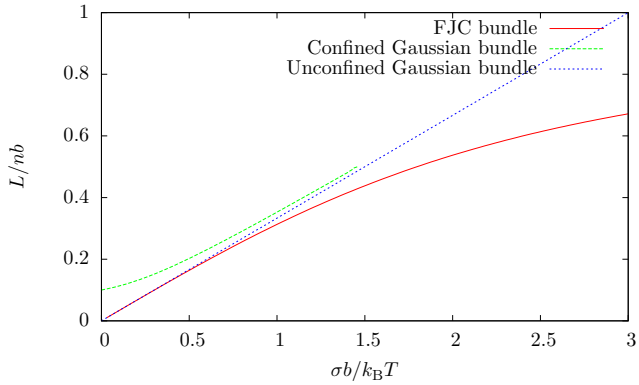

Figure 2.1: Stress-strain curves for the three models. We have here set the parameter $n = 100$.

This is supported by the analysis of the Gaussian chain. However, the Gaussian chain is a continuous chain model, only valid in the limit of large n, and its stress-strain curve approaches that of a linear spring in the large separation limit. In this case, the FJC is almost fully stretched and becomes increasingly rigid. Hence, the Gaussian chain is only valid as an approximation of the FJC under conditions where the latter is approximately distributed as a Gaussian, as is reflected in Figure 2.1.

Hence, we have in the above two descriptions for which one systematically underestimates the separation at a given force, and one systematically overestimates the separation. Note, however, that these approaches should only be regarded as approximations with respect to the model for which we carry out simulations in the forthcoming.

In this spirit, an interpolation between the two approaches would capture the essential mechanism for a FJC bundle confined between two plates. Namely, the effect of confinement from Gaussian chain (effective confinement), and the large separation limit from the FJC bundle.

2.7 Adiabatic stretching

Due to its simplicity, equation (2.24) is practical for illustration purposes, since it is easy to treat analytically. We turn to the case of adiabatic stretching, i.e. the case where the system is thermally insulated, or in mathematical terms,

$$\mathrm{d}Q = 0, \tag{2.25}$$

and assume that the process is so slow that the system is at all times at equilibrium, and that no chains break during stretching. The equation-of-state is then given by

$$\sigma = \frac{3L}{\beta n b^2}, \tag{2.26}$$

and the thermodynamic identity (2.15) becomes

$$C_L \mathrm{d}T = N\sigma \mathrm{d}L \tag{2.27}$$

$$= \frac{3NL}{\beta n b^2}\mathrm{d}L. \tag{2.28}$$

Integrating both sides, we obtain

$$T = T_0 \exp\left[\frac{3Nk_{\mathrm{B}}}{2nb^2C_L}(L^2 - L_0^2)\right] \tag{2.29}$$

where (L_0, T_0) is some reference state. This shows that the temperature will increase when we stretch the chain adiabatically. We perform work on the system, increasing the energy of the system. This is contrary to the case of adiabatic expansion of an ideal gas – for which the temperature decreases as the gas performs work on the surroundings upon expanding.

2.8 Physical problems

The above described models are advantageous in spirit of their simplistic description and their analytical tractability. However, these advantages come at the expense of their ability to describe real systems. In real polymeric systems, the monomers will interact not only with their nearest-neighbour monomers, but with other surrounding monomers. The effect could be accounted for by incorporating the feature of *excluded volume* in the models. This generally leads to less volume being available, and hence a swelling of the polymer coil. The description of such a free chain would correspond to the self-avoiding random walk, rather than the standard random walk associated with the conformation of a FJC. However, in the context of our numerical simulations, it would be pointless to include such effects in the theoretical models, as they are not present in the numerical model. The described theoretical models will suffice, as we are not including interactions between non-neighbouring monomers in our numerical schemes. Moreover, such polymers exist in reality [46], under certain conditions. In polymer solutions, monomers will interact with the solvent. In a good solvent, non-neighbouring monomers will repulse each other, leading to swelling. In a poor solvent, the monomers will attract each other, leading to a contraction of the coil. When the solvent is precisely poor enough to exactly cancel the effect of excluded volume, the chain–solvent pair is at its so-called Theta point, and the FJC becomes a good description of the chain.

Another discrepancy in the above models is that they do not incorporate covalent bonds – i.e. an anharmonic interaction potential – instead of rigid rods, as in the FJC, or entropic springs, as in the Gaussian chain. Such anharmonicity is generally hard to treat analytically, but possible numerically by using e.g. molecular dynamics. In principle, the FJC could correspond to such a chain only in the limit of infinitely rigid bonds. Hence, none of these models correspond precisely to real systems, not even at the theta point. Moreover, they do not allow for bonds to break, which is the property we are mostly interested in in the present thesis. However, they may be good models for understanding the static properties of such simple, idealized polymers.

Another interesting aspect of the above described theory, is that it only provides the static description of such conformations – at equilibrium. Dynamic properties, such as collective modes, sound velocities, etc. are not contained in these models, and more refined models (e.g. the Rouse model [8]) must be employed. Generally, out-of-equilibrium effects will also be present. Close to equilibrium, the presented framework may be a fair approximation. Moreover, the thermodynamics employed in the above refers to a system in the macroscopic limit – where the system consists of infinitely many particles and may be seen as a continuum wherein thermal fluctuations may be neglected. This may not the case in the numerical experiment we are to present.

2.9 Rupture of polymer chains

Breakage, or rupture, of *single polymer chains* has been studied extensively, both theoretically and numerically, in itself constituting a field of research affiliated under reaction rate theory [17, 37]. Intact chains are generally in a metastable state, and hence it is energetically favourable for the chain to break, but this requires a certain threshold energy leading to a certain lifetime. There are several aspects and assumptions that can be, and have been, taken into account in such studies:

- Thermally induced rupture. In the absence of an applied load, chains will break solely due to thermal fluctuations. Variable parameters are chain length, strength of thermal coupling, dissociation energy and temperature [38].
- Rupture under stress-controlled conditions. In this case the applied force is held constant, and hence the length of the chain will fluctuate with a magnitude dependent on the temperature [39]. In addition to the mentioned parameters, now the force can be varied to compute the expected lifetime.
- Rupture under strain-controlled conditions. In this case the length is held fixed, and thus the force will fluctuate. Hence the strain replaces the force in the above expression.

In the case of a stress-controlled stretching of bundle of non-interacting chains (except through the confining plates), the rupture of the single chains composing the bundle may correspond to all of these. In the case of a large bundle, the fluctuations will vanish and the conditions can be regarded as strain-controlled. In the case of a small bundle, the conditions will be more towards stress-controlled. Analytical approaches [37] and numerical simulations [38] have been carried out to uncover this behaviour. The essential part of these studies consists of determining how the *mean first breakage time* (MFBT) depends different parameters. Note however that these studies generally do not incorporate the effect of a sudden onset of force, nor the effect of the deformation of the chain as it is stretched. The presence of unstable modes, which is directly related to the way the applied force is applied, may also severely influence the breaking process [14].

For the theoretical insight into the breaking process, Kramers-Langer theory has been extensively applied. We now present the simplest physical interpretation of such breaking events. Assuming that each bond in the chain $i = 1, \ldots, N$ has the same rupture probability, manifested by the characteristic lifetime τ_1 such that $p_i(t) = \exp(-t/\tau_1)$. Moreover, assuming that the rupture events for the different bonds in the chain are independent, the total rupture probability can be written as in [17], namely

$$p(N,t) = \prod_{i=1}^{N} p_i(t) = \exp(-Nt/\tau_1) = \exp(-t/\tau_N) \tag{2.30}$$

so that the collective lifetime becomes

$$\tau_N = \tau_1/N. \tag{2.31}$$

This suggests that the lifetime should depend on the chain length as $\tau \sim N^{-1}$.

The next step consists of considering the individual bonds as effective two-particle potentials. Considering one of the particles as fixed, the problem can be seen as equivalent to that of particle

diffusing in an anharmonic potential. In the presence of an applied constant force, the two-particle potential may be superimposed by a linear potential, thus modifying the barrier height. The stronger the force, the lower the barrier becomes. According to the theory of Kramers [27], based on the predictions of Arrhenius [2], the lifetime of the particle in such a potential can be expressed as

$$\tau_1^{-1} = A \exp\left(-\beta E_a\right), \tag{2.32}$$

where $E_a = E_0 - \alpha F$ is the resultant modified potential, α an effective distance from the bottom of the potential to the barrier with the original height E_0, and the factor A depends on the shape of the potential. It turns out that the single-particle treatment results in an overestimation of the factor A compared to numerical results, and that collective effects tend to reduce the breaking rate significantly. Recently, a multidimensional Kramers approach [14] has been used to predict these rates, in which the order of magnitude of the lifetime agrees with the numerical simulations.

We now turn to a phenomenological description of this breaking process, stating the findings of some recent numerical simulations. The simulations indicate that the breaking rate is dependent both on temperature and applied load. Such simulations were performed to measure the effect of thermal rupture of a polymer chain with a Morse-like coupling between beads [38], and the effect of an applied force [39]. The findings indicate that $\tau \sim N^{-\chi}$ where $0 < \chi < 1$ for applied forces and $\chi \simeq 1$ in the absence of an applied force. This indicates that the intuitive prediction that the lifetime decays with an increased number of beads per chain was correct. In the presence of an applied force, the value of the exponent $\chi < 1$, however, reflects that correlation effects are present, as the lifetime does not decay as it would with independent bond rupture events. Moreover, it is found that the Arrhenian relationship $\tau \sim \exp(\beta(E_0 - \alpha F))$ is in good agreement with the simulations for sufficiently strong stretching forces.

As mentioned briefly earlier, the situation of stretching a bundle of polymers does not correspond exactly to any of these simulations. In our scenario, force is applied fairly suddenly, and this may correspond to a dynamic probing of the system, moving the system, and the individual chains out of equilibrium. Furthermore, single breaking events may trigger further breakings, since a snapping chain may introduce fluctuations and enhancement of the force each chain must withstand, and hence, the system is neither performed under constant strain nor stress for any chains. Moreover, both breaking and stretching may cause the temperature[3] to fluctuate, and hence also the temperature may vary throughout the process. However, in a metastable state – close to equilibrium – it may be a reasonable assumption to regard the breaking rate – inverse lifetime – as a state function of the system parameters: temperature, strain, number of beads, etc.

[3]Which is, strictly speaking, not unambiguously defined out of equilibrium.

3 Fiber bundle models

In materials science and engineering, a class of models known as fiber bundle models (FBMs) have found extensive use in describing a large variety of systems. These models describe a bundle of elastic fibers subject to a load. The fibers fail successively, and for each failure, the load distribution on the individual fibers changes. The different variants of the FBMs may differ in, e.g., the way fibers fail, the way force is redistributed between fibers, or the incorporation of thermal effects. Due to these models being just at the edge of what is analytically treatable, much insight into the field of fracture mechanics can be gained from studying them [41].

In this context, such models are interesting for two reasons. The first is that we are interested in applying such models to understand the microscopic mechanisms in our experiment, namely the stretching and breaking of a bundle of polymers. The second reason is that the simulations we are to present, may be more realistic than the macroscopic, theoretical models, and thus provide phenomenological input to these models.

Thus, in Section 3.1 we first present the generic fiber bundle model, with equal load sharing, discrete time and a heterogeneous bundle, and an extension of this thermally induced failure. In Section 3.2, we propose a continous-time model for the thermal failure of a fiber bundle, viewing the breaking process as a non-linear Markovian one-step process, with transition rates accounting for breaking and recombination of fibers. In Section 3.3 we consider limitations and extensions of the approach taken.

3.1 Equal-load-sharing model

The simplest and oldest fiber bundle model is known as the equal-load-sharing (ELS) model, which was introduced by Pierce [34]. Herein, when a fiber breaks, the load it previously carried is distributed equally among the remaining intact fibers of the bundle. This inherent mean-field nature of the model makes it possible to treat analytically to a large extent. Time is here viewed as a discrete variable, and the breaking proceeds in bursts – multiple simultaneous breaking events – as force is redistributed and the load is increased on the remaining fibers, until either all of the remaining fibers are strong enough to withstand the applied stress – and equilibrium is reached –, or the whole bundle fails. Taking N_t to denote the number of intact fibers at timestep t, the recursive breaking dynamics can be stated as

$$N_{t+1} = N\left[1 - P\left(\frac{F}{N_t}\right)\right], \tag{3.1}$$

where N is the total number of fibers in the bundle, and $P(x) = \int_0^x \mathrm{d}x' p(x')$ is the cumulative distribution function for the failure thresholds $p(x)$ of the fibers, i.e. the maximum applied stress that a single fiber can withstand. Introducting the applied stress $\sigma = F/N$, the fraction of remaining fibers $u_t = N_t/N$, and the effective stress at timestep t, $x_t = \sigma/u_t$, we get the recursion relations

$$x_{t+1} = \frac{\sigma}{1 - P(x_t)}, \quad x_0 = \sigma, \tag{3.2}$$

and

$$u_{t+1} = 1 - P(\sigma/u_t), \quad u_0 = 1. \tag{3.3}$$

These recursion relations yield the fixed points $x^* \equiv x_{t+1} = x_t$ and $u^* \equiv u_{t+1} = u_t$ at equilibrium. For given probability distributions $p(x)$ these can be solved exactly around and beyond the fixed points.

In a heterogeneous bundle, the fibers have different threshold strengths. Exact analytical solutions have been found for a variety of threshold distributions [41]. Due to the time regarded discrete, multiple fibers will break simultaneously, and the breakdown of the bundle proceeds in bursts, i.e. multiple fibers failing simultaneously. However, if the applied load is sufficiently low, the bundle does not break completely down. For probability distributions with load curves $\sigma = x[1 - P(x)]$ that have a quadratic maximum in the interval $[x_{\min}, x_{\max}$ (the domain of the effective applied stress), the system is shown to undergo a phase transition from partial failure to complete failure of the bundle. Around the critical stress $\sigma = \sigma_c$, the characteristic timescales are summarized as

$$t_f \sim (\sigma - \sigma_c)^{-1/2}, \quad \sigma > \sigma_c, \tag{3.4}$$

$$u - u_c \sim t^{-1}, \quad \sigma = \sigma_c, \tag{3.5}$$

$$t_r \sim (\sigma_c - \sigma)^{-1/2}, \quad \sigma < \sigma_c. \tag{3.6}$$

Herein, t_f is the lifetime of the bundle, while t_r is the relaxation time of the bundle towards a state where breaking stops. Regarding the branching ratio as the order parameter, it has been argued that the system undergoes a continuous (second-order) phase transition at this point [35].

In addition to this critical average behaviour, it has been proven that under the same assumptions as mentioned above, the *burst distribution* $D(\Delta)$, where Δ is the number of simultaneous breaking events, follows a power law distribution $D(\Delta) \sim \Delta^{-5/2}$ [20]. In the case of imminent failure – logging only the breaking events close to complete failure – the distribution becomes a power law with the distribution $D(\Delta) \sim \Delta^{-3/2}$. Due to the discrete nature of time in this model, the concept of simultaneous breakings is given naturally.

3.1.1 Thermally induced failure in FBMs

The richness of this class of fiber bundle models does not stop here. The model presented up to this point constitutes a static model. Considering a single simulation of such a mode, the fiber strengths are initially set from the start, and do not change throughout the process. Hence, as soon as the individual thresholds are set, the process proceeds deterministically. In our case, however, we consider fibers (chains) which are intrinsically equal – a homogeneous bundle – but break spontaneously due to thermal fluctuations in either the applied force or the chains themselves. It is clear that such mechanisms are not captured in the macroscopic fiber bundle model described above.

Thermal fluctuations introduce Gaussian noise in loaded materials. Roux [42] incorporated this effect in a fluctuating force

$$\sigma = \sigma_i + \eta, \tag{3.7}$$

where η is a random noise drawn from a Gaussian probability distribution with mean 0 and variance kT, $\sigma_i = F/(N - i)$ where F is the total applied force on the bundle, and i is the

number of broken fibers from a bundle initially consisting of N fibers. Thus, the initial applied stress is $\sigma_0 = F/N$. The homogeneity of the bundle is contained in a homogeneous threshold strength σ_c of all fibers. Clearly, such a model must proceed to complete failure within a finite time, due to the fact that there is no healing mechanism incorporated, and that there is always a nonzero probability of fibers breaking. At the first timestep the probability that a single chain survives is given by $p_1(t) = 1 - P(\sigma_c - \sigma_0)$, where $P(\eta)$ is the probability that the noise value exceeds η. Hence, the probability that the *entire bundle survives after t timesteps* is

$$p_N(t) = [1 - P(\sigma_c - \sigma_0)]^{Nt} \equiv \exp(-t/\tau_1), \tag{3.8}$$

which defines a timescale for the process. Generalizing the above relation for τ_i, recursively solving it by replacing σ_0 with σ_i, and taking into account the dominant terms, one finds the asymptotic failure time

$$t_f \simeq \frac{\sqrt{2\pi kT}}{\sigma_0} \exp\left(\frac{(\sigma_c - \sigma)^2}{2kT}\right) \tag{3.9}$$

in the limit of low thermal noise. We note that although this model may be applicable to the system under consideration, it still regards time as a discrete parameter. In the following, we attempt to describe the failure process of a fiber bundle as a process occuring in continuous time.

3.2 The breaking process modelled as a one-step process

We now present now a simple model for the breaking process, based on the equal-load-sharing model, but viewing it in continuous time. The model is in principle a standard one-step process, with transition rates accounting for the failure and possible healing of fibers – similar to birth-death models [25] – but we make certain assumptions on the transition rates. Consider now a bundle initially consisting of initially N fibers, of which n are intact at an instance t. We assume, as in the ELS model, that the applied force is distributed evenly among the intact fibers. Moreover, we assume that the only relevant parameter for an individual fiber to fail is the applied effective stress, in this case

$$\sigma_n = \frac{F}{n}, \tag{3.10}$$

where F is the total applied force, which is taken to be constant. Hence, by assuming the state of the bundle at time t to be characterized only the number n of remaining fibers, we assign a probability $p_i(t)$ to each of these states $i = 0, \ldots, n$. The breaking process is hence governed by two rates:

- Breaking rate b_n. The probability for any fiber of the bundle to break within an infinitesimal time window should be proportional to the number of intact fibers. Moreover, for each individual fiber, the breaking probability per time should be the same, namely a monotonically increasing function f of the applied stress – since an increased load on a fiber should enhance the probability of it breaking. Thus, given the applied stress σ_n on each chain, we may write the total breaking rate b_n – i.e. the rate of jumping from state n to state $n-1$ – as

$$b_n = nf(\sigma_n). \tag{3.11}$$

However, for a bundle initially consisting of N fibers, under a constant applied force F, the applied stress when the bundle contains n intact fibers can be expressed as

$$\sigma_n = \frac{F}{n} = \frac{N}{n}\frac{F}{N} = \sigma\frac{N}{n}. \tag{3.12}$$

- Recombination rate r_n. This rate should, similarly as above, be given by the product of the number of broken fibers – i.e. fibers that may recombine – times the single-chain rate. Moreover, an increased stress on a fiber should decrease the probability for it to recombine. Hence, the recombination rate – i.e. the rate of jumping from state n to $n+1$, becomes

$$r_n = (N-n)g(\sigma_n), \tag{3.13}$$

where g is a monotonically decreasing function. We may also consider the case where a fiber is allowed to recombine with any other broken fiber. In that case, the recombination rate becomes

$$r_n = (N-n)^2 g(\sigma_n). \tag{3.14}$$

In the forthcoming, we assume the form (3.13), as this is what corresponds to the system we are inspecting in the scope of this thesis. In particular, one can realize that then g will decay with an increased σ, since this corresponds to expanding the available volume, making it less probable for a chain to recombine.

Given this definition, it is clear that the bundle represents a stationary Markov process [25] – the transition rates are only dependent on the present state of the system. We now write down the master equation of this process.

3.2.1 Master equation

Breaking the bundle can be viewed as a one-step (Markovian) process. Writing the master equation, with $p_n(t)$ denoting the probability of being in a state of n remaining fibers at time t, given the rates described above,

$$\frac{\mathrm{d}p_n}{\mathrm{d}t} = -\left(b_n + r_n\right)p_n + b_{n+1}p_{n+1} + r_{n-1}p_{n-1}, \quad n \in [1, N-1]. \tag{3.15}$$

For the boundary cases $n = 0$ and $n = N$, we have

$$\frac{\mathrm{d}p_0}{\mathrm{d}t} = -r_0 p_0 + b_1 p_1, \quad \text{and} \tag{3.16}$$

$$\frac{\mathrm{d}p_N}{\mathrm{d}t} = -b_N p_N + r_{N-1}p_{N-1}. \tag{3.17}$$

Naturally, the initial condition is

$$p_n(0) = \delta_{n,N}, \tag{3.18}$$

meaning that all fibers are intact at time $t = 0$.

Expansion

In order to analyse the behaviour of this fiber bundle model under general considerations, we make the ansatz [25]

$$n = Nu + N^{1/2}\xi, \tag{3.19}$$

where ξ is a Gaussian noise containing the fluctuations around the macroscopic expectation value of the fraction of remaining fibers, which we define as

$$u = \frac{\langle n \rangle}{N}. \tag{3.20}$$

In Appendix A.4, we show that the master equation 3.15 can be expanded to yield the macroscopic equation for the system:

$$\frac{\mathrm{d}u}{\mathrm{d}t} = -b(u) + r(u), \tag{3.21}$$

where

$$b(u) = \phi f(\sigma/u) \quad \text{and} \quad r(u) = (1-u)g(\sigma/u). \tag{3.22}$$

From (3.21) we can obtain the expected macroscopic behaviour of the system under these assumptions. The fluctuations are given as the solutions of the Fokker–Planck equation

$$\frac{\partial \Pi}{\partial t} = \left[b'(u) - r'(u)\right] \frac{\partial \xi \Pi}{\partial \xi} + \frac{1}{2}\left[r(u) + b(u)\right] \frac{\partial^2 \Pi}{\partial \xi^2}. \tag{3.23}$$

3.2.2 Macroscopic breaking dynamics

We now consider the case where one allows for recombination of broken chains. In this case, there will be a competition between the two microscopic mechanism controlling the bundle – the spontaneous breaking and the recombination. These two mechanisms will, in a sense, have opposite dependence on the applied stress. An increased stress will enhance the probability for a chain to spontaneously break, and decrease the probability of a chain to recombine, as stretching the bundle enlarges the available volume. Hence, considering the temperature T as fixed, the dynamics can be captured in one variable, namely the applied force F – or equivalently in applied initial stress σ. Depending on how we tweak σ, there will be either a two local fixed points (one stable and one unstable) or no fixed points. At a critical value $\sigma = \sigma_c$ we undergo a saddle-node bifurcation. Over this value of σ, the chain will break within a finite time, and under this the bundle may relax towards an equilibrium value. Due to the analogy to the phase transition seen in the equal-load-sharing model [41], we use this terminology here as well – although it may be imprecise.

We now disregard fluctuations, and solely consider the average behaviour of the system. This corresponds to letting $N \to \infty$ and considering the remaining fraction of intact fibers $u(t)$ as the evolving quantity. The evolution equation becomes

$$\frac{\mathrm{d}u}{\mathrm{d}t} = -b(u) + r(u). \tag{3.24}$$

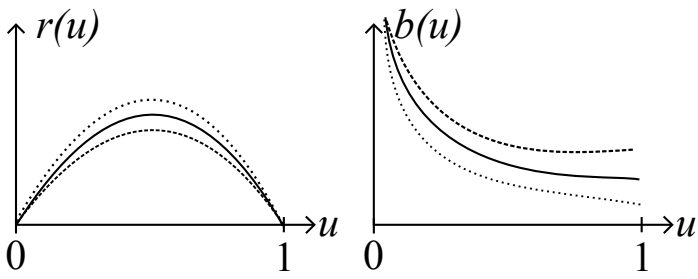

Figure 3.1: The two rate functions describing the macroscopic dynamics of the bundle. The dashed line represents the effect of an increased applied load on the rates, and the dotted line represents the effect of a decreased load.

The natural initial condition is thus $u(0) = 1$. The functional form of b and r now completely determines the process. We assume these to be as simple as possible, shown qualitatively in Figures 3.1. We adopt the notation

$$Q(u) = -b(u) + r(u) \tag{3.25}$$

for the net rate determining the evolution of the bundle. This function is illustrated in Figure 3.2. These rates depend on the applied load σ, so we henceforth write $Q(u, \sigma)$, meaning that the macroscopic equation of the system can be written as

$$\frac{\mathrm{d}u}{\mathrm{d}t} = Q(u, \sigma). \tag{3.26}$$

We assume that Q depends continuously on both σ and u, and that Q is a monotonically decreasing function of σ. The latter follows from the fact that we already assumed that both r and b depend continuously on σ, monotonically, in the opposite manner of each other. In other words, since

$$\frac{\partial r}{\partial \sigma} \leq 0 \quad \text{and} \quad \frac{\partial b}{\partial \sigma} > 0 \quad \forall u \in [0, 1], \tag{3.27}$$

then we have that

$$\frac{\partial Q}{\partial \sigma} = \frac{\partial}{\partial \sigma}(r - b) < 0 \quad \forall u \in [0, 1]. \tag{3.28}$$

Now, by tuning σ one may find three distinct cases determining the dynamics of the system. The flow diagram for the three cases is sketched in Figure 3.3. We see that below a certain threshold stress, the bundle has two fixed points in the "remaining fraction space" spanned by $u \in [0, 1]$: one stable and one unstable. In this case, the bundle will relax towards the stable fixed point. Below this threshold, there are no fixed points and the bundle moves towards breakdown ($u = 0$). At the limiting value inbetween, $\sigma = \sigma_c$, the fixed-point is half-stable. This is an example of a saddle-node bifurcation, as we see the emergence of a pair of fixed points at a critical value of our control parameter σ. The phase diagram for the bundle is illustrated in Figure 3.4

The fixed points $u^*_\pm$ are given as the solution of the equation

$$Q(u^*_\pm, \sigma) = 0, \quad \sigma \leq \sigma_c. \tag{3.29}$$

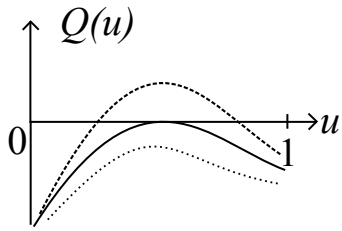

Figure 3.2: The net rate function $Q(u) = -b(u) + r(u) = \mathrm{d}u/\mathrm{d}t$ determining the process.

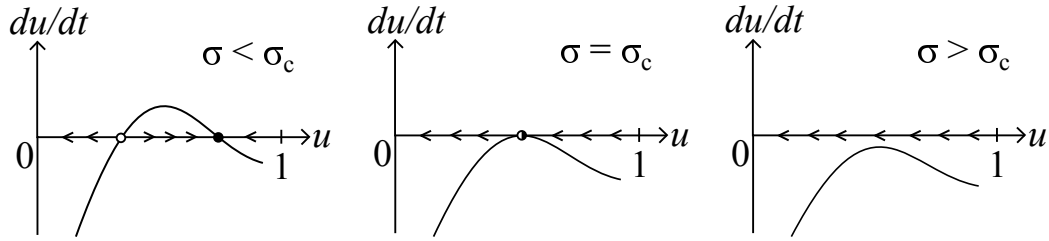

Figure 3.3: Flow diagrams for different values of applied stress, showing the transition at $\sigma = \sigma_c$.

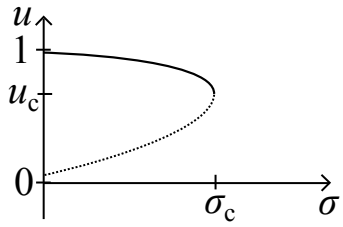

Figure 3.4: Phase diagram of the bundle.

When $u_+^* = u_-^* \equiv u_c$ we are at the critical stress $\sigma = \sigma_c$. In this case, due to the smoothness of Q, we have $\partial Q/\partial u = 0$. Assuming that Q has a quadratic maximum as a function of u, and is monotonically decreasing in σ, we expand the function around the point (u_c, σ_c) by introducing the displacement coordinates

$$\eta = u - u_c, \quad \text{and} \quad \delta = \sigma - \sigma_c \tag{3.30}$$

so that

$$Q(u_c + \eta, \sigma_c + \delta) = \left.\frac{\partial Q}{\partial \sigma}\right|_c \delta + \frac{1}{2}\eta^2 \left.\frac{\partial^2 Q}{\partial u^2}\right|_c + \mathcal{O}(\delta^2, \delta\eta^2). \tag{3.31}$$

Under the assumption of $Q(u_c)$ being a quadratic maximum, we may truncate the series after the second term, provided that we choose $\delta \sim \eta^2$ small enough. The smoothness of Q guarantees that $\partial^2 Q/\partial u \sigma|_c$ does not blow up.

For simplicity we define

$$\kappa_1 = -\left.\frac{\partial Q}{\partial \sigma}\right|_c > 0 \quad \text{and} \quad \kappa_2 = -\frac{1}{2}\left.\frac{\partial^2 Q}{\partial u^2}\right|_c > 0. \tag{3.32}$$

The macroscopic evolution equation sufficiently close to the fixed point can thus be cast as

$$-\frac{\mathrm{d}\eta}{\mathrm{d}t} = \kappa_1 \delta + \kappa_2 \eta^2. \tag{3.33}$$

This is the so-called normal form of a saddle-node bifurcation [47].

At the bifurcation point, $\delta = 0$ and

$$-\frac{\mathrm{d}\eta}{\mathrm{d}t} = \kappa_2 \eta^2, \tag{3.34}$$

which yields the solution

$$\eta = \frac{1}{\kappa_2 t}, \tag{3.35}$$

so that $u - u_c \sim t^{-1}$, the same asymptotic behaviour as was found for the critical state in the equal-load-sharing model [41], indicating a critical slowing down.

Supercritical stress

At stresses slightly above, but sufficiently near, the critical stress σ_c, the total failure time will be dominated by the time the bundle spends close to the fixed point. Here, $\delta > 0$ and the failure time is approximated by

$$t_f = \int_0^{t_f} \mathrm{d}t \simeq -\int_{-\Delta}^{\Delta} \frac{\mathrm{d}\eta}{\kappa_1 \delta + \kappa_2 \eta^2}, \tag{3.36}$$

where Δ is a small characteristic length scale in u-space for which the quadratic maximum is a good approximation. Then

$$t_f = 2(\kappa_1 \kappa_2 \delta)^{-1/2} \arctan\left(\Delta \sqrt{\frac{\kappa_2}{\kappa_1 \delta}}\right) \sim \delta^{-1/2} \tag{3.37}$$

for sufficiently small δ. Hence, the characteristic timescale for the breakage of the bundle diverges as $t_f \sim (\sigma - \sigma_c)^{-1/2}$ sufficiently close to the fixed point.

Subcritical stress

Slightly below the critical stress, $\delta < 0$ and the stable fixed point may be approximated by

$$\eta^* \simeq \sqrt{\frac{\kappa_1(-\delta)}{\kappa_2}}, \tag{3.38}$$

and thus

$$\frac{\mathrm{d}(\eta - \eta^*)}{\mathrm{d}t} = -2\kappa_2\eta^*(\eta - \eta^*) + \mathcal{O}(\eta^2). \tag{3.39}$$

Close to the fixed point this guarantees the exponential relaxation

$$\eta - \eta^* \propto \exp(-t/t_r), \tag{3.40}$$

for which the characteristic relaxation time t_r is given by

$$t_r = (2\kappa_2\eta^*)^{-1} = \left(2\sqrt{\kappa_2\kappa_1(-\delta)}\right)^{-1} \sim (\sigma_c - \sigma)^{-1/2}. \tag{3.41}$$

Hence, to sum up, sufficiently close to the critical point we have

$$t_f \sim (\sigma - \sigma_c)^{-1/2}, \quad \sigma > \sigma_c \tag{3.42}$$

$$u - u_c \sim t^{-1}, \quad \sigma = \sigma_c \tag{3.43}$$

$$t_r \sim (\sigma_c - \sigma)^{-1/2}, \quad \sigma < \sigma_c, \tag{3.44}$$

which is the same asymptotic behaviour as seen in the canonical equal-load-sharing model (with quadratic maximum in the load curve expression) – although the breaking process is intrisically different.

Note that the above approximations are only valid in the utmost vicinity of the critical point, and that away from this point, the bundle behaves differently – the behaviour must typically be calculated numerically.

Role of fluctuations

In a bundle of finite size, stochasticity will influence the breaking process, so even well below the threshold $\sigma = \sigma_c$ the entire bundle will break. The linear noise approximation **??** is valid in some neighbourhood around the stable fixed point. However, since the fixed point is only local, and has a certain finite basin of attraction, there is a non-vanishing probability that the fluctuations may become so large that the system escapes from the basin of attraction, surpasses the unstable fixed point, and proceeds towards complete failure. The probability for this is typically of the order $\exp(-N)$ [25], and it is evident that such terms could not be a part of the linear noise approximation.

The situation can be understood qualitatively by regarding the state of the bundle as similar to that of a diffusing particle in a smooth potential well, interpreting now the state of the bundle u as a position coordinate. By looking at the subcritical Q, we can imagine that Q is derived from some potential V, see fig. 3.5. Herein, the combined magnitude of the reaction assumes the role of the (nonlinear) diffusion coefficient $D \propto r(u) + b(u)$, and controls the magnitude of the fluctuations. The particle diffuses in the bottom of the well, around the fixed point, but

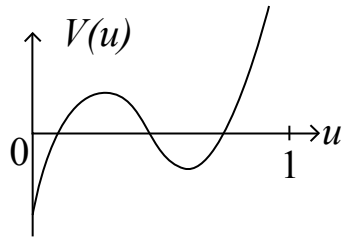

Figure 3.5: The potential $V(u)$ that could be imagined to yield the effective rate function $Q(u)$.

may, within a finite time, escape the well – i.e. the basin of attraction – and jump over the barrier never to return. As we approach the critical stress σ_c from below, the fixed points come closer to each other – the "barrier" is lowered – and the escape rate increases, leading to a finite expected lifetime of the bundle even at (macroscopically) subcritical stress.

In fact, the described problem is related to the celebrated Kramers' escape problem and escape rate theory [25, 27]. We make no efforts in quantitatively resolving the problem here, but merely state that it will be present as long as the system is of finite size. In fact, it might limit us from observing the described critical behaviour in systems of finite size – as is the case in our experiment.

We note also that the magnitude of the rates can be computed by measuring the fluctuations around the stable fixed points, by assumption well inside their respective basins of attraction. At the fixed point, we have that necessarily

$$r(u) = b(u), \tag{3.45}$$

Since the linear noise approximation is valid here, we consider the stationary solution of it around this stable fixed point. It can be shown [25] that the autocorrelation of the fluctuatuons n in the stationary state is given by

$$\operatorname{corr}\{n(0), n(t)\} = \frac{1}{N} \frac{r(u) + b(u)}{2\,|Q'(u)|} \exp(-\,|Q'(u)|\,t) \tag{3.46}$$

$$= \frac{1}{N} \frac{b(u)}{|Q'(u)|} \exp(-\,|Q'(u)|\,t). \tag{3.47}$$

Assuming ergodicity, one could then fit the latter relation to experimental data, effectively yielding the factors $|Q'(u)|$ and $b(u) = r(u)$ for that particular value of σ. Figure 6.31 shows how this could be done.

3.2.3 Disallowing recombination

We now return from the macroscopic description to the stochastic description of the bundle, and regard the case of no recombination, also accounting for fluctuations. In the case of no recombination, we simply let $r_n = 0$. Thus, the master equation reads

$$\frac{\mathrm{d}p_n}{\mathrm{d}t} = -b_n p_n + b_{n+1} p_{n+1}, \quad n \in [1, N-1], \tag{3.48}$$

$$\frac{\mathrm{d}p_0}{\mathrm{d}t} = b_1 p_1, \quad \text{and} \quad \frac{\mathrm{d}p_N}{\mathrm{d}t} = -b_N p_N. \tag{3.49}$$

With this assumption, there evidently is no σ_c for forces below which there exists an equilibrium state for the bundle.

In this case it is trivial to solve for the waiting times, as we can never return to a state of higher n. The probability of being in state n at time is $p_n(t)$. Since the transition rates are time-independent, the conditional probability of staying in the state n during a time t is simply given by

$$p_{n|n}(t) = e^{-b_n t}. \tag{3.50}$$

We let the stochastic variable τ_n denote the waiting times for a breaking event, i.e. jumping to state $n-1$ from state n. The waiting time distribution is given by

$$w_n(\tau) = b_n e^{-b_n \tau}. \tag{3.51}$$

The expected time of staying in state n is readily found as

$$\langle \tau_n \rangle = b_n^{-1} \tag{3.52}$$

and $\langle \tau_n^2 \rangle = 2b_n^{-2}$. The total expected time of breaking a chain is

$$\langle \tau \rangle = \sum_{n=1}^{N} \langle \tau_n \rangle = \sum_{n=1}^{N} b_n^{-1}, \tag{3.53}$$

and the variance

$$\operatorname{var}\{\tau\} = \left\langle (\tau - \langle \tau \rangle)^2 \right\rangle = \sum_{n=1}^{N} \sum_{m=1}^{N} \left(\langle \tau_n \tau_m \rangle - \langle \tau_m \rangle \langle \tau_n \rangle \right) \tag{3.54}$$

$$= \sum_{n=1}^{N} \left(\langle \tau_n^2 \rangle - \langle \tau_n \rangle^2 \right) \tag{3.55}$$

$$= \sum_{n=1}^{N} b_n^{-2} \tag{3.56}$$

since the waiting times of different states are independent. Introducing the functional form of b_n we obtain

$$\langle \tau \rangle = \sum_{n=1}^{N} (nf(F/n))^{-1} \simeq \int_1^N (nf(F/n))^{-1} \, \mathrm{d}n, \tag{3.57}$$

and

$$\operatorname{var}\{\tau\} = \sum_{n=1}^{N} (nf(F/n))^{-2} \simeq \int_1^N (nf(F/n))^{-2} \, \mathrm{d}n, \tag{3.58}$$

where we in the rightmost equalities assume N to be large and consider n a continuous variable. To evaluate these integrals further knowledge is needed about the function f.

Scaling form of breaking rate

We do not know the functional form of the breaking rate function f, other than that it should be positive and monotonically increasing. Moreover, it should go to infinity as $\sigma \to \infty$ and tend to a small value as $\sigma \to 0$. There are infinitely many functions that satisfy these criteria. Intuitively, under constant T, one would assume the single-fiber breaking rate to depend on the Arrhenian relation [2] as

$$f(\sigma) \sim \exp(\alpha\sigma/k_{\mathrm{B}}T), \tag{3.59}$$

where we have omitted the part that is not due to the superponed linear potential discussed in 2.9. However, as this is neither particularly tractable analytically, nor valid in the context of our numerical experiment, where the temperature changes, we hereby leave this approach.

In the spirit of Kun et al. [29] we try the scaling form

$$f(\sigma) = \alpha\sigma^{\gamma}, \tag{3.60}$$

where $\alpha > 0$ and $\gamma > 1$ are parameters controlling the damage accumulation due to stress. The waiting time integrals (3.57), (3.58) are now easily solved to yield

$$\langle\tau\rangle = \int_1^N n^{-1} f(F/n)^{-1}\,\mathrm{d}n = \alpha^{-1}\int_1^N n^{-1}(F/n)^{-\gamma}\,\mathrm{d}n \tag{3.61}$$

$$= \alpha^{-1}(N\sigma)^{-\gamma}\int_1^N n^{\gamma-1}\,\mathrm{d}n \tag{3.62}$$

$$= \alpha^{-1}(N\sigma)^{-\gamma}\frac{N^{\gamma}-1}{\gamma} \tag{3.63}$$

$$\simeq \frac{\sigma^{-\gamma}}{\alpha\gamma}. \tag{3.64}$$

Similarly,

$$\mathrm{var}\{\tau\} = \int_1^N (nf(F/n))^{-2}\,\mathrm{d}n \tag{3.65}$$

$$= \alpha^{-2}(N\sigma)^{-2\gamma}\int_1^N n^{2\gamma-2}\,\mathrm{d}n \tag{3.66}$$

$$= \alpha^{-2}(N\sigma)^{-2\gamma}\frac{N^{2\gamma-1}-1}{2\gamma-1} \tag{3.67}$$

$$\simeq \frac{\sigma^{-2\gamma}}{\alpha^2 N(2\gamma-1)} \tag{3.68}$$

This shows that in this case, the lifetime is independent of N under a given applied stress, as one would intuitively expect. Moreover, $\mathrm{var}\{\tau\} \to 0$ as $N \to \infty$ which shows that in this limit, the behaviour of the bundle is deterministic – it consequently breaks at a well-defined time, given an initial applied stress. Moreover, it shows that the mean lifetime of the bundle is a power law with the same exponent as the microscopic breaking rate, as is the standard deviation of the mean lifetime. This relation is in fact seen in a large variety of materials, and is known as the Basquin law of fatigue [5].

Macroscopic breaking process

Now we consider the macroscopic limit in the case of a power-law breaking rate. Equation 3.21 can then be solved analytically to yield

$$t = -\int_1^u b^{-1}(u')\,\mathrm{d}u' = \alpha^{-1}\sigma^{-\gamma}\int_u^1 (u')^{\gamma-1}\,\mathrm{d}u' \tag{3.69}$$

$$= \frac{\sigma^{-\gamma}}{\alpha\gamma}(1-u^\gamma) = \langle\tau\rangle\,(1-u^\gamma) \tag{3.70}$$

so

$$u = (1 - t/\langle\tau\rangle)^{1/\gamma}. \tag{3.71}$$

The above analysis illustrates that if the rate controlling the breaking is a power law, then the fraction of remaining chains will be a power law dependent of the normalized time-to-failure, which we define as

$$\tau_{\mathrm{ttf}} = 1 - t/\langle\tau\rangle\,. \tag{3.72}$$

However, as mentioned, it is not obvious that *microscopic breaking rate* should be a power law.

Lifetime under no applied force

In the case of a bundle under no applied force, the single-chain breaking rate becomes $f(0) = c$, where c could be some temperature-dependent constant. Hence, from (3.57)

$$\langle\tau\rangle = c^{-1}\ln N, \tag{3.73}$$

which diverges as $N \to \infty$, which is consistent with the model described in section 3.1.1. This illustrates that the scaling form (3.60) can not hold exactly – for small F, the breaking rate must approach some finite, positive value for it to hold true.

3.2.4 Considerations

In this subsection, we discuss the proposed one-step model, and connect it to the numerical experiment we are to present in the forthcoming. In the experimental scenario of stretching a polymeric bundle, we have three characteristic time scales associated with their respective mechanisms:

- Redistributing the force. After a chain has broken, the applied force must be redistributed among the remaining chains.
- Spontaneous breaking. This rate is associated with the breaking of bonds due to the thermal motion the beads. Applying a force stretching the chain effectively lowers the energy barrier required to break a bond. Hence, increasing the applied stress should be associated with an increased rate of spontaneous breaking.
- Recombination of broken bonds. This time scale is related to the probability of a broken chain recombining with itself. The rate of recombination is inversely proportional to the available volume, and proportional to the number of broken chains.

In the one-step model lies the assumption that the time scale related to the redistribution of forces is small compared to the others, i.e. the applied force is instantly distributed democratically among the surviving chains when a fiber breaks. Moreover, since time is regarded as continuous, we consider only cases where one chain breaks at the time, since the probability of two random events to occur simultaneously is zero – one can always find a small time window to separate the two events. Hence, it may be reasonable to view the process as a *one-step process*.

However, one aspect of the numerical experiment carried out is significantly different: the onset of force. In the experiment, a force is applied to stretch the bundle, and during the onset it perturbs the system out of equilibrium. This means that the breaking process can not be a stationary Markovian process – the breaking rate may in this case be time-dependent.

3.3 Limitations and extensions

All the models presented in this section can be said to belong to the class of mean-field fiber bundle models, in the sense that load is shared in the same manner between the surviving fibers, and the position of the fibers in the bundle is irrelevant. In real systems, such locality effects will be present, and they are often crucial, as the load which a failed fiber previously carried will generally distributed more heavily on fibers close to this fiber. This opens up for the possibility of locality effects, such as crack propagation, generally leads to a significantly shorter lifetime of the bundle than what is predicted by equal-load-sharing models [41]. This effect is accounted for in the subclass of fiber bundle models called local-load-sharing (LLS) models. There has been proposed several ways of distributing the load between surrounding fibers, the simplest of which is the nearest-neighbour load-sharing. Herein, all the load carried by a fiber is shared solely among the nearest neighbours of the failing fiber. Another extensively studied and much more realistic model is the soft-clamp model, where the fibers are assumed to be anchored to an elastic medium [6]. When a force is applied to a given fiber, the elastic medium responds with a deformation falling off inversely proportional to the distance from the fiber – similar to the effect of pulling a hair on your arm. When a single fiber fails, the deformation changes, and other fibers may subsequently fail. This model generally requires a minimum of phenomenological input, e.g. values for clamp stiffness. This could be obtained by means of molecular dynamics simulations where the chains interact.

However, in the forthcoming numerical simulations, we will consider a bundle of polymeric chains which only interact through the plates they are anchored to. This means that position of single chain is irrelevant for the other chains – it is only the force it exerts on the plates that is relevant. This inherent mean-field nature of the system we are considering makes it pointless to employ sophisticated LLS models at the present stage – the natural framework for understanding this lies in the within the ELS class. However, at later stages, when chain-chain interactions are accounted for in the molecular models, comparison with and input for LLS models may be provided.

A natural point in question is also whether or not the proposed one-step model may be extended to account for locality effects – we have not attempted to do so here.

4 Numerical methods

In this section, we present the numerical methods and algorithms necessary for carrying out the simulations in the present work. In Section 4.1, we present the idea behind molecular dynamics – solving Newton's equation of motions on the particle-level – and proceed to describing the Verlet algorithm in detail. Finally, we describe limitations and possible extensions for future simulations. The theory presented in this section is largely based on the classic textbook by Frenkel [13].

4.1 Molecular dynamics

On the particle level, we know how nature works. For the constituents of most materials, assuming them to be classical particles – particles that obey the laws of classical mechanics – is an excellent approximation [13]. At short distances these particles repulse each other, and at large distances they attract each other. In principle, from this fact one could derive all the properties of classical matter, by integrating Newton's equation of motions for all the involved particles. Before the age of computers, however, this procedure was too cumbersome to perform. In recent years, it has been possible to this: the techniques for doing this numerically constitute the field of molecular dynamics simulations. We present in the following the scheme for studying the natural time evolution of such a system.

4.1.1 Numerical integration algorithms

The algorithms we are to use must be chosen with care. Especially in the numerical integration of the equations of motion, replacing analytic expressions with numerical approximations always encompasses error. We need algorithms that to a large extent provide simulations that obey the laws of physics, but at the same time are not too computationally costly. There are several aspects we may emphasize in the numerical integration schemes:

1. Numerical stability.
2. Energy conservation. Here we distinguish between short-term and long-term energy drift. For the statistical properties of a system, the latter is considered more important, as we expect short-term temporal fluctuations in the energy to vanish when averaging over an ensemble.
3. Time-reversibility. Newton's equations of motion are time-reversible, and so should the numerical schemes we employ.
4. Volume-preservation. From classical mechanics, we know that Hamiltonian dynamics leaves the magnitude of any volume in phase space unchanged [16].
5. Computational aspects, such as speed and memory consumption.

To this end, we employ the velocity Verlet algorithm [48, 51] to integrate the equations of motion. In the following we present it, and discuss its accordance with the above points.

4.2 Velocity Verlet

Verlet-type algorithms are not just among the simplest algorithms for integrating Newton's equations of motion, but usually also the best [13]. The variant cast in a form that uses the positions and velocities at equal times is called the Velocity Verlet algorithm. The fundamental requirement for the use of Verlet-type algorithms is that the Hamiltonian be separable, i.e. that the potential from which the forces between particles are derived can be found from only knowing the position vectors of the particles. This means that

$$\mathbf{a}(t) = \frac{\mathbf{F}(t)}{m} = -\frac{\nabla V(\mathbf{r}(t))}{m}, \tag{4.1}$$

where $\mathbf{a}$ is the acceleration, $\mathbf{F}$ is the force, V the potential, and m is the mass of each particle. For simplicity we abuse notation slightly, as the equations are supposed to hold for all involved particles, but we denote each one by the general $\mathbf{r}$.

The basic Verlet algorithm [51] is derived by expanding the particle coordinate $\mathbf{r}(t + \Delta t)$ around t,

$$\mathbf{r}(t + \Delta t) = \mathbf{r}(t) + \Delta t \cdot \mathbf{v}(t) + \frac{\Delta t^2}{2}\mathbf{a}(t) + \frac{\Delta t^3}{3!}\dddot{\mathbf{r}}(t) + \mathcal{O}(\Delta t^4), \tag{4.2}$$

and likewise,

$$\mathbf{r}(t - \Delta t) = \mathbf{r}(t) - \Delta t \cdot \mathbf{v}(t) + \frac{\Delta t^2}{2}\mathbf{a}(t) - \frac{\Delta t^3}{3!}\dddot{\mathbf{r}}(t) + \mathcal{O}(\Delta t^4). \tag{4.3}$$

Summing these two expressions, we obtain that

$$\mathbf{r}(t + \Delta t) = 2\mathbf{r}(t) - \mathbf{r}(t - \Delta t) + \Delta t^2 \cdot \mathbf{a}(t) + \mathcal{O}(\Delta t^4), \tag{4.4}$$

implying that the updating formula for the position vector,

$$\mathbf{r}(t + \Delta t) = 2\mathbf{r}(t) - \mathbf{r}(t - \Delta t) + \Delta t^2 \cdot \mathbf{a}(t), \tag{4.5}$$

is of order four. In order to compute quantities of interest, such as energy, temperature, etc., we need to compute the temperature. It turns out that we can calculate velocities and position vectors in the same timestep, and at the same time obtain a global error of $\mathcal{O}(\Delta t^2)$ in both.

4.2.1 Numerical scheme

To this end, we adopt the convention by Frenkel [13], and introduce the updating formulae

$$\mathbf{r}(t + \Delta t) = \mathbf{r}(t) + \Delta t \cdot \mathbf{v}(t) + \frac{\Delta t^2}{2}\mathbf{a}(t), \tag{4.6}$$

which is identical to the forward Euler scheme, and

$$\mathbf{v}(t + \Delta t) = \mathbf{v}(t) + \frac{\mathbf{a}(t + \Delta t) + \mathbf{a}(t)}{2}\Delta t, \tag{4.7}$$

wherein we have used the new position $\mathbf{r}(t+\Delta t)$ to calculate $\mathbf{a}(t+\Delta t)$. This can be interpreted as a predictor-corrector approach for the velocity, as we are using the predicted position $\mathbf{r}(t+\Delta t)$

to compute the acceleration in the next time-step. This can be seen from splitting (4.7) into two steps:

$$\mathbf{v}'(t+\Delta t) = \mathbf{v}(t) + \mathbf{a}(t)\Delta t, \tag{4.8}$$

$$\mathbf{v}(t+\Delta t) = \mathbf{v}'(t+\Delta t) + \frac{\mathbf{a}(t+\Delta t) - \mathbf{a}(t)}{2}\Delta t. \tag{4.9}$$

Herein, $\mathbf{v}'$ is to be interpreted as the (intermediate) predictor value. The first step is the regular Euler scheme, and the second is correcting by using the predicted accelerating. Assuming $\mathbf{a}$ to be independent of $\mathbf{v}$, adding them together obviously yields (4.7). This was actually the approach chosen in the final programs.

Hence, we can sum up the scheme as

1. Compute $\mathbf{r}(t+\Delta t)$ from (4.6).
2. Compute $\mathbf{a}(t+\Delta t)$ from the newly obtained $\mathbf{r}(t+\Delta t)$ and (4.1).
3. Compute $\mathbf{v}(t+\Delta t)$ from the newly obtained $\mathbf{a}(t+\Delta t)$ and (4.7).
4. Repeat for next timestep.

We emphasize that each of these steps should be taken for all particles involved, before proceeding to the next step.

4.2.2 Error terms

We now consider the error encompassed in the presented scheme. Equation(4.6) can be translated in time to yield

$$\mathbf{r}(t+2\Delta t) = \mathbf{r}(t+\Delta t) + \Delta t \cdot \mathbf{v}(t+\Delta t) + \frac{\Delta t^2}{2}\mathbf{a}(t+\Delta t), \tag{4.10}$$

so that, subtracting (4.6)

$$\mathbf{r}(t+2\Delta t) + \mathbf{r}(t) = 2\mathbf{r}(t+\Delta t) + \Delta t \cdot [\mathbf{v}(t+\Delta t) - \mathbf{v}(t)] + \frac{\mathbf{a}(t+\Delta t) - \mathbf{a}(t)}{2}\Delta t^2 \tag{4.11}$$

$$= 2\mathbf{r}(t+\Delta t) + \mathbf{a}(t+\Delta t)\Delta t^2, \tag{4.12}$$

where in the last line we have used (4.7). This expression is equivalent to (4.5), and hence error in $\mathbf{r}$ from the updating scheme (4.6) and (4.7) is of order four in Δt. The error in the velocity $\mathbf{v}$ is of order two in Δt, which can be realized by comparing (4.7) to the Taylor expansion

$$\mathbf{v}(t+\Delta t) = \mathbf{v}(t) + \Delta t \cdot \mathbf{a}(t) + \mathcal{O}(\Delta t^2). \tag{4.13}$$

4.3 Summary and limitations

The basic algorithm we have presented, the velocity Verlet algorithm, is on many accounts a good algorithm. It is fast, requires little memory, it is time-reversible, fairly stable, symplectic, and undergoes little energy drift in the long run. However, as is the problem with most numerical integrators of such systems, the solution will depend sensitively on initial conditions, and will

thus suffer from Liyapunov instabilities [33]. This means that no matter how small timestep we choose, a small perturbation in the initial conditions will result in an exponential divergence in trajectories. The equations are never solved exactly. However, this is not the purpose of MD simulations, as we seek *statistical* properties of a system. Significant numerical evidence indicate that the trajectories for particles obtained through MD simulations lie close to the "true" trajectories of the systems [15]. This, however, is evidence, and not proof, so MD simulations are still largely based on belief [13].

A problem with MD in general is also the computational cost. Since we are facing only finitely powerful computers, this limits us in system size, i.e. the number of particles to include in the simulations. Hence, it is important to use effective algorithms to speed-up the process, e.g. by parallelization. The most time-consuming part of the simulation process is the computation of the forces, and hence the number of force evaluations should be kept at a minimum, but not at the cost of obtaining physically feasible simulations.

5 Model of a polymer bundle

In this chapter we present a model which is as simple as possible, yet sufficiently rich to realistically capture the process of stretching and breaking a bundle of polymers. We first present the many-body model which is be solved numerically by means of molecular dynamics, using the algorithms presented in Chapter 4. Then we present a brief overview of the program, with an emphasis on complexity and possibilities of parallellization.

5.1 Requirements

We need a model which can be implemented in order to capture the physics of breaking a polymer bundle through numerical simulations, using molecular dynamics. As a first approach, the model should be as simple as possible, in order to see which physical features this provides us with.

As a basic starting point, the bundle should consist of an array of identical fibers. We take each fiber in the bundle to consist of an ideal chain with anharmonic coupling between neighbouring beads along the chain. However, in order to simulate the breaking process using molecular dynamics, the beads should interact through smoothly varying potentials [13]. Moreover, in order to allow for the bundle to break as time evolves, these potentials should vanish at a certain maximum separation between beads, also in a smooth way. We expect the chain to possess similar physical features as those of an ideal chain, although with an internal energy contribution originating from the anharmonic potentials. The property of no excluded volume is apparent also in this model. The chains will approach ideal chains in the limit $T \to 0$, as the bonds in this limit become increasingly rigid.

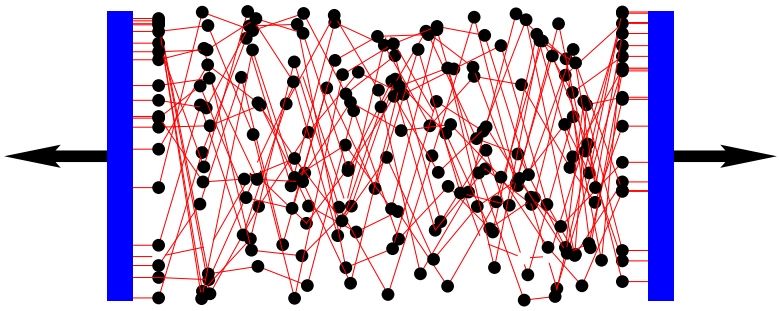

Figure 5.1: A schematic view of the polymer bundle.

The relatively few links in this model ensures that the model is computationally feasible, compared to a model with interaction between each pair of particles. Although there are few real systems that have these properties, there exist certain systems – at the theta point, mentioned in Section 2.6 – that do. Moreover, it is in itself an important first case to consider, as one can

hardly think of a simpler model of a polymer bundle to be simulated by means of molecular dynamics.

5.2 The model

We let the bundle be thermally insulated, and to consist of n_c polymeric chains. Each chain is attached to two parallel planar surfaces which are perpendicular to the (vertical) z-axis and located at z_L and z_R, respectively, for convenience oriented such that $z_L < z_R$. Each chain consists of n_b regular beads, which which we take to be point particles of mass m, in addition to two endpoints. The endpoints are constrained to lay on the boundary planes, but are free to move along the x and y directions. For each chain $j = 1, \ldots, n_c$, we denote the position vectors of beads $i = 0, 1, \ldots, n_b, n_b + 1$ as $\mathbf{r}_i^{(j)}$, so that $\mathbf{r}_0^{(j)}$ and $\mathbf{r}_{n_b+1}^{(j)}$ denote the position vectors of the two endpoints. The boundary plane constraint is thus fulfilled through $z_0 = z_L$ and $z_{n_b+1} = z_R$. A sketch of the bundle is shown in Figure 5.1.

5.2.1 Endpoint–bead interaction

Each endpoint interacts with its nearest regular bead through a harmonic potential

$$V_{\text{end}}(r) = \frac{1}{2} k_{\text{end}} r^2, \tag{5.1}$$

where r is the distance between the interacting beads, and k_{end} is the corresponding spring constant.

5.2.2 Bead–bead interaction

Regular beads interact only with their nearest neighbours along the chain, through a truncated Morse potential

$$V_M(r) = \begin{cases} D_0 \left[\exp(-2a_0(r - r_0)) - 2\exp(-a_0(r - r_0))\right] & r < r_{\text{c,i}}, \\ a_s(r - r_{\text{c,o}})^2 + b_s(r - r_{\text{c,o}})^3 & r_{\text{c,i}} \le r < r_{\text{c,o}}, \\ 0 & r \ge r_{\text{c,o}}, \end{cases} \tag{5.2}$$

where r is the distance between neighbouring beads, D_0 is the dissociation energy, a_0 is a parameter determining the width of the well, r_0 is an equilibrium distance. The truncation of the potential is determined by $r_{\text{c,i}}$ and $r_{\text{c,o}}$, which are respectively, the inner and outer radii of the cutoff section, and the coefficients a_s and b_s are determined such that $V_M(r)$ and $V_M'(r)$ are continuous everywhere.

This analytic expression for the truncated Morse potential yields a simple way to compute a critical threshold force at which interparticle bonds become mechanically unstable, since increasing their elongation decreases the restoring force. Any force beyond the magnitude corresponding to the inflection point, i.e. the maximum value of $V_M'(r)$, will break the bond.

5.2.3 Confining potential

In principle, with a model as described up to this point, chains will be allowed to cross the boundary plates. Close to equilibrium, chains will be distributed nearly as ideal chains, i.e.

coiled up in a shape given by a random walk – as was described for the freely jointed chain in Chapter 2. The separation of the two walls will then be short, and regular beads can be found on either sides of the pulling planes. This effect might limit the ability of our model to represent real systems, where one would expect the plates to be impenetrable. Moreover, constraining the beads to a limited portion of spaces reduces the entropic breaking, and enhances the probability for bonds to reform.

Hence, in order to restore important qualitative features of real systems, a soft repulsive potential is added to the regions outside the plates, pushing beads towards the inside of the portion of space delimited by the two parallel plates. The analytic expression for the added potential is

$$V_{\text{wall}}(\mathbf{r}) = \frac{1}{2}k_{\text{wall}}\left[(z - z_L)^2\theta(z_L - z) + (z - z_R)^2\theta(z - z_R)\right] \tag{5.3}$$

where $\mathbf{r}$ is the position vector of the bead it is acting on, and θ is the Heaviside step function, defined by

$$\theta(z) = \begin{cases} 0 & \text{for } z < 0, \\ 1 & \text{for } z > 0. \end{cases} \tag{5.4}$$

The contributions for particles 1 and n_b should be omitted in order to avoid straining bonds that by necessity are located close to the boundary planes – they already feel the force from the walls through the endpoint–bead interactions. This moderately repulsive potential does not strictly prevent particles to enter the external portion of space, but given a sufficiently large k_{wall} it should be sufficient to drastically reduce the spill-out of beads, thus enforcing the role of the plates as the exterior boundary of the simulated sample. The total plate separation $z_R - z_L$ should be significantly larger in the presence of a confining potential, than in the absence of one, as the end beads are forced towards the exterior of the system. Especially, this effect is present in the absence of external forces.

5.2.4 Stretching the bundle

Through the above equations it is implied that beads belonging to different chains interact only through the boundary plates. The z-component of the force on each of the endpoints is given by

$$F_{z,L}^{(j)} = k_{\text{end}}(z_L - z_1^{(j)}) \tag{5.5}$$

at the leftmost plate, and

$$F_{z,R}^{(j)} = k_{\text{end}}(z_R - z_{n_b}^{(j)}) \tag{5.6}$$

at the rightmost plate. The total force from the end beads on the left plate is then given by

$$F_{z,L} = \sum_{j=1}^{n_c} F_{z,L}^{(j)} = k_{\text{end}} \sum_{j=1}^{n_c} (z_L - z_1^{(j)}) = k_{\text{end}} \left(n_c z_L - \sum_{j=1}^{n_c} z_1^{(j)} \right) \tag{5.7}$$

and similarly on the right plate by

$$F_{z,R} = \sum_{j=1}^{n_c} F_{z,R}^{(j)} = k_{\text{end}} \left(n_c z_R - \sum_{j=1}^{n_c} z_{n_b}^{(j)} \right). \tag{5.8}$$

Moreover, the force contribution from the half-harmonic confining potential to the left can be written as

$$\tilde{F}_{z,L} = k_{\text{wall}} \sum_{j=1}^{n_c} \sum_{i=2}^{n_b-1} (z_L - z_i^{(j)}) \theta(z_L - z_i^{(j)}) \tag{5.9}$$

$$= k_{\text{wall}} \left(\tilde{n}_L z_L - \sum_{j=1}^{n_c} \sum_{i=2}^{n_b-1} z_i^{(j)} \theta(z_L - z_i^{(j)}) \right), \tag{5.10}$$

where $\tilde{n}_L = \sum_{j=1}^{n_c} \sum_{i=2}^{n_b-1} \theta(z_L - z_i^{(j)})$ is the number of particles to the left of z_L. Similarly, to the right, the force contribution from the confining potential is

$$\tilde{F}_{z,R} = k_{\text{wall}} \left(\tilde{n}_R z_R - \sum_{j=1}^{n_c} \sum_{i=2}^{n_b-1} z_i^{(j)} \theta(z_i^{(j)} - z_R) \right), \tag{5.11}$$

where $\tilde{n}_R = \sum_{j=1}^{n_c} \sum_{i=2}^{n_b-1} z_i^{(j)} \theta(z_i^{(j)} - z_R)$ is the number of particles to the right of z_R. The force on the plates is due both to the harmonic spring linking the end-of-chain beads, and to the repulsive interaction of regular beads.

We want to apply an external force F in order to stretch the bundle. This can be done in at least two ways:

1. Keep one of the plates fixed at a constant value at all times, and apply a force F to the other.

2. Apply a force $-F$ to the leftmost plate (at z_L) and a force F to the rightmost plate.

In our experiment, we choose the latter case to keep the symmetry. This force constraint effectively determines the plate positions z_L and z_R, and thereby the end values $z_0^{(j)}$ and $z_{n_b+1}^{(j)}$ for the endpoints of each chain j.

This corresponds to letting

$$F_{z,L} + \tilde{F}_{z,L} = -F \quad \text{and} \quad F_{z,R} + \tilde{F}_{z,R} = F. \tag{5.12}$$

For the left side, this yields

$$z_L = \frac{1}{k_{\text{end}} n_c + k_{\text{wall}} \tilde{n}_L} \left[\sum_{j=1}^{n_c} \left(k_{\text{end}} z_1^{(j)} + k_{\text{wall}} \sum_{i=2}^{n_b-1} z_i^{(j)} \theta(z_L - z_i^{(j)}) \right) - F \right], \tag{5.13}$$

and for the right side,

$$z_R = \frac{1}{k_{\text{end}} n_c + k_{\text{wall}} \tilde{n}_R} \left[\sum_{j=1}^{n_c} \left(k_{\text{end}} z_{n_b}^{(j)} + k_{\text{wall}} \sum_{i=2}^{n_b-1} z_i^{(j)} \theta(z_i^{(j)} - z_R) \right) + F \right]. \tag{5.14}$$

The above equations are non-linear relations where z_L and z_R are determined implicitly, since $\tilde{n}_R$ and $\theta(z_i^{(j)} - z_R)$ depends on z_R, and correspondingly for z_L. These can, however, easily be solved iteratively, and the iterative solver converges quickly e.g. by using the numerical value

from the previous time ste as an initial guess, or initially by use of the expressions for z_L and z_R in the case of vanishing confining potential, where we have

$$z_L = \frac{1}{n_c}\left[\sum_{j=1}^{n_c} z_1^{(j)} - \frac{F}{k_{\text{end}}}\right] \quad \text{and} \quad z_R = \frac{1}{n_c}\left[\sum_{j=1}^{n_c} z_{n_b}^{(j)} + \frac{F}{k_{\text{end}}}\right]. \tag{5.15}$$

In other words, we treat the two plates as massless objects, instantaneously adjusting their position to the force from the bundle, in such a way that the externally applied force is constant.

5.2.5 Energy

Collecting the contributions stated in the previous subsections, the total potential energy of the system is given by

$$\begin{aligned} &V(\{\mathbf{r}_i^{(j)}\}) \\ &= \sum_{j=1}^{n_c}\left[V_{\text{end}}(|\mathbf{r}_1^{(j)} - \mathbf{r}_0^{(j)}|) + \sum_{i=1}^{n_b-1} V_M(|\mathbf{r}_i^{(j)} - \mathbf{r}_{i+1}^{(j)}|) + V_{\text{end}}(|\mathbf{r}_{n_b}^{(j)} - \mathbf{r}_{n_b+1}^{(j)}|) + \sum_{i=2}^{n_b-1} V_{\text{wall}}(\mathbf{r}_i^{(j)})\right]. \end{aligned} \tag{5.16}$$

The total kinetic energy of the system is given by

$$K(\{\mathbf{p}_i^{(j)}\}) = \frac{1}{2m}\sum_{j=1}^{n_c}\sum_{i=0}^{n_b+1}(\mathbf{p}_i^{(j)})^2, \tag{5.17}$$

where $\mathbf{p}_i^{(j)} = m\dot{\mathbf{r}}_i^{(j)}$ is the momentum of particle i of chain j. Hence, the Hamiltonian of the system is given by

$$H(\{\mathbf{r}_i^{(j)}\}, \{\mathbf{p}_i^{(j)}\}) = V(\{\mathbf{r}_i^{(j)}\}) + K(\{\mathbf{p}_i^{(j)}\}). \tag{5.18}$$

We note that energy during a stretching will not be conserved, but will increase, as the will be transferred to the system upon adiabatic stretching, given that $F > 0$, as the applied force is opposed by the entropic-spring-like behaviour of the individual chains. Thus, work is performed on the system, and the energy increases.

5.2.6 Observable quantities

We now turn to identifying the most important quantities that we want to measure during the simulations, in addition to total kinetic and potential energy.

If the process is non-stationary, the notion of temperature is tricky to define, and in this case we rather interpret this as a measure of the kinetic energy of the system, measured in temperature units. Hence, we define the instantaneous temperature T according to

$$T = \frac{2K}{k_{\text{B}} N_f}, \tag{5.19}$$

where the number of degrees of freedom N_f can be calculated as

$$N_f = 2 + 2 \cdot 2n_c + 3n_c n_b - 3 \tag{5.20}$$

$$= 3n_c n_b + 4n_c - 1, \tag{5.21}$$

i.e. the sum of the 1 degree (z-direction) of freedom per 2 plates, 2 degrees of (xy-plane) freedom per $2n$ endpoints, the regular 3 degrees of freedom for the remaining beads, minus the 3 degrees of freedom for fixed momentum. Traditionally the "true" temperature is rather defined as the ensemble average

$$T_{\text{true}} = \langle T \rangle \tag{5.22}$$

The temperature fluctuations close to an equilibrium state will be of the order of $N_f^{-1/2}$. Assuming ergodicity one could then accurately estimate the true temperature by averaging over many fluctuations.

Moreover, we need to count the number broken bonds as time evolves. We define a bond as broken if the affiliated distance r between subsequent beads is larger than $r_{\text{c,o}}$, the outer truncation radius. Hence, the number of broken chains k is defined as the total number of chains which has at least one such bond.

We define the plate separation, or elongation L, as

$$L = z_R - z_L, \tag{5.23}$$

which by assumption is positive. The mean-field estimate of the applied force per chain, which we define as the *effective stress*, is

$$\sigma_{\text{eff}} = \frac{F}{n}, \tag{5.24}$$

where n is the number of remaining intact chains.

5.2.7 With or without recombination

Recombination of bonds will physically only correspond to a perfectly clean laboratory. In most experimental cases, however, one would expect that broken bonds rarely reform, as one could imagine that a free end could rather recombine with a free particle (e.g. a hydrogen) from the surroundings instead of reforming. The effect of allowing or disallowing for recombination is an nteresting point in question, and it is easy to test its effect by simulation.

5.2.8 Boundary conditions

In order for the chains not to drift off into the infinities in the xy plane, we apply periodic boundary conditions to the system. We take B to be length of the unit cell. The available volume then becomes finite, as the chains lie in a box with the volume LB^2. This drastically enhances the probability of chains recombining, especially when the plate separation L is small. Since chains in this model only can recombine with themselves, B acts as a characteristic interaction distance. Note that this is strictly not physical, but serves to restore a qualitative feature of the system.

5.2.9 Some remarks

Strictly speaking, the system is not *globally* stable at any non-zero temperature T, as long as there is enough energy in the system to break all chains at least once. Bonds will break spontaneously, and not reform due to entropy, as there is infinite empty space to diffuse into

once all chains are broken and the plates moves towards $\pm\infty$. However, due to the volume confinement, with limited space to diffuse into, the system may be locally stable given that the probability of recombination compensates for the probability of breaking, and that the fluctuations due to the finite size of the system are sufficiently small for the system to stay close to this local stable state at all times – this can be understood, at least qualitatively, by employing the model presented in Section 3.2.

5.3 Numerical implementation

The model that has been described may readily be implemented for molecular dynamics simulations using the velocity Verlet algorithm described in Chapter 4. However, in order to provide feasible simulations, there are some important aspects that first need to be adressed. These concern the conditions under which the simulation is run. Firstly, we need to initialize the system in such a way that it resembles a physical system near equilibrium when the simulation of the breaking process is started. Then we must consider the way we apply the force.

5.3.1 Initialization and equilibration

In order to run simulations that are uncorrelated, and obtain robust statistics, we need the system to be in an *equilibrated* state before a high load is applied. Strictly speaking, it is not an equilibrium state, since such a state would not exist for such a system when a force is applied other than when the plate separation approaches infinity. To initiate uncorrelated initial states need, however, a metastable initial state where we are guaranteed that almost[1] no bonds are broken.

This is done by adding a smooth half-harmonic contribution, given by

$$V_{\mathrm{eq}}(r) = \begin{cases} k_{\mathrm{eq}}(r - r_{\mathrm{c,o}})^2, & \text{if } r > r_{\mathrm{c,o}}, \\ 0 & \text{otherwise} \end{cases} \tag{5.25}$$

to the outer part of the truncated Morse potential, so that bonds that are extended beyond the outer cutoff radius $r_{\mathrm{c,o}}$ will feel the attractive force from this potential, and quickly return to a feasible length. For such a system, a globally stable state will exist. Equilibration among chains is ensured by the common contact with the end plates.

A preliminary initial state is produced by distributing the beads and chains in a regular manner, with separations r_0, but slightly perturbed in a random direction. These perturbations each add a small contribution to potential energy of the system. Then, we let the system evolve over a very long time, using the velocity Verlet algorithm – under a small external load F_{eq} in order to keep the system fairly stretched. During this time, we expect the potential energy contribution due to the perturbations in the positions to be distributed on the available degrees of freedom of the system, and an equilibrium state to be reached. Then a snapshot of the system – i.e. all the positions and momenta of the particles – is stored, constituting one initial state of the system. The system is then let evolve over a time interval that we assume to be sufficiently long for the state of the system to be uncorrelated to the state at which the snapshot was taken. Then, a new snapshot of the system is stored, and so forth, until we have a sufficient amount of initial states in order to provide feasible statistics.

[1] *Almost* in the sense that we do not consider a single broken bond in a large bundle as influental on the final outcome.

5.3.2 Numerical experiment

In order to initiate simulations of stretching and breaking the bundle, we turn off the half-harmonic contribution to the bead–bead interaction potential. The system is now in an equilibrated state – and we can start to experimentally investigate the effect of applying a tensile force F.

However, care must be taken while applying this force, in order to avoid excessive breaking due to high-frequency oscillatory modes[2]. We start the simulation at time $t = 0$, with the equilibration tensile force, i.e. $F(0) = F_{\text{eq}}$, and smoothly increase the load. Defining the *onset time* t_{onset}, the force $F(t)$ on the bundle is given by

$$F(t) = \begin{cases} F_{\text{eq}} + \frac{1}{2}\left(1 - \cos(2\pi t/t_{\text{onset}})\right)(F' - F_{\text{eq}}) & \text{if } t < t_{\text{onset}} \\ F' & \text{if } t > t_{\text{onset}} \end{cases} \tag{5.26}$$

where F' is the final, constant force we want to apply during single simulations. We assume herein the onset time t_{onset} to be small compared to the total simulation time.

5.3.3 Units and parameter set

In the simulations, we are using scaled units. These can be related to real systems by rescaling time and space, but are in any case sufficient to describe the qualitative behaviour of a variety of systems. The actual parameter values for the simulations were chosen somewhat heuristically, and we chose to mimic a scenario where temperature effects are present, and the chains are long enough and many enough for us to consider primarily the statistical properties of the breaking process.

Generally, a schematic model in scaled units represents many systems at the same time, and this is an advantage more than a disadvantage [4]. Moreover, the aim of this model is to provide an intuitive realisation of the FBM. Large-scale simulations are planned to extend the explorations of such an idealised model. In the future, simulations of more realistic models will become feasible, and will certainly be carried out.

In Table 5.1, the parameter set that was adopted for the major part of the simulations is summarized, in scaled units. By applying dimensional analysis, this can be related back to real units. As an example we consider the realistic values [52]

- Length: 1 nm (10)
- Energy: 0.1-1 eV
- Mass: 120 atomic units (10 carbon atoms)

This gives the unit of time in our system to be in the order 10^{-12} seconds [4].

We chose a time step $dt = 0.025$ for which we verified that energy was well conserved whenever F is set to zero, i.e., when the system is isolated. Our longest simulations covered a 200 million step run under the force $F = 5$[3]. In this sense, a such a simulation covers ~ 10 microseconds, which is not very short for a simulation. Moreover, we are using a coarse grained model, and time runs faster in coarse-grained models than in atomistic models [1], so the actual simulation time may be in the order of 0.1 microseconds.

[2] This was seen to be present when we increased the force in a discontinuous manner.

[3] Unfortunately, we did not obtain sufficiently reliable data for this to be included in Chapter 6.

Physical quantity	Variable	Value
Number of beads per chain	n_b	100
Number of chains in the bundle	n_c	400
Dissociation energy	D_0	6.0
Equilibrium radius of interaction potential	r_0	1.5
Inner cutoff radius of interaction potential	$r_{\mathrm{c,i}}$	3.0
Outer cutoff radius of interaction potential	$r_{\mathrm{c,o}}$	3.5
Potential width parameter	a_0	1.0
Endpoint–bead interaction potential strength	k_{end}	0.2
Confining potential strength	k_{wall}	0.2
Equalibration potential strength	k_{eq}	0.4
Equilibration force	F_{eq}	5.0
Initial temperature	T_0	0.33
Onset time of increasing tensile force	t_{onset}	250
Boltzmann constant	k_{B}	1
Unit cell length	B	20

Table 5.1: Parameter set chosen in the major part of the simulations.

Note that the temperature T_0 is only the initial temperature. Since we are not coupled to a thermostat, the temperature T will change during a single simulation, since energy is added by the stretching force, and may be dissipated into broken bonds. An overview and discussion related to the numerical implementation of thermostats is given in Appendix B.1. The long simulation time indicates that a discrepancy of the simulations carried out is the lack of a thermostat. Adiabatic stretching corresponds to a very fast stretching, or that the experiment takes place in vacuum.

5.3.4 Computational complexity and parallelization

We now consider the complexity of the program. For a system with n_c chains of n_b beads[4], there are $n_c n_b$ equations of motion that need to be solved, and thus, the number of operations to be performed in a time-step is thus of the order $\mathcal{O}(n_c n_b)$. In principle, these operations could be split on several, say N, processor cores on a supercomputer, reducing the expected computation time by a factor N. However, at each timestep, the confining plates are adjusted to a new position depending on the updated positions of all the beads in the system. This requires the processors to communicate, and is a bottleneck for the process. Thus, another timestep can not be initiated until all the processors have fully performed their operations, and hence the slowest one of the N processors is limiting the running time of the program. Since we in any case need many simulations to acquire robust statistics, a more efficient way of spending the computational resources is by running simultaneous instances of the unparallelized program on the N parallel cores, where we are guaranteed a speedup of N. For the final simulations, this was the approach that was adopted.

However, note that in order to run long simulations – meaning a low applied force – a genuine parallel implementation would be needed.

[4]For simplicity omitting the endpoints

6 Results

A large amount of simulations with the model described in Chapter 5 were carried out. In this chapter we present the main results from these simulations. First, in Section 6.1, we present results and considerations regarding the equilibrated bundle – i.e. the bundle wherein chains are not allowed to break. This also includes inspecting some thermodynamic properties of an equilibrated system. Then, in section 6.2 we state the conditions under which the numerical experiments are run. In Section 6.3, we qualitatively present the breaking process by focusing on single simulations. We then move to inspecting the average behaviour of bundles in Section 6.4. In section 6.5 we present the fluctuations around these averages. In Section 6.6 we briefly present a further exploration of the parameter space, varying other parameters than the applied stress. Finally, in Section 6.7, we inspect some of the rheological properties of the model.

Remark: In the figures in this chapter, we are always using scaled units, as were addressed in Section 5.3.3.

6.1 Equilibrated bundle

In this section we present results for the bundle during the equilibration stage. Here, the bead-bead interaction potential is modified by a half-harmonic addition effectively preventing bonds from breaking, as was described in Section 2.8. The main point of these simulations is to verify the implementation of the model, by ensuring that the behaviour of the bundle is physically feasible. Secondly, it should be verified that the equilibrated configuration actually corresponds to a state of thermal equilibrium. Moreover, it is in many aspects important for the forthcoming analysis to identify the behaviour of a system for which a well-defined equilibrium state exists.

One important physical feature that the equilibrated model should encompass is that it should conserve energy. During a stretch, upon extending the chain, it is expected that the energy of the system increases. In the stable equilibrated state, however, the energy may fluctuate on a short timescale, but the average, yielding the system temperature, should be stable. Figure 6.1 shows how energy is conserved in a single simulation of the bundle under a small applied tensile stress ($F = 5$), wherein the bundle has reached the equilibrated state. The plot shows as expected that the energy fluctuates rapidly on the short timescale, but that in the long run energy is well conserved, with only a slight observable energy drift during the first 2 million timesteps. This energy drift is assumed vanishingly small compared to the overall inaccuracies related to the system in scope. The relative fluctuations in the temperature are of the order 1%, which is typical for a system of $\sim$ 40000 particles – this gives the number of degrees of freedom in the order $N_f \approx 10^5$, which yields $1/\sqrt{N_f} \approx 1\%$ [13]. Figure 6.2 shows a portion of a bundle of 400 chains with 100 chains per bead after equilibration. The beads are overlapping to a large extent, but seem to be largely concentrated between the confining plates. In Figure 6.3, the relative density of beads along the z-axis is shown. From Figure 6.3, we see that the beads are mostly distributed between the confining plates, i.e. the confining potential is effectively pushing the beads towards the center. The high density towards the middle portion of space indicates that the chains are in a fairly coiled-up conformation. The distribution also appears fairly symmetric around $z = 0$, which is what one would expect given the inherent symmetry of

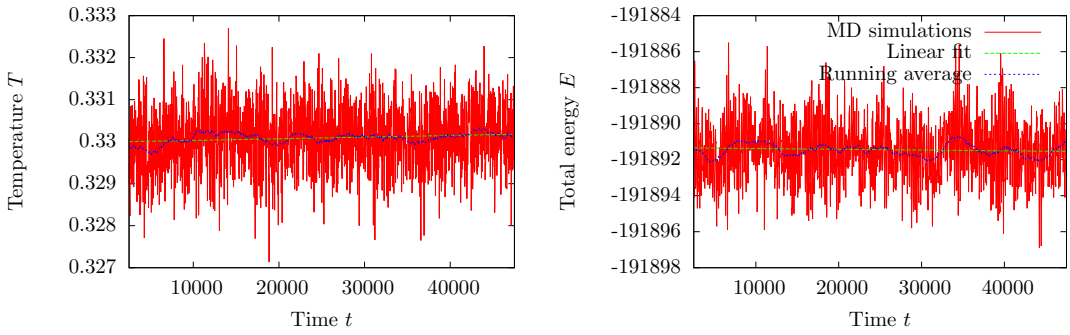

Figure 6.1: Plot showing how the energy of the system evolves during a single simulation. The running average is taken over 2500 time units, i.e. 100000 timesteps. The energy fluctuates on the short time scale, but is fairly stable on the long time scale.

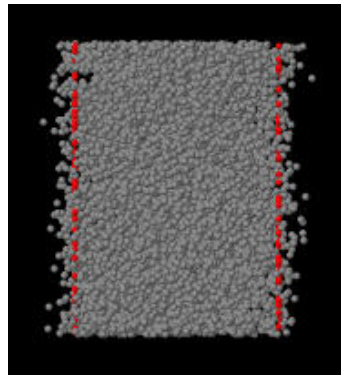

Figure 6.2: A snapshot of a portion (25% of the chains) of the bundle equilibrated under a small applied tensile stress of $F = 5$, immediately after the confining potential preventing bonds from breaking has been switched off. The red beads are the endpoints confined to the plates, and regular beads are shown in gray.

the model. Similarly, in Figure 6.4, the distributions of the z-component of the velocities and the kinetic energy of the individual beads are shown, along with fitted Maxwell-Boltzmann distributions. The measured values are found to fit well with their corresponding Maxwell-Boltzmann distributions, effectively yielding the sample temperature $T = 0.33$.

The computed stress-strain curve of the bundle where bonds are not allowed to break is shown in Figure 6.5. It is seen here that the Gaussian bundle represents the bundle well at short separations, albeit slightly overestimating the strain at low forces. This is attributed mainly to the fact that the analytic expression 2.10 was obtained under the assumption of chains being attached to hard walls, while the confining potential of the molecular dynamics simulations were assumed soft. At longer separations, it is seen that the bundle approaches the curve of the FJC bundle, but that in the large force range becomes more elastic than the FJC, in agreement with the experimental findings of Smith et al. [44] on stretching DNA. This intermediate behaviour can be attributed to the fact that the bonds are not as rigid as assumed in the derivation of the

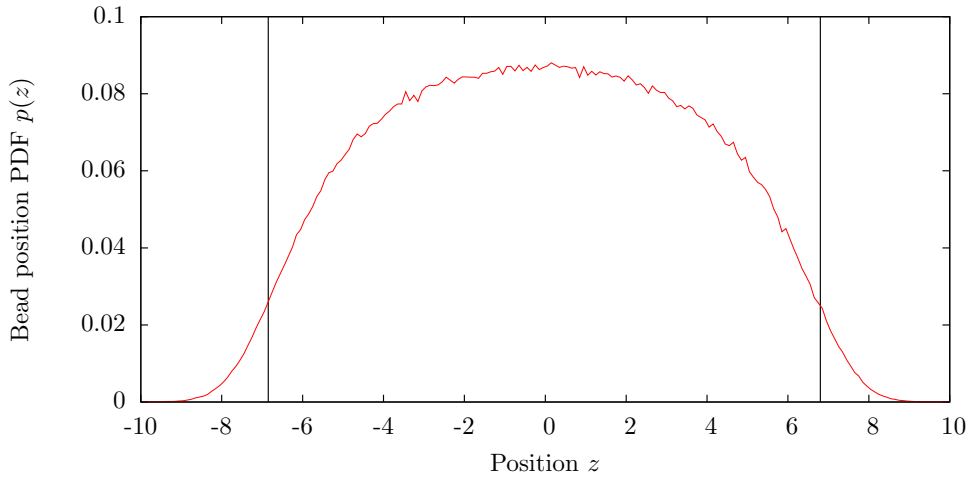

Figure 6.3: Histogram showing the experimental PDF of the positions of beads in the system along the z-direction immediately after equilibration. The z-axis has been shifted to set the center of mass of the system at $z = 0$, and 62 equilibrated samples (initial states) have been used to produce the histogram. The endpoints have intentionally been omitted, and hence the vertical lines show the average positions of the confining plates.

FJC, but much more rigid than what was assumed in the derivation of the Gaussian bundle.

By inverting equation (2.29) for the adiabatic stretching of a bundle we can also inspect the validity and applicability of the equation-of-state which was derived in Chapter 5 for the linear stretching regime (moderate stretching), i.e. for the unconfined Gaussian bundle. Preventing bonds from breaking yields the expression

$$\frac{3k_{\mathrm{B}}}{2nb^2}L^2 = c_L \ln T + C, \tag{6.1}$$

where $c_L = C_L/N$ is the heat capacity per chain, and the initial equilibrium state (T_0, L_0) has been suppressed into the constant C, which we regard as a fitting parameter. The left hand side during adiabatic stretching of the non-breaking bundle has been plotted against $\ln T$ in figure 6.6, displaying, except during the very initial stretching regime, a linear dependence. This indicates that the assumption of regarding the internal energy of the bundle as solely and linearly dependent on the temperature T was a valid one, at least in the temperature region in scope – i.e. $[0.35, 0.45]$. Moreover, the heat capacity is readily identified by estimating the slope of the graph.

6.2 Experimental conditions

In this section we discuss the conditions under which the major portion of the numerical experiments have been carried out. We simulate a *thermally insulated* system and *stress-controlled* conditions, i.e. we control the force that is applied on the bundle, and not the length of it. The simulations are based on a set of equivalent initial states that have been equilibrated at a temperature $T = 0.33$ under a small tensile load $F = 5$.

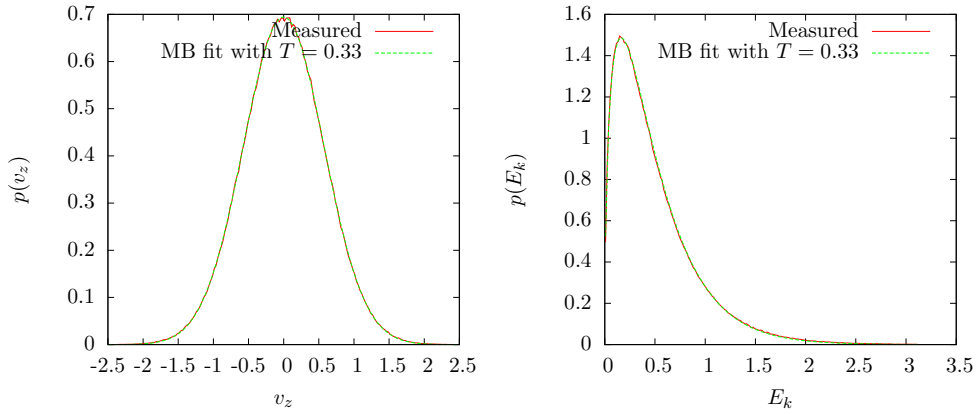

Figure 6.4: Histogram showing the experimental PDF of the z-component of the velocities of the beads, and the kinetic energy distribution of beads. 62 equilibrated samples (initial states) have been used to produce the histograms.

Even though the system is thermally insulated, we note that the temperature will change throughout the process as a force is applied, performing work on the system and thus effectively transferring energy to it. Although this process may, and will, perturb the system out of equilibrium, we call it *adiabatic stretching*, as it may be regarded as thermodynamically analogous to the process of expanding a gas which is thermally insulated from the surroundings. However, in the present context, energy may be dissipated into broken bonds.

6.3 Qualitative features of the breaking process

We now present qualitative features of the breaking process in the model by focusing on a representative set of single simulations. Depending on the magnitude of the tensile load we apply, the bundle will behave differently, as will be presented in the forthcoming.

The simulations have been carried out under two different model assumptions: One part allowing for recombination of broken bonds, and one part disallowing recombination. We begin by the former.

6.3.1 With recombination

The simulations with recombination showed two distinct behaviours for the bundle under stress, in a sense reminiscent of what is found for the discrete-time FBM with heterogeneous bundle. Regarding the applied tensile force F as the control parameter, it was observed from a series of simulations with equivalent initial states that at sufficently high F, the bundle breaks down, whereas for sufficiently low F, the bundle settles towards an equilibrium state where only a finite number of chains are broken. This suggests that the bundle undergoes what may be a continuous phase transition – at some critical force $F = F_c$ the behaviour changes suddenly from relaxing towards a stable state, to complete failure. We henceforth call forces, or equivalently applied tensile stress, above this threshold *supercritical stress* ($F > F_c$) , and correspondingly forces below *subcritical stress* ($F < F_c$). Due to the finite size of the system, fluctuations will

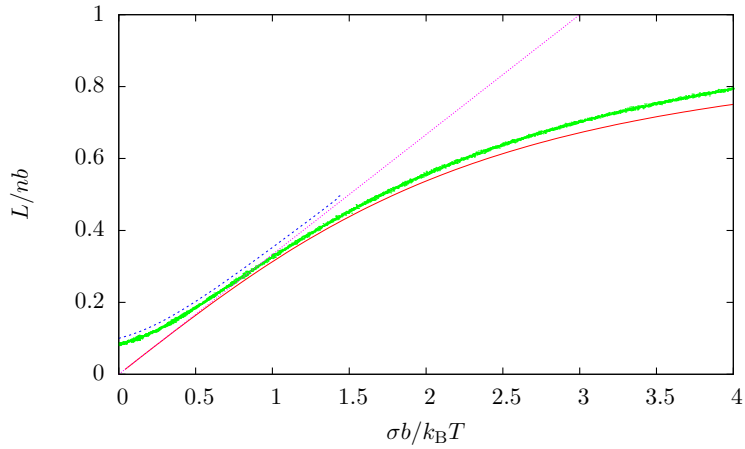

Figure 6.5: Comparison of stress-strain curves. The stress-strain curve for the proposed model for the polymeric bundle is shown in green, as obtained by molecular dynamics simulations. The simulation data were provided during a single slow stretching of a bundle while preventing bonds from breaking. The other curves represent the unconfined Gaussian bundle (dashed blue), the confined Gaussian bundle (pink) and the FJC bundle (red).

play a major role, as the simulations are not deterministic. However, much insight can be gained by first studying representative single simulations before proceeding to statistical averages.

Supercritical stress

In a bundle under supercritical stress, the applied tensile stress is sufficiently high for the bundle to reach complete failure within a finite time. Figure 6.7 shows a portion of a bundle of 400 chains, with 100 beads per chain as it evolves in time under an applied tensile stress $F = 60$. For the sake of visual clarity only 25 % of the chains are shown. As time proceeds, more and more chains break, and consequently more load is shared between the surviving chains. During the same time, the bundle becomes increasingly elongated. Chains steadily break, the load on the remaining chains increase, and ultimately the entire bundle fails. Intuitively this agrees with the class of equal-load-sharing fiber bundle models. As chains spontaneously break, the average force on the remaining ones increase. Since the strain of a polymer increases with the applied stress, the individual chains, and thus the entire bundle, becomes increasingly elongated as time proceeds and more and more chains are broken.

In figure 6.8, four different quantities of the same single run are shown, namely the number of intact chains, the elongation, the instantaneous temperature and the excess potential energy (V_0 is the theoretical ground state energy of the system, at $T = 0$). From this single run, which corresponds to 6.7, focusing on the number of broken chains and elongation as the quantities evolve in time, it is observed that the breaking process consists of three distinct regimes, namely an initial regime of a high rate of breaking, which decays as we approach a secondary regime, with a seemingly constant breaking rate. This proceeds for a while, until we reach the tertiary regime – the regime of imminent failure. At this point, it seems as if the load on each chain is approaching a critical threshold, and the breaking rate accelerates rapidly before the bundle breaks completely down.

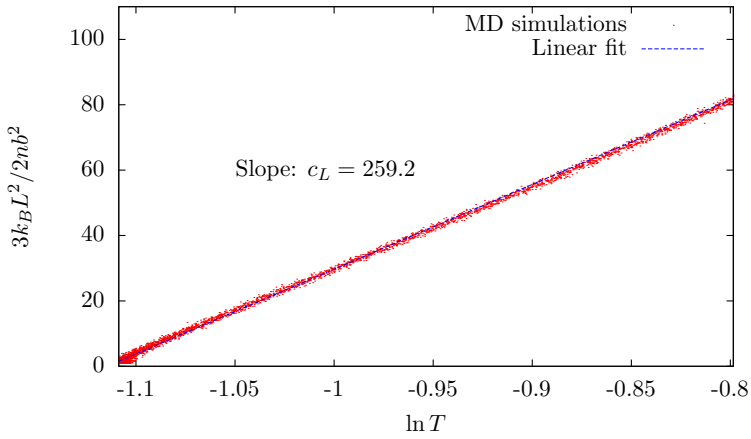

Figure 6.6: Estimation of the heat capacity of the non-breaking bundle, based on molecular dynamics simulations and Equation (6.1). The linear fit displayed effectively yields the heat capacity per chain c_L as the slope of the graph.

Figure 6.9 shows a density plot of the beads in the bundle at an instance of time before the bundle completely fails. It is clear that beads from, respectively, broken and unbroken chains are distributed differently. The beads from the intact chains seem to be distributed almost evenly – corresponding to the chains being in a fairly stretched state –, whilst the beads from broken chains are located close to the confining plates – indicating that they are predominantly in a coiled-up state where one end is attached to the plates. In figure 6.10 the velocity and kinetic energy distributions of the individual beads are shown.

Subcritical stress

In a bundle under subcritical stress, the applied load is sufficiently low for the bundle to withstand the applied force and not reach complete breakdown. It rather relaxes towards a local equilibrium state where only a portion of the chains are broken. Figure 6.11 shows snapshots of a bundle under such conditions at several instants of time. The bundle is first stretched due to the sudden onset of the force, as many chains break, whereupon it shrinks again. This is seen quantitatively, for the same single simulation, in figure 6.12. A large amount of chains break immediately, but then many of the chains recombine, and the bundle slowly shrinks.

It is clear that at low applied loads, the same regimes as was observed for supercritical loading can not be found. The primary regime has qualitatively the same features – a quick rise in the number of broken chains – but it decays. After an initial stage, recombination starts to dominate. This proceeds until the rates of recombination and breaking again are competing, and the bundle settles and fluctuates around equilibrium where only a few chains are broken.

In figure 6.13, the density plot of the z-component of beads are shown, for a simulation where equilibrium is reached. The beads from intact chains are seemingly distributed almost uniformly between the plates, whilst the broken ones seem to be coiled up close to the plates they are attached to.

The velocity components and kinetic energy distribution for individual beads of the bundle of the same state is shown in figure 6.14. By a least squares method, regarding the temperature T

as the free variable, the distribution is fit to a Maxwell–Boltzmann distribution. The accurate fit indicates that the bundle is close to thermal equilibrium in this state, yielding also a well-defined temperature.

Critical stress

The observation of two distinct behaviours for the bundle under tensile stress, namely the subcritical regime and the supercritical critical regime, suggests that there should exist a well-defined *critical* value of $F = F_c$ where the transition takes place. However, large fluctuations in the simulation trajectories take place. For a small interval of applied loads, the same applied load may lead to individual simulations either settling to equilibrium or leading to complete failure. These *finite-size effects* are present due to the numerical limitations involved. For a more precise description and identification of this point, simulations with larger bundles are necessary. For the model parameters studied here, we heuristically identified $F_c \simeq 42$ as this critical value.

In figure 6.15, four quantities of the bundle are shown for two distinct simulations under equivalent initial conditions, from two different initial states. It is seen that one leads to the bundle completely breaking down, and the other leads to the bundle relaxing towards equilibrium. The quantities of the bundle evolve in the same manner, until a point, at about $t = 80000$, when one of the bundles seems to spontaneously cross a threshold value of broken chains, reminescent of an unstable fixed point. From this point on, the two trajectories are completely different. The bundle that crossed the threshold is stretched, more and more bonds are broken, and eventually it fails completely. The other bundle shrinks slowly and seems to reach stable state where almost all chains are intact, and the temperature is stable.

We note that in a bundle of finite size, we would expect that the bundles will fail in a finite time, also under a subcritical load, given that the fluctuations around equilibrium are so large that the bundle state will surpass the unstable fixed point within a finite time.

6.3.2 Without recombination

Extensive simulations were also carried out without allowing for recombination. In this model assumption the bundle proceeds to ultimate breakdown no matter how low the force. Simulations were carried out at values down to $F = 5$, yielding a lifetime in the order of 5 million time units, e.g. 200 million timesteps, showing a significant decrease in the breaking rate during simulation. Simulation snapshots of a portion of the bundle at $F = 60$ where recombination is disallowed are shown in figure 6.16. The bundle proceeds in qualitatively the same way as the one without recombination at this high applied force, but breaks in a marginally shorter amount of time, since no bonds are allowed to reform. The corresponding quantities during the same single simulation are shown in figure 6.17.

6.3.3 Bond breaking

A point in question which can be answered by means of the present numerical model is where in the chains bonds break. Since we, in the present context, are considering a bundle of 400 chains with 100 beads per chain, we need the averages over many simulations to create reliable histograms.

For the model assumption of allowing for recombination, the breaking histograms for different forces are shown in Figure 6.18. This figure shows the experimental probability of a bond being

broken after the bundle has completely broken down. It is clear that for larger forces, the bonds break more likely close to the plates, and for lower forces this effect decays. Due to limited data, the cases for $F = 60$ and $F = 43$ are almost indistinguishable, but it is likely that the later stage of breaking may be responsible for the excessive breakings close to the plates. The distribution of the rupture PDF is symmetric, as anticipated due to the symmetry in the model.

In figure 6.19, a histogram over the bond length at different instants of time is shown. It is seen that the bond length distribution changes only slightly during loading, indicating that the chains break mainly due to the thermal fluctuations, corresponding to the tails of the bond length distributions. The inflection point of the Morse potential is indicated with an arrow. Beyond this point, the bond becomes less resistant to perturbations and may more easily break – boyind this point bonds may become mechanically unstable.

6.3.4 Effective stress–strain curve

In Chapter 2, we identified the *effective stress–strain relation* in thermodynamic equilibrium as a relation between the dimensionless quantities

$$\frac{L}{L_c} \quad \text{and} \quad \frac{\sigma_{\text{eff}} b}{k_B T}, \tag{6.2}$$

where $\sigma_{\text{eff}} = F/n$ is the effective stress, or average force per remaining intact chain, and $L_c = n_b b$ is the contour length. The quantities L, F, n and T will all change through the course of a simulation, but they are at all times kept track of. In this sense, they can be regarded as parametrized by the time t. Eliminating t yields a parametrized curve in the plane constituted by the quantities in (6.2).

In Figure 6.20, these curves are plotted for a range of representative single simulations with different applied forces. For all the simulations, the curves more or less coalesce, resulting in a remarkable data collapse. For all of the forces involved, the trajectories follow qualitatively the same behaviour, meaning first an unsettled regime with deviations from the common stress–strain curve, before the curves settle for a regime of steady strain. The common curve deviates from the both the theoretical curves and the experimental curve for the non-breaking bundle, indicating that chains break in a predictable manner when they become sufficiently elongated. We see that the FJC approach seems to hold fairly well during moderate stretching, and that the Gaussian bundle holds under small stretching. No one of the models hold over the entire effective-stress span, as was expected initially. The trajectories from the different forces seem to follow the same curve, indicating that there exists a predictable stress-strain relationship – in effect an equation-of-state relating the above variables to each other.

Primarily this indicates that the evolution of the stretching-and-breaking process of the polymeric bundle happens, for the dominant part of time, close to a thermodynamical equilibrium state of the system, potentially allowing for employment of close-to-equilibrium thermodynamics. Secondly, the data collapse may indicate that the effect of fluctuations in the force is small, since the computed curves are based on a simple mean-field approach for the effective applied stress – average load per surviving chain. Thirdly, the presence of broken chains seems to have little influence on the process, as the curves fall on top of each other for a large span in magnitudes of the applied initial stress – at least for the region where the data collapse is observed. An alternative option, that we strictly must hold open, is that two or more of these effects cancel, yielding the same curve.

6.4 Average behaviour

In this section we present the average behaviour of the bundle. To calculate the averages, general methods are needed in order to unambiguously define the trajectories of the quantities we are interested in.

6.4.1 Definition of the averages

The evolution of the bundle under stress depends largely on fluctuations, and the parameters of the process are changing constantly throughout a simulation. Figure 6.21 shows the number of broken chains as a function of time for many independent simulations with equivalent initial conditions under the same applied tensile load $F = 60$, for which the bundle ultimately fails. Based on this limited set, one gets an intuitive impression of both the mean, and the magnitude of its deviations, but it is necessary to quantify it in a systematic manner.

We are interested in obtaining the average evolution of the system under a given applied force F. A major question is thus how to define the average evolution of this process. When the bundle breaks completely down, many quantities, such as the force per chain and temperature, will diverge, and hence it is clear that a naive application of averaging over many samples at the same time t will not suffice for such an unstable system.

If we consider the first-time breakage of each chain, we can, however, obtain a well-defined average by defining the time of breakage for the ith chain $t(i)$ as

$$t(i) = \frac{1}{N_s} \sum_{j=1}^{N_s} \hat{t}_j(n), \tag{6.3}$$

where N_s is the total number of simulations, and $\hat{t}_j(i)$ is the time in simulation j at which the ith chain breaks. Correspondingly, the empirical variance $(\Delta t(i))^2$ is given by

$$(\Delta t(i))^2 = \frac{1}{N_s - 1} \sum_{j=1}^{N_s} (\hat{t}_j(i) - t(i))^2. \tag{6.4}$$

We note that higher moments can be computed in a similar manner, but generally require larger data sets than we have acquired to this point. It follows then that the empirical mean time of failure is given by

$$t_f = t(N), \tag{6.5}$$

and the corresponding standard deviation is

$$\Delta t_f = \Delta t(N). \tag{6.6}$$

The latter two quantities are unambiguosly well-defined as long as the bundle comes to a complete breakdown within the simulation time. This is the case for sufficiently large applied forces, and is also guaranteed[1] for the model assumption of disallowing recombination. For the model assumption with allowing for recombination, this definition will tend to overestimate the number of broken bonds, as broken bonds may heal. Moreover, other quantities that are not monotonically increasing in time requires other methods of averaging. Hence other methods are generally

[1] As long as there is sufficient energy in the system to initiate breaking after the initial stretch.

required. However, we adopt this averaging approach for the number of bonds under the model assumption of no recombination.

For all other cases, we propose to separate the simulations in two categories: The ones that ultimately fail, and the ones that approach equilibrium. For the first case, we have a well-defined timescale for the process under a given applied tensile load through the average lifetime t_f, obtained from the definition above. From this, we can scale the time t_i for every single simulation by their respective failure time $t_{f,i}$. In this way, the total time of the simulation is fixed. Taking $\tau = t_i/t_{f,i}$ to be the new dimensionless *normalized* time running from 0 to 1 for each simulation, we can unambiguously define the averages for any quantity that evolves during the simulation. For an arbitrary quantity X with measurements $X_i(\tau)$ we then define the empirical average

$$X(\tau) = \frac{1}{N_s}\sum_{i=1}^{N_s} X_i(\tau), \tag{6.7}$$

and correspondingly the variance

$$(\Delta X)^2 = \frac{1}{N_s - 1}\sum_{i=1}^{N_s}(X_i(\tau) - X(\tau))^2. \tag{6.8}$$

This is perhaps not the only way to define this average, but to our knowledge, it is the simplest, and will suffice for the present work.[2]

6.4.2 With recombination

In the bundle assumption *with* recombination, we have observed two distinct behaviours depending on the applied load, identified as the cases of sub- and supercritical loading. In the forthcoming we focus on the latter.

Lifetime dependence upon applied load

In Figure 6.22, the lifetime of the bundle is plotted as a function of applied initial stress, for a bundle wherein recombination is allowed. All simulations are carried out under thermal insulation. A power law $t_f \sim F^{-\gamma}$ is fitted to the data, yielding the exponent $\gamma = 4.0 \pm 0.1$ with a least squares method. This is reminiscent of the Basquin law of fatigue [5] known from materials science, which has shown to be valid for a range of materials under cyclic loading [29], and recently for polymeric materials under constant load [32]. The estimated exponent is valid only for approximately half a decade in the applied force F, based on a somewhat limited data set, and the results are therefore not sufficiently statistically robust to conclude that it is indeed a power law.

[2] For the simulations that approach equilibrium, no such finite time-scale exists (although one could define a characteristic relaxation time for approaching equilibrium), and the natural averaging procedure is simply given by

$$X(t) = \frac{1}{N_s}\sum_{i=1}^{N_s} X_i(t), \tag{6.9}$$

and correspondingly for the variance. t is the unscaled time.

In Figure 6.22, we are limited by the phase transition we observed and commented on in section 6.3. At the threshold value of $F \simeq 42$, the behaviour of the bundle crosses over from approaching equilibrium to proceeding to ultimate failure, and hence we are limited from including any lower values of F in this plot. At any higher values of applied tensile load, we are limited by the fact that the lifetime of the bundle becomes comparable to the time window we have chosen for the onset of force, i.e. of the order $t_f \sim 250$.

6.4.3 Without recombination

As already mentioned in section 6.3, it is evident that in the case of disallowing recombination, the bundle proceeds to complete failure no matter how small the applied load is. We therefore present the results concerning the averages of the evolving quantities in the context of this model assumption, since this allows us to investigate a larger span of applied forces.

Lifetime dependence upon applied load

The lifetime of the bundle as a function of applied force is shown in figure 6.23. Compared to the case with recombination, shown in Fig. 6.22, the lifetimes are slightly shorter, but of the same order of magnitude. The power law observed for a short range in F is not found for all inspected F in the case of no recombination. In this case we observe a crossover behaviour at $F \simeq 50$. In the range of large forces, the exponent obtained for the case with recombination seems to agree well with the data. However, the error bars are too large to obtain a reliable estimate of the exponent in this case, and the line in Figure 6.23 corresponding to $\sim F^{-\gamma}$, with the exponent $\gamma = 4$, is thus merely meant as a guide to the eye.

In this case, the simulations for low forces were only limited by the computational resources available. Carrying out enough simulations to obtain reliable statistics at low forces proved to require a disproportionate amount of time. At large forces, the simulations are limited in the same manner as the case with recombination.

Evolution of observable quantities

The average evolution of different quantities of interest were computed according to the methods described in subsection 6.4.1 for a range of forces. The simulation time is thus scaled, or normalized, by the lifetime of the bundle, for which the averages are shown in Figure 6.23. In Figure 6.24, the number of broken chains are shown as a function of the scaled time, for a range of forces. It is evident that the evolution of the bundle depends continuously on the magnitude of the applied load.

The existence of the three regimes that were pointed out in section 6.3 are now evident. The *primary regime* consists of a stage of high breaking rate which smoothly decays. At sufficiently high forces, and correspondingly short bundle lifetimes, it is observed that the finite time window for the continuous onset of force makes a significant impact on the breaking process. At the highest force, $F = 150$, this time window corresponds to roughly 25% of the lifetime of the bundle, and hence may the validity of the related data point in figure 6.23 be questioned. At sufficiently low forces, this *onset effect* becomes vanishingly small, and it is seen that the primary stage lasts for roughly the same relative amount of time for all the forces, $\sim 10\%$ of t_f. The height of this regime is however dependent on the applied force – we see that more chains are broken during this primary stage when a lower force is applied.

The characteristic feature of the *secondary regime* is a constant breaking rate. The slopes of the curves in Figure 6.24 are essentially the same in this regime, implying that the lifetime of the bundle is mainly determined by the breaking rate in the secondary regime. The secondary regime lasts until the breaking rate again starts to accelerate. This marks the onset of the *tertiary regime* – the regime of imminent breakdown of the bundle.

The relative time at which the tertiary regime sets in depends on the load. At larger forces, it sets in earlier than at low forces – for $F = 150$ it begins at $\sim 0.8t_f$, while at $F = 20$ it begins at $\sim 0.98t_f$. The main characteristic feature of the tertiary regime is, as mentioned, the increasing breaking rate which leads to the ultimate breakdown of the bundle.

In Figure 6.25, the average elongation as a function of scaled time is shown. The bundle starts with the equilibrated elongation $L \simeq 13$, which as we remember was obtained at a small tensile load $F = 5$. As the tensile load is applied[3], the bundle starts oscillating around a certain "equilibrium" elongation L_0 which is steadily increasing. This rippling effect is reminiscent of the phenomenon called *creep ringing* of viscoelastic materials [24] – which we will investigate in more detail in Section 6.7. In Figure 6.25, this effect is most apparent at large forces, but it is also present at low forces, but in this case the relaxation time for the oscillations to die out becomes small compared to the total failure time of the system. Additionally, the averaging procedure may reduce the amplitude of the oscillations.

Disregarding the oscillations, it is seen that the elongation depends continuously on the applied force, in the sense that an increased load leads to a higher strain, in agreement with the observations pointed out in Subsection 6.3.4. The elongation between curves corresponding to different applied loads are seen to differ by a seemingly constant separation throughout the process. The presence of the primary regime is harder to see in this case than by regarding the breaking rate. However, a slight decrease in the *strain rate*, which we define as $\dot{L} = \mathrm{d}L/\mathrm{d}t$, is observed for the lower forces until $\sim 0.1t_f$. This is consistent with what the so-called *primary creep* of viscoelastic materials [49]. The secondary regime is seen to behave according to a constant breaking rate – which is consistent with the concept of *steady state creep* [49]. The strain rate starts to increase between $0.8 - -0.9t_f$, indicating imminent breakdown – i.e. the onset of the tertiary regime. The tertiary regime is characterized by a accelerating increase in the strain until the bundle breaks completely down around the contour length $L \sim 150$. Interestingly, the bundle is seen to behave in the same manner during the entire process, differing only the equilibrium elongations – also near the end – as long as the applied load is not too large ($F \lesssim 100$).

In Figure 6.26, the average temperature evolution for a range of forces is presented. It is clear that the also the temperatures depend continuously on the applied load – a lower force generally leads to a lower temperature during the stretching. This is consistent with the fact that we are considering a bundle under adiabatic stretching, meaning that a large applied load leads to a longer stretching – transferring more energy to the system. It is evident from Figure 6.26 that at large forces, the bundle temperature is significantly increased; at moderate forces, it is practically constant, and at sufficiently low forces the temperature decreases throughout the process. This decrease is in agreement with the large amount of broken bonds in the primary regime for low forces, since broken bonds effectively lead to energy being dissipated from the system. The common point for all the simulations is that the temperature drastically increases in the tertiary regime, suggested that the velocity of the particles are increased, in accordance the observed increased strain rate in 6.25.

In Figure 6.27, the fraction of broken bonds per chain as a function of normalized time is

[3]Strictly speaking, it is *increased*, as a load is present already at the equilibration.

displayed. The trajectories are in agreement with Figures 6.24 and 6.26, displaying that chains may break in more than one place, leading to more energy being dissipated.

6.4.4 Scaling behaviour

Inspecting Figure 6.25 we noticed a similarity between the strain curves as a function of time. Eliminating the mentioned equilibrium elongation by subtracting L_0, regarding it a fitting parameter dependent only on the applied load, we see that the trajectories for the different loads fall on the same curve. This is shown in Figure 6.28, where the deviation $L - L_0$ is plotted against the normalized time. This remarkable data collapse hints to universality in the breaking process, suggesting the very same behaviour at timescales of dramatically different amplitude. Inspecting Figure 6.23 shows that the timescales span from

In order to inspect the regime of imminent failure (the tertiary regime), we introduce the normalized time-to-failure

$$\tau_{\text{ttf}} = 1 - t/t_f. \tag{6.10}$$

In Figure 6.29 the elongation difference $L - L_0$ is plotted against this normalized time-to-failure. We found that the data is well fitted by a logarithmic relation

$$L = a \log \tau_{\text{ttf}} + C, \tag{6.11}$$

where a and C are constants, seemingly valid over roughly one and a half decade. This suggests that in the regime of imminent failure, the strain rate is given by

$$\dot{L} \propto \frac{\mathrm{d} \ln \tau_{\text{ttf}}}{\mathrm{d}t} = \frac{1}{\tau_{\text{ttf}}} \frac{\mathrm{d}\tau_{\text{ttf}}}{\mathrm{d}t} \tag{6.12}$$

$$\sim \tau_{\text{ttf}}^{-1} \tag{6.13}$$

This is in excellent agreement with the experimental findings of Leocmach et al. [32], who found the *shear rate* $\dot{\Gamma}$, in the regime of imminent failure, to depend on the time-to-failure as $\dot{\Gamma} \sim \tau_{\text{ttf}}^{-1}$ – the same relation as was deduced above for the present numerical model. The present findings indicate that this may be a universal fingerprint of such simple polymeric systems at imminent failure.

In any case, it may be another indication that that the model suffices to reproduce phenomena known from experiments, showing promise to bridge the gap between the microscopic and macroscopic scales of understanding failure phenomena.

6.5 Fluctuations

The main focus until this point has been the average behaviour of the bundle under tensile load. However, fluctuations at the microscopic scale is the driving mechanism behind the breakdown of the bundle. These become present at large scales, resulting in large fluctuations – making the evolution of single simulation highly unpredictable. In this section we briefly present these variations around the average behaviour.

6.5.1 Lifetime dependence upon applied load

The estimated standard deviations Δt_f of the lifetimes t_f are plotted in Figure 6.30, and show reminiscent features of Figures 6.22 and 6.23, suggesting a proportional relation between them. Based on a somewhat limited dataset, one finds that the curves may be fitted to power laws on the form $\Delta t_f \sim F^{-\lambda}$, in particular, for the case with recombination, this yields the exponent $\lambda = 4.4 \pm 0.8$. The exponent estimated earlier for the average lifetime, $\gamma = 4.0 \pm 0.1$, lies well inside this interval. From the model presented in Section 3.2 it was shown that if the microscopic breaking rates were power laws, then both the average lifetime and the corresponding standard deviation would be power laws with the same exponent. One could use this to argue the other way around; i.e. that if the lifetime and standard deviation were power laws, then the microscopic rate must be one. However, the data set is far too limited and the values obtained are too unreliable to conclude this.

6.5.2 Fluctuations in the metastable state

We now inspect the equilibrium state of a bundle under subcritical applied tensile stress, in the case with recombination. In Figure 6.31 a time series from a single bundle showing the number of broken bonds as a function of time, and the related autocorrelation function, is displayed. The approximate exponential distribution suggests diffusive behaviour, indicating that the linear noise approximation may be fair. The deviations from exponential behaviour in the long time limit indicate long-term correlations, that may origin from the slow oscillations of the bundle. However, the data set is too limited to conclude from this.

6.5.3 Without recombination

The computed relative standard deviations in the simulations for which the average behaviour was inspected in Section 6.4 are plotted in figure 6.32. The curves are fairly unpredictable due to the limited data set used, but one gets an impression of the magnitude of the variations from sample to sample. The elongation is seen to deviate significantly in the beginning at large forces, but the estimated deviation is generally below 5 %, with respect to both elongation and broken bonds. The relative deviation in the temperature is seen to lie below 0.5 % seemingly regardless the applied force, except early in the simulations for large tensile loads.

6.6 Further exploration of the parameter space

The present results have until now been based on a finite set of initial states, varying mainly the applied load F. However, a large parameter space could be explored, based on different initial states – by varying the temperature, chain length, bundle size, etc. – a whole range of parameters. We present now a few simulations that does this for two parameters, namely initial temperature and chain length.

Initial temperature

The effect of the initial temperature was studied to some extent by means of single simulations, which can be summarized in Figure 6.33. The initial samples were equilibrated at $T = 0.09$. Compared to the force at which we ran most of our simulations, the bundle at low temperature seems to require much larger forces for the bundle to break down within a reasonable amount of

time. The instantaneous temperature is also seen to increase significantly, and doubles during the course of the initial stretching. Moreover, it is seen that the bundle is almost fully stretched in this case, corresponding to the beads being confined to the bottom of their interaction potentials, and the bundle approaching an FJC bundle. This is consistent with the idea of considering the chain as an entropic spring – at low temperature the spring is weaker.

Chain length

Figure 6.34 summarizes the dependence of the breaking time as a function of chain length. More beads per chain leads to a weaker chain and shorter lifetime, and correspondingly, fewer beads per chain leads to a longer lifetime. This is in agreement with what was discussed towards the end of Chapter 2.

6.7 Connections to materials science

In this section, we explore the ability for the model to reproduce two known properties of viscoelastic media, manifested in single simulations. To this end, we inspect the two rheological phenomena *creep ringing* and *stress relaxation*.

6.7.1 Creep ringing

The decaying oscillation of the elongation after the initial onset of an applied force is not an artifact of the simulation, but a known rheological property of viscoelastic materials. It turns out that this initial stage of the bundle evolution can be modelled in terms of Kelvin–Voigt element [30], i.e. a damped oscillator modeled as a spring and a dashpot serially coupled. Figure 6.35 shows the beginning of a simulation fitted to a damped oscillator model with a linear drift, yielding a well-defined period and exponential decay. Evidently, this stage is fairly predictable. More sophisticated methods of modelling the creep ringing regime is e.g. by means of fractional calculus [26], but this is not inside the scope of this thesis.

6.7.2 Strain-controlled conditions: Stress relaxation

A set of experiments were carried out for states during *strain-controlled conditions*. In this case, the equilibrated bundle is brought to a certain elongation, and the net force it exerts on the plates is kept track of. At time t, the confining potential preventing bonds from breaking is turned off, and the chains start breaking, reducing the stress on the plates. Figure 6.36 shows the fraction of broken chains as the bundle evolves in time, along with the net force the bundle exerts on the plates at each instant of time. It is seen that the fraction of remaining chains decays approximately exponentially, after a short settling regime.

We note that under these conditions, only the *single-chain properties* matter, after the plate separation has been fixed. This is due to the fact that the chains can communicate only through the plates. In this sense, one would – assuming a low rate of recombination – referring to the theory in Section 3.2, expect an exponential decay of the number of intact chains. From this type of experiments, one could thus in principle obtain the probability distribution for the lifetime of single chains under a given strain.

Experimentally, this is known as a stress relaxation test [53]. A common feature of viscoelastic materials is that at constant strain the viscoelastic material will exert a force on the pulling

device, that will decay in time. The measurements of the force 6.36 are in our case fluctuating too much in time for it to tell us anything useful[4]. However, by assuming that each remaining chain contributes with the same average force, only dependent of the strain, we can, by utilizing the fact that they are independently evolving, deduce that the force exerted on the plates is proportional to the number of remaining chains, i.e.

$$F \propto n \sim \exp\left(-t/\tau_1\right), \tag{6.14}$$

where τ_1 is the characteristic lifetime for a single chain. Hence the behaviour of the model is verified also in the case of stress relaxation.

[4]One approach could, however, consist of a time-averaging over many fluctuations.

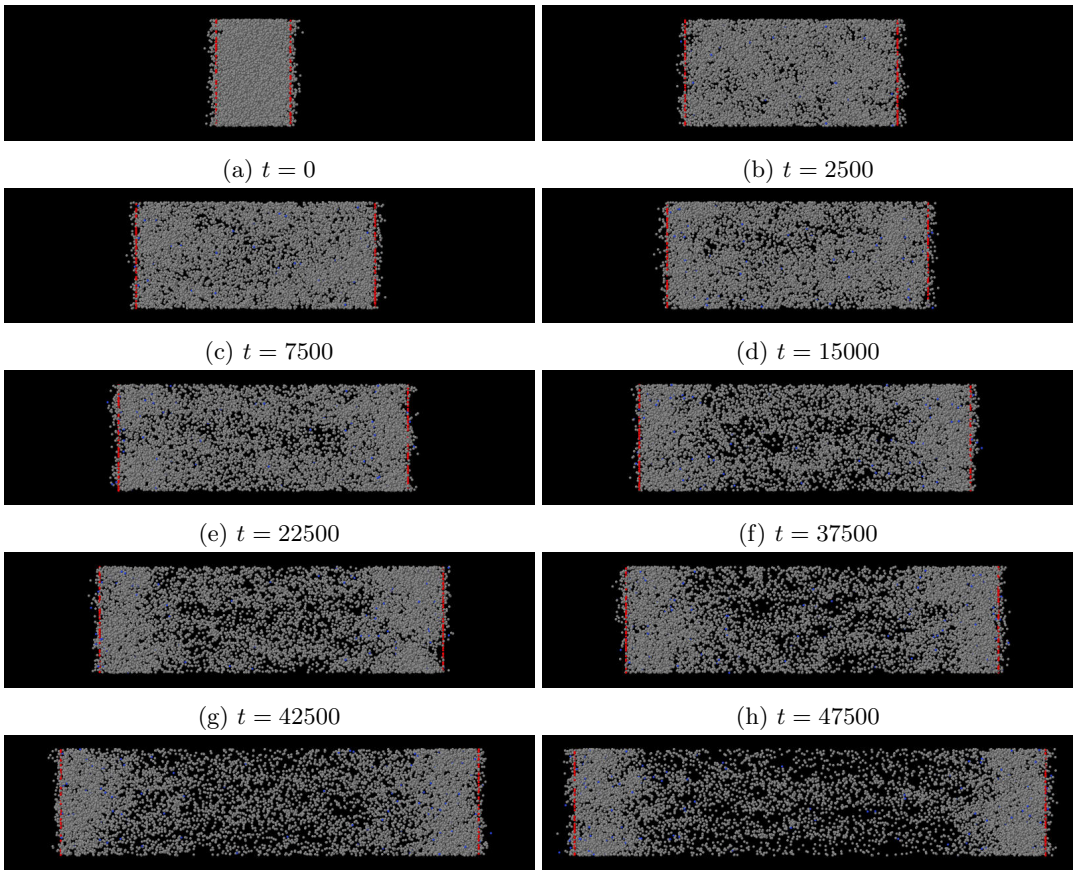

(a) $t = 0$ (b) $t = 2500$

(c) $t = 7500$ (d) $t = 15000$

(e) $t = 22500$ (f) $t = 37500$

(g) $t = 42500$ (h) $t = 47500$

(i) $t = 52500$ (j) $t = 55000$

Figure 6.7: Evolution of a polymer bundle under applied tensile stress, where recombination of broken bonds is allowed. Subfigures (a)–(j) show snapshots of a portion (25% of the chains) of bundle of 400 chains with 100 beads per chain, under a constant applied external force $F = 60$ at different times t. The red beads are endpoints fixed to the confining plates, and the blue beads signify broken bonds. The rest of the regular beads are gray.

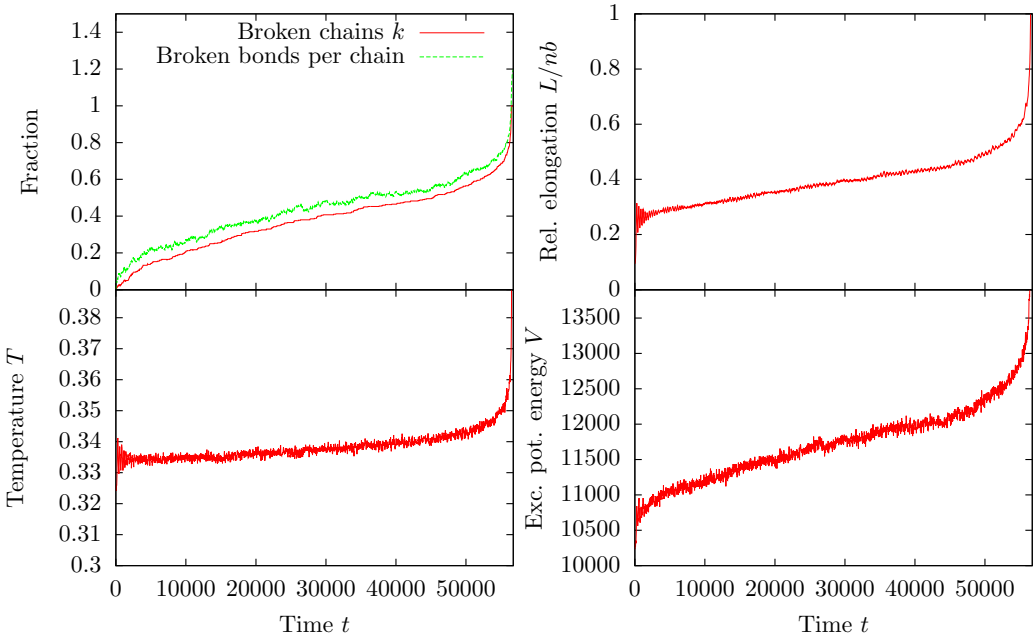

Figure 6.8: Evolution of different observable quantities during a single simulation of a bundle under a constant applied force $F = 60$, where recombination of broken bonds is allowed.

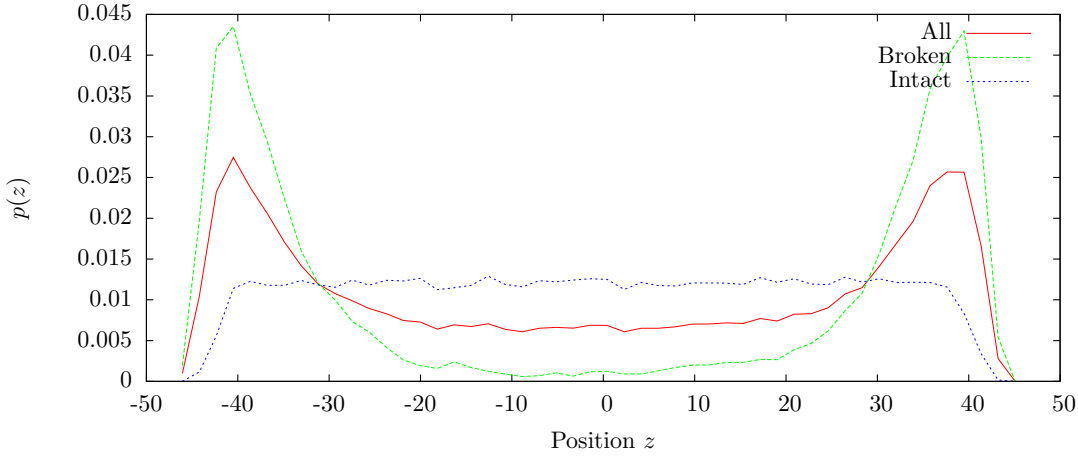

Figure 6.9: Normalized density plot of the positions along the z-axis of beads of a single simulation of a bundle under supercritical stress $F = 90$ at imminent failure. Roughly half of the chains in the bundle are broken. Normalized PDFs of beads corresponding to broken and unbroken chains are compared. All sets have been normalised to 100 %, irrespective of the different number of particles in the set.

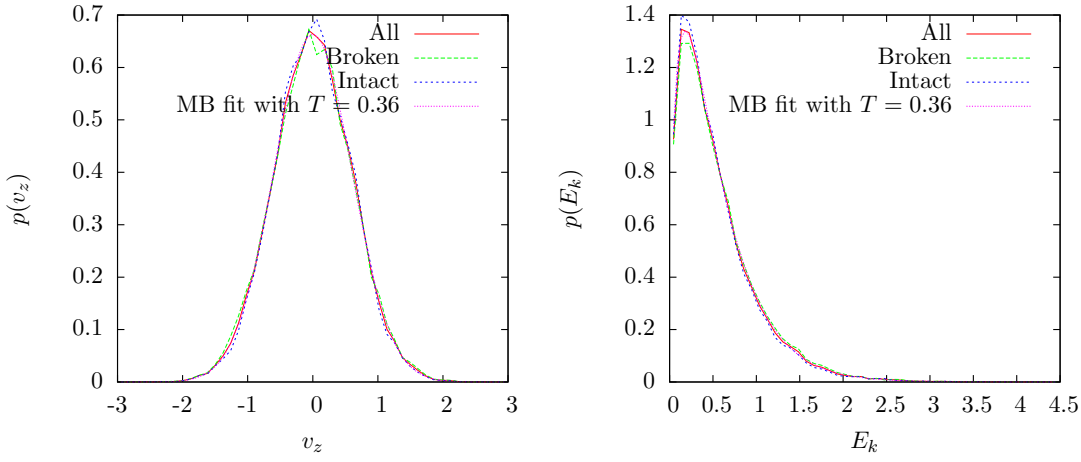

Figure 6.10: Velocity and kinetic energy distribution of single beads of a single simulation of a bundle under supercritical stress $F = 90$, after the bundle has settled towards equilibrium. The distributions are fitted to Maxwell–Boltzmann distributions yielding the temperature $T = 0.36 \pm 0.01$.

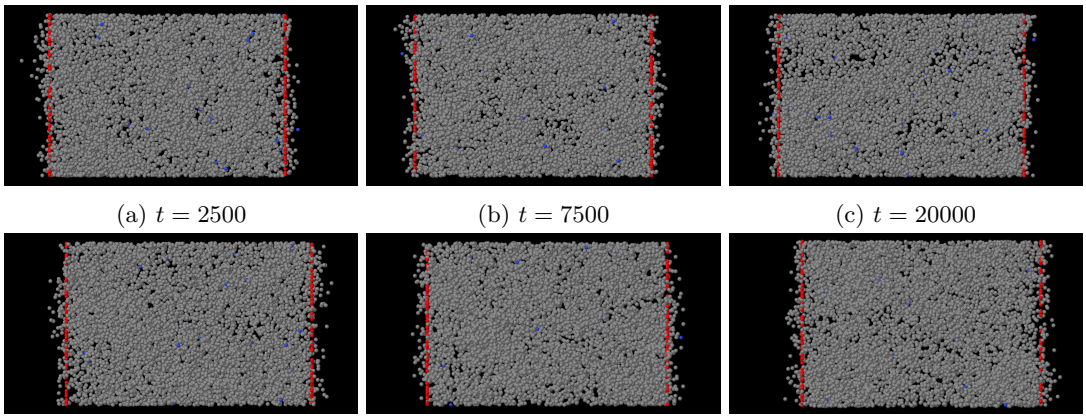

(a) $t = 2500$ (b) $t = 7500$ (c) $t = 20000$

(d) $t = 40000$ (e) $t = 80000$ (f) $t = 180000$

Figure 6.11: Evolution of a polymer bundle under applied tensile stress, where recombination of broken bonds is allowed. Subfigures (a)–(j) show snapshots of a portion (25% of the chains) of bundle of 400 chains with 100 beads per chain, under a constant applied external force $F = 40$ at different times t. The red beads are endpoints fixed to the confining plates, and the blue beads signify broken bonds. The rest of the regular beads are gray. The initial state is the same as in Figure 6.7.

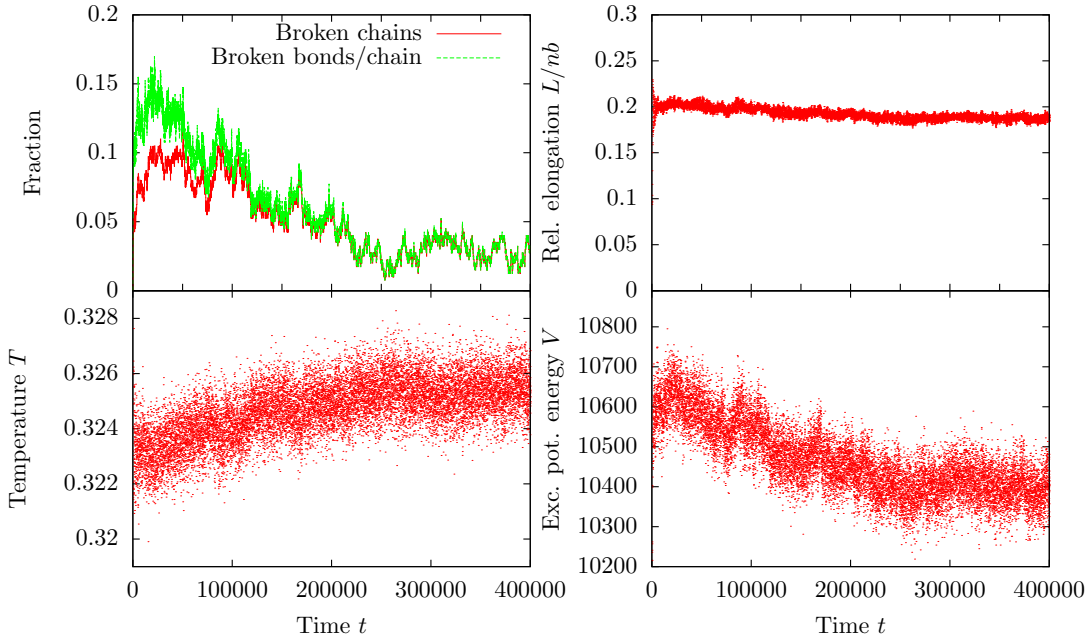

Figure 6.12: Different observable quantities during a single simulation of a polymer bundle under subcritical load.

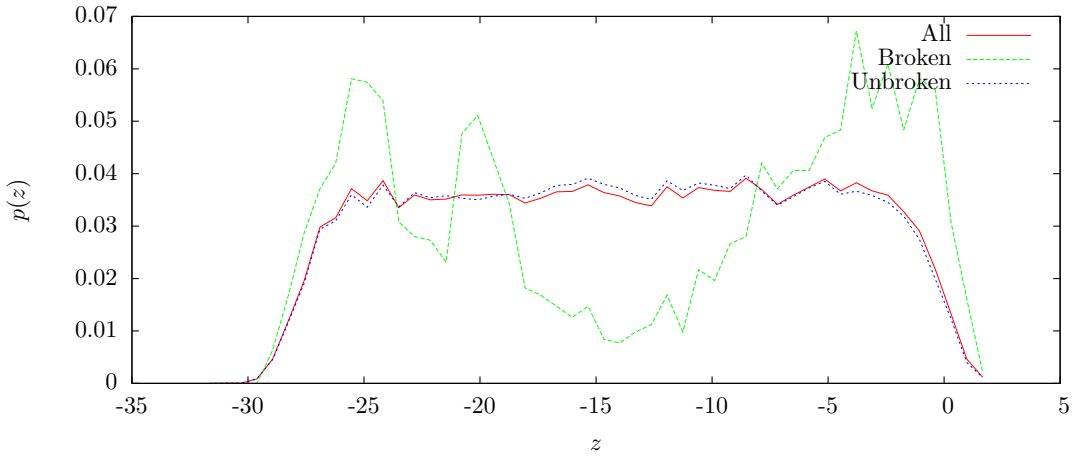

Figure 6.13: Normalized density plot of the positions along the z-axis of beads of a single simulation of a bundle under subcritical stress $F = 40$ after a bundle has started to settle towards equilibrium. Normalized density plots of beads corresponding to broken and unbroken chains are compared.

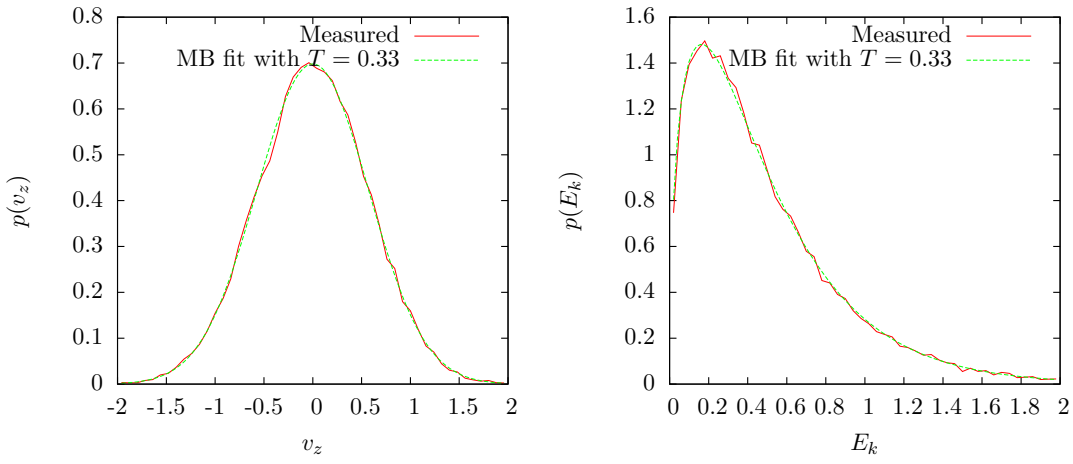

Figure 6.14: Velocity distribution along the z-axis and kinetic energy distribution of single beads of a single simulation of a bundle under precritical stress $F = 40$, after the bundle has settled towards equilibrium. The distributions are fitted (with least squares method, using T as the free parameter) to the Maxwell–Boltzmann distributions for velocity and energy, respectively, which yield the measured temperature $T = 0.33 \pm 0.01$.

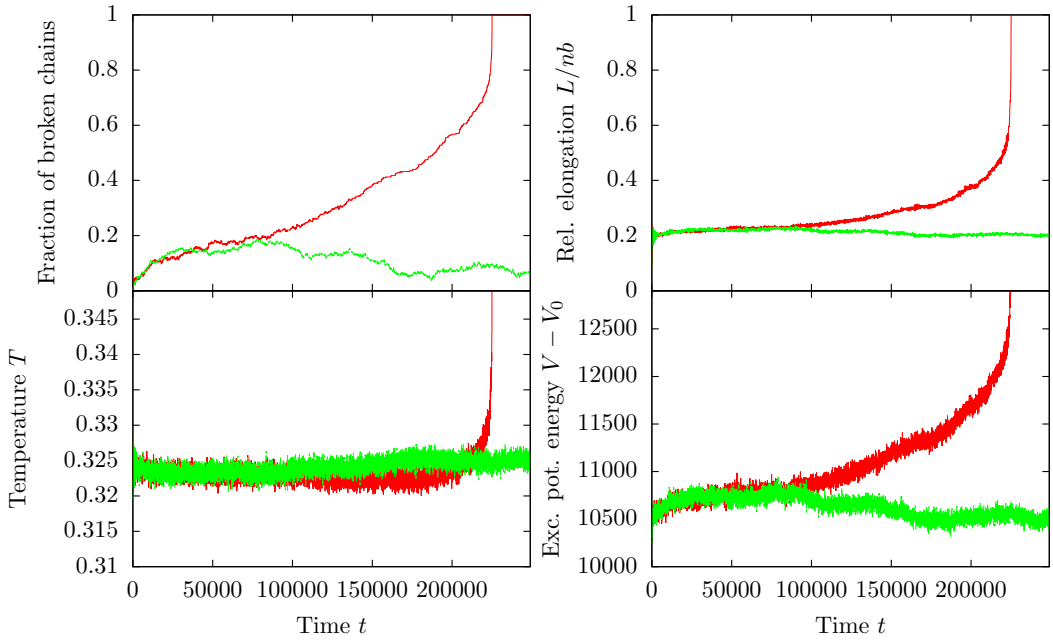

Figure 6.15: Different observable quantities during simulations from two equivalent initial states of a polymer bundle under applied tensile load. One of the bundles reach equilibrium, whilst the other reaches complete breakdown.

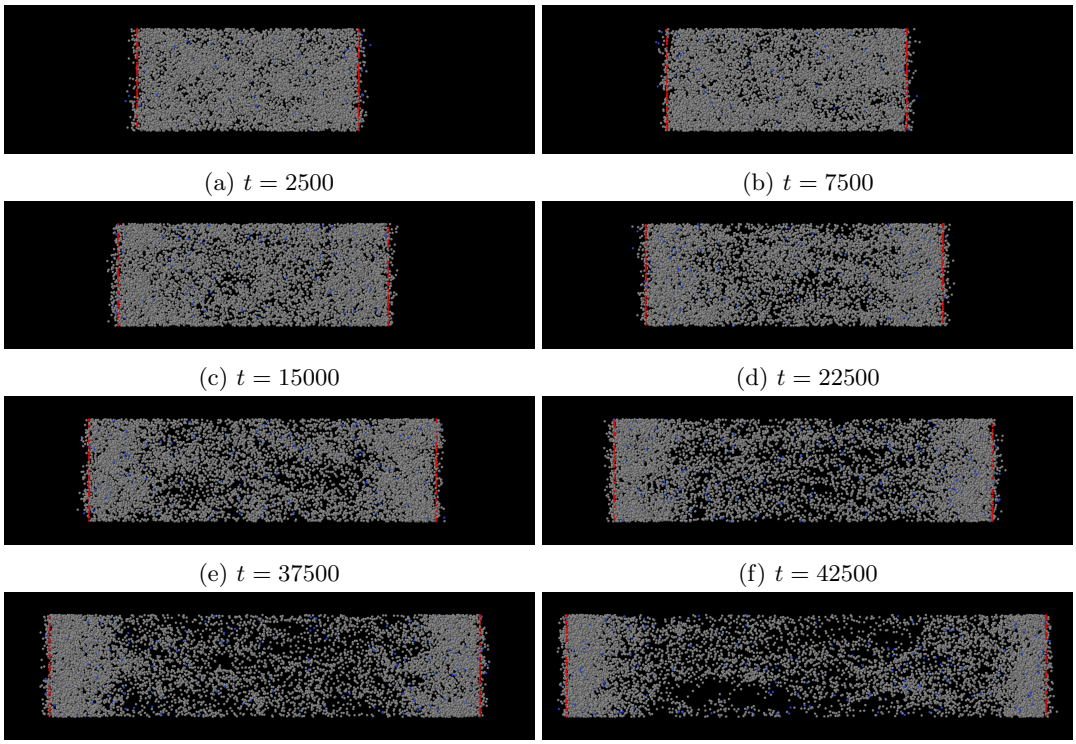

(a) $t = 2500$ (b) $t = 7500$

(c) $t = 15000$ (d) $t = 22500$

(e) $t = 37500$ (f) $t = 42500$

(g) $t = 47500$ (h) $t = 50000$

Figure 6.16: Evolution of a polymer bundle under applied tensile stress, where recombination of broken bonds is disallowed. Subfigures (a)–(h) show snapshots of a portion (25%) of bundle of 400 chains with 100 beads per chain, under a constant applied external force $F = 60$ at different times t. The red beads are endpoints fixed to the confining plates, and the blue beads signify broken bonds. The rest of the regular beads are gray. The initial equilibrated state is the same as in Figure 6.7.

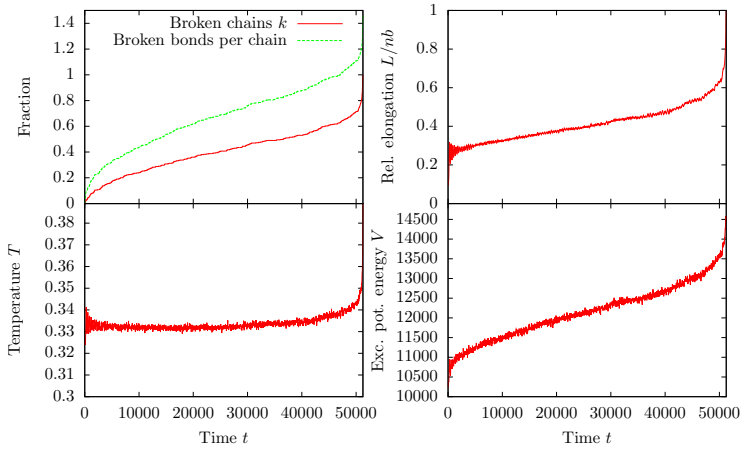

Figure 6.17: Evolution of different observable quantities during a single simulation of a bundle under a constant applied force $F = 60$, where recombination of broken bonds is allowed.

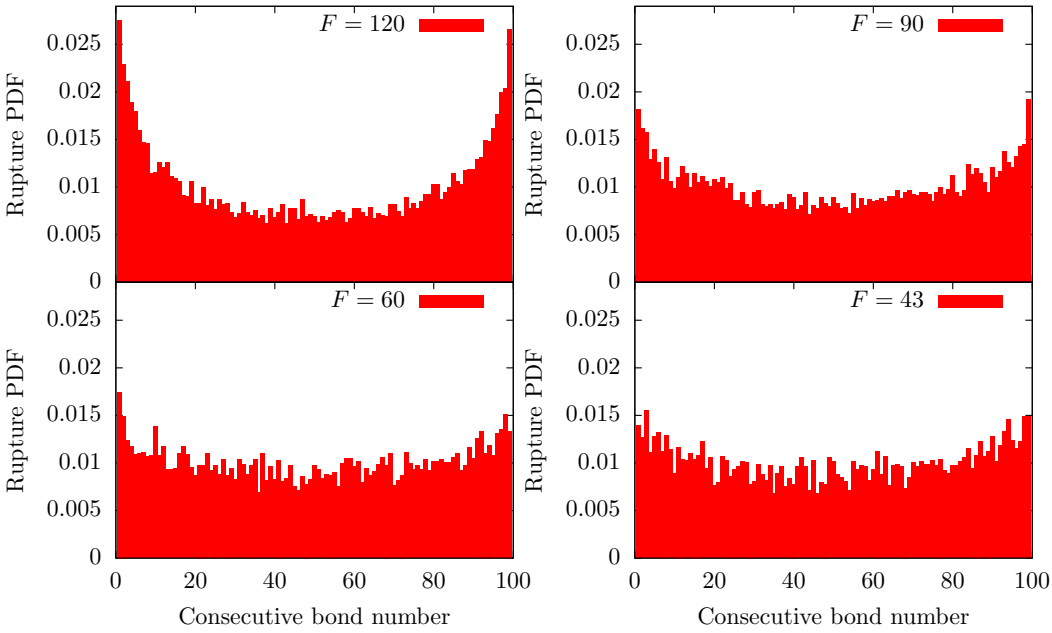

Figure 6.18: Histogram showing the position of bond breakages in chains from a bundle where recombination is allowed.

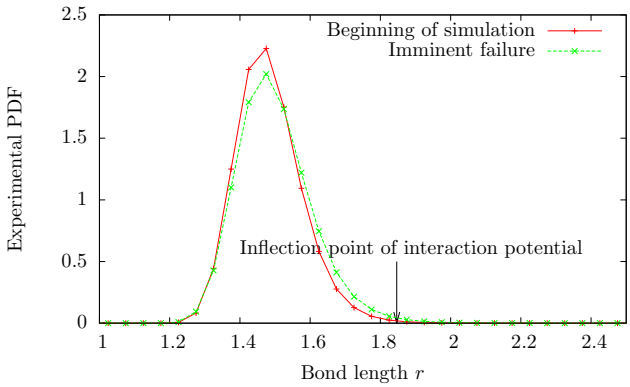

Figure 6.19: Histogram showing the bond length distribution at the beginning and the end of a simulation with applied tensile stress $F = 90$. Recombination is allowed.

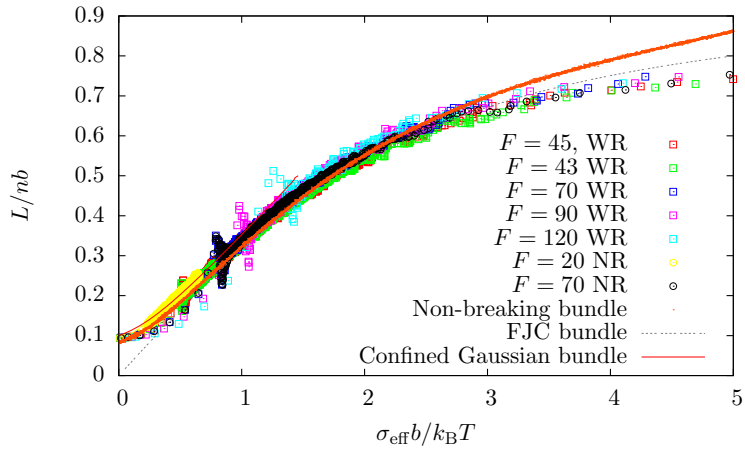

Figure 6.20: Effective stress-strain curve for a range of simulations, for model assumptions both with recombination (WR) and with no recombination (NR). The simulated stress-strain curve for a non-breaking bundle is included for comparison, and so are the theoretical curves for the FJC bundle, and for the confined Gaussian bundle. Note that in order for comparison to theoretical values, the elongation of the bundle has been compensated for the plate displacement due to the onset of force – effectively it is the distance between the first and last *regular* beads that is measured here.

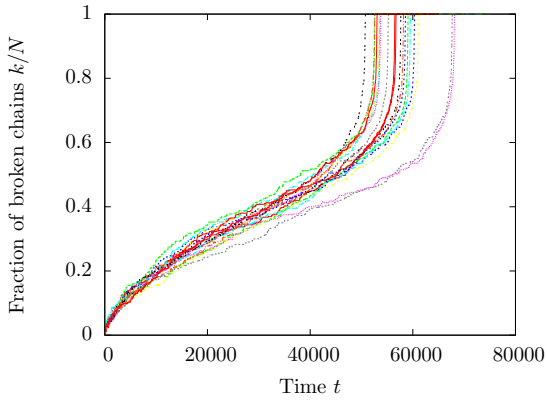

Figure 6.21: The fraction of broken chains as a function of time for an ensemble of 19 realizations.

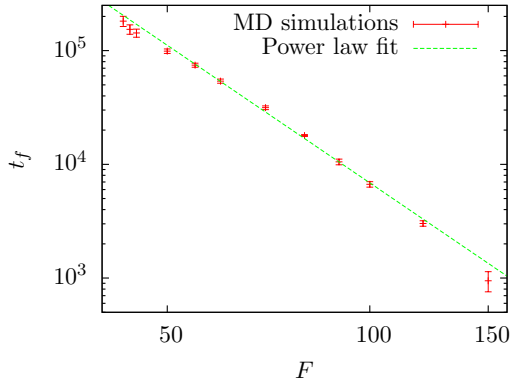

Figure 6.22: The *average lifetime* t_f as a function of applied force F, for a bundle where recombination is allowed. The error bars correspond to the computed variances of the average lifetime. The averages are computed from between 6 and 20 samples for each value of F, and the bundle consists of 400 chains with 100 beads per chain.

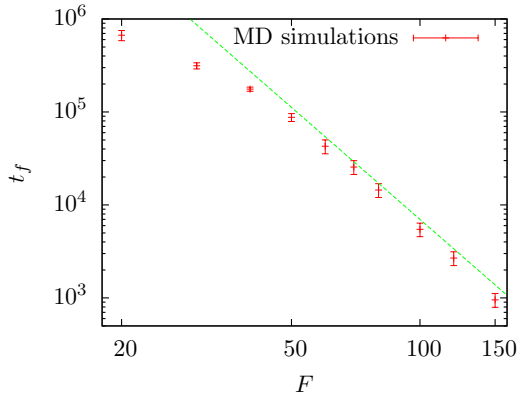

Figure 6.23: The average lifetime t_f as a function of applied force F, for a bundle where recombination of bonds has been disallowed. The error bars correspond to the computed variances of the average lifetime. The averages are computed from between 6 and 20 samples for each force.

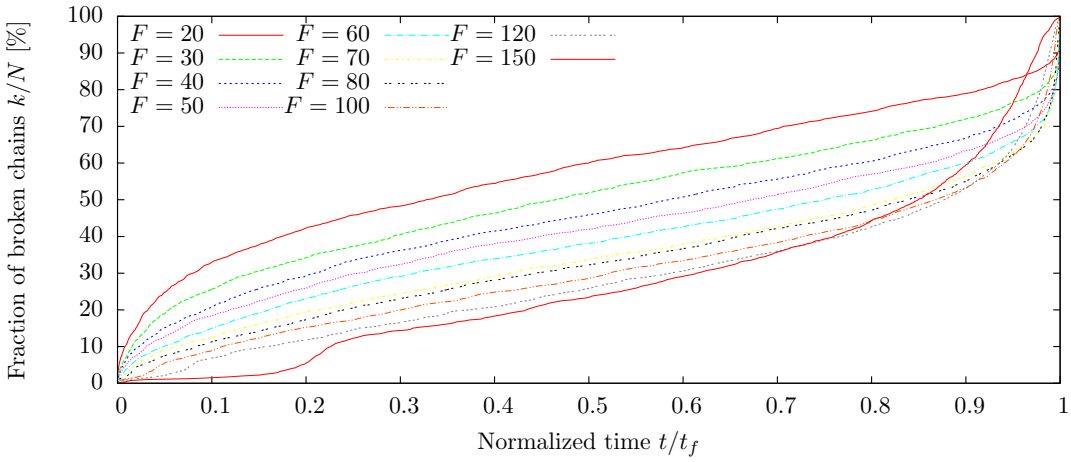

Figure 6.24: Fraction of broken chains as a function of normalized time for a range of applied tensile loads. The trajectories are based on averages over 6 samples per applied load.

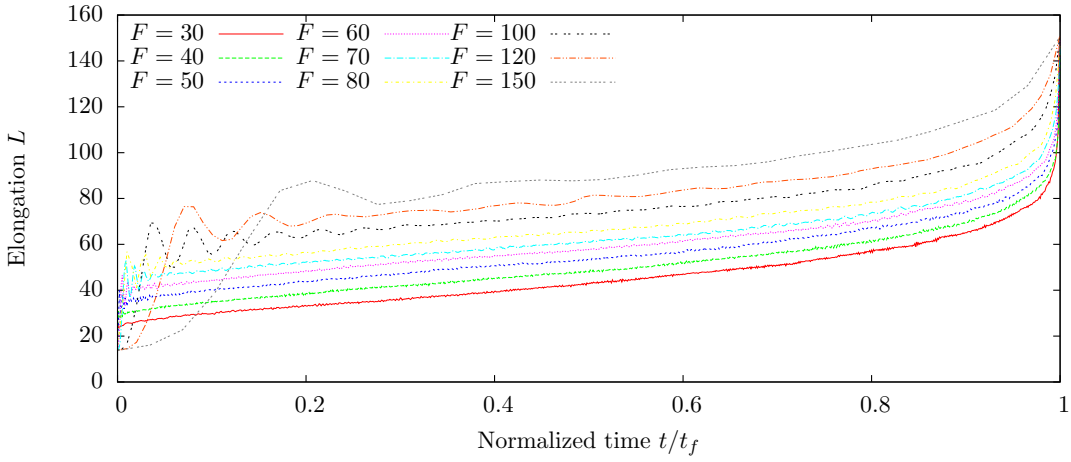

Figure 6.25: Elongation as a function of normalized time for a range of applied tensile loads. The trajectories are based on averages over 6 samples per applied load. Recombination is not allowed.

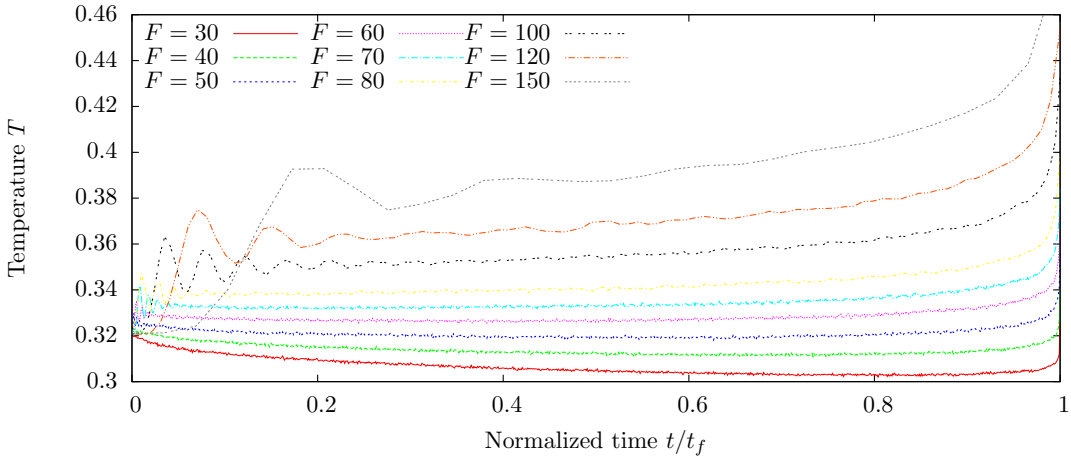

Figure 6.26: Temperature as a function of normalized time for a range of applied tensile loads. The trajectories are based on averages over 6 samples per applied load. Recombination is not allowed.

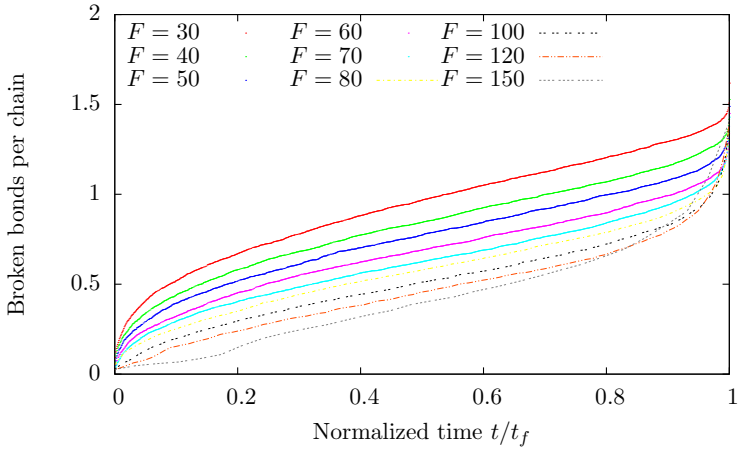

Figure 6.27: Fraction of broken bonds per chain as a function of normalized time for a range of applied tensile loads. The trajectories are based on averages over 6 samples per applied load. Recombination is not allowed.

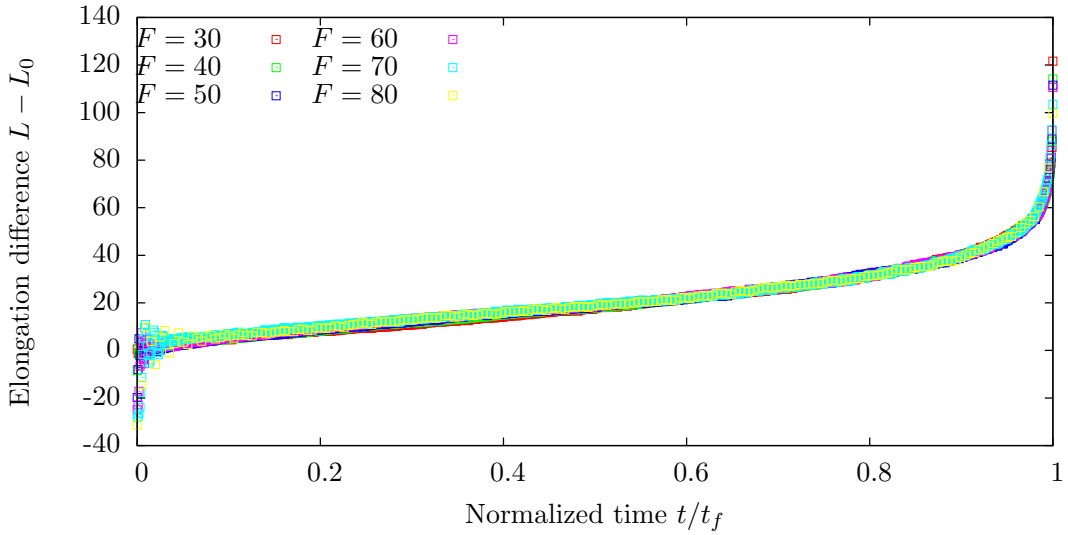

Figure 6.28: Deviation from the elongation as a function of normalized time for a range of applied tensile loads. The trajectories are based on averages over 6 samples per applied load. Recombination is not allowed.

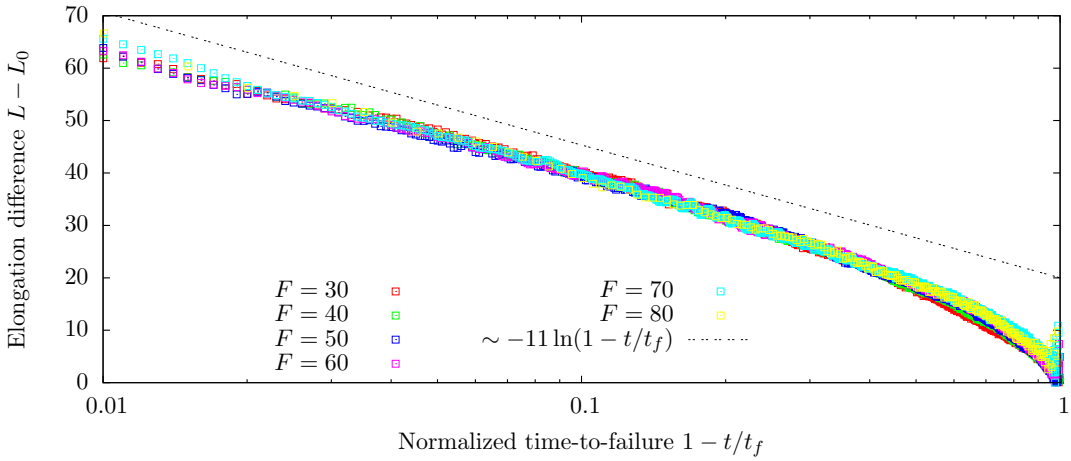

Figure 6.29: Deviation from the elongation as a function of normalized time-to-failure for a range of applied tensile loads. The trajectories are based on averages over 6 samples per applied load, and recombination of broken bonds is not allowed.

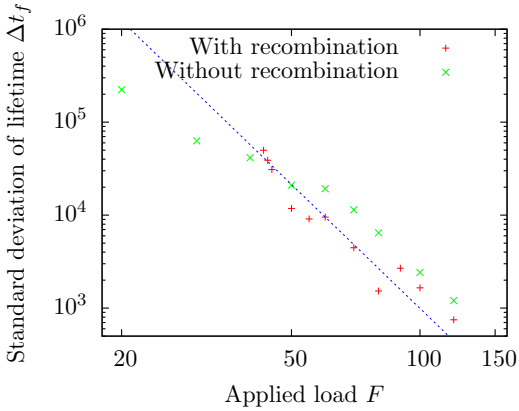

Figure 6.30: The standard deviation of the average lifetime t_f as a function of applied force F, for a bundles both with and without recombination. The averages are computed from between 6 and 20 samples for each value of F. The line corresponds to a power law $\sim F^{-\lambda}$ fitted to the data for the case with recombination, yielding the exponent $\lambda = 4.4 \pm 0.8$.

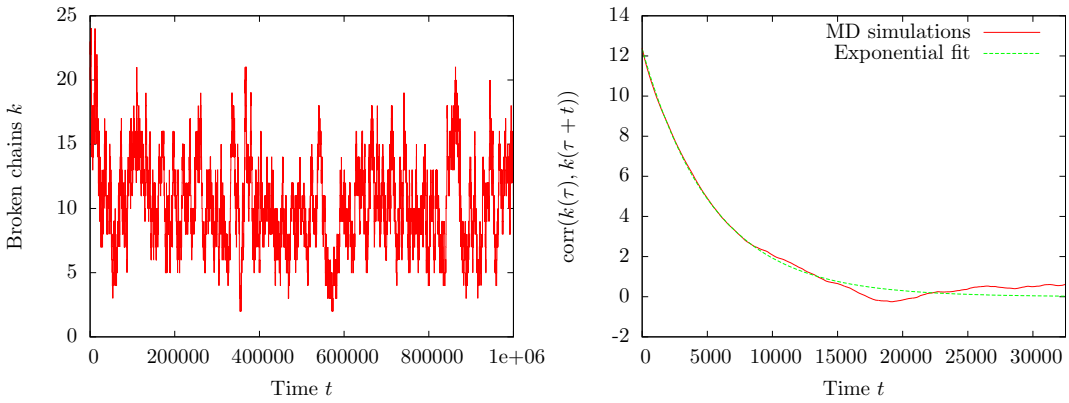

Figure 6.31: Autocorrelation function of the breaking-recombination process of a bundle under subcritical tensile load, after equilibrium is approached (right) and the long time series it was obtained from (left). The correlation function was calculated by assuming ergodicity in the steady state.

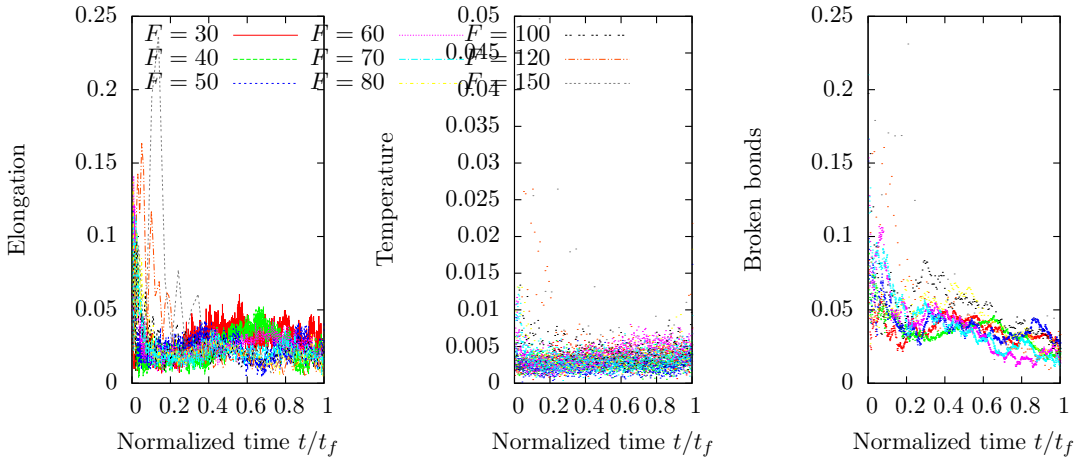

Figure 6.32: The relative standard deviation of the quantities temperature, broken bonds as a function of normalized time. The values are based on 6 samples per force, yielding somewhat unreliable estimates.

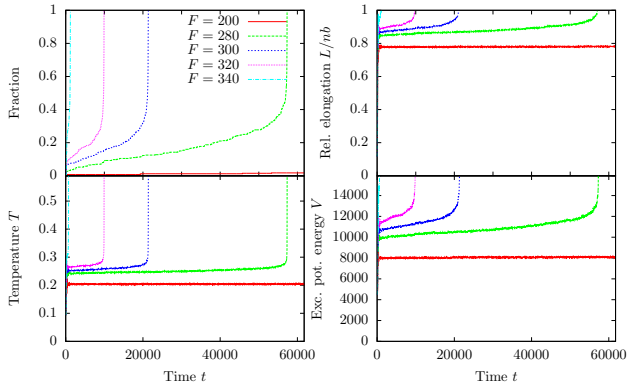

Figure 6.33: Single simulations showing the evolution of the bundle under stress, for initial states equilibrated at $T = 0.09$. Recombination is not allowed.

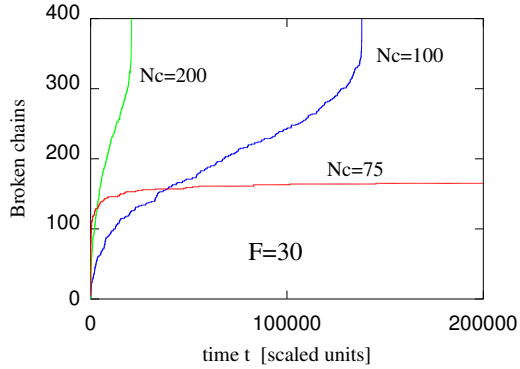

Figure 6.34: The effect of chain length upon the evolution of the bundle. The initial temperature is the same in all cases, and so is the applied tensile force.

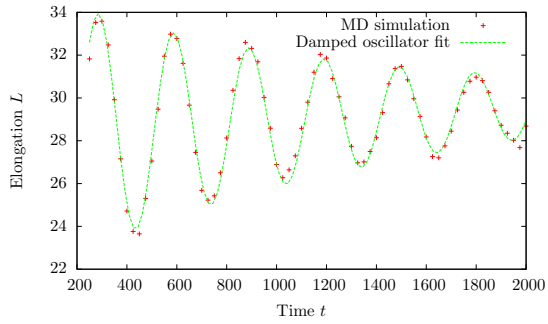

Figure 6.35: The creep ringing regime after soon after a tensile load $F = 40$ is applied.

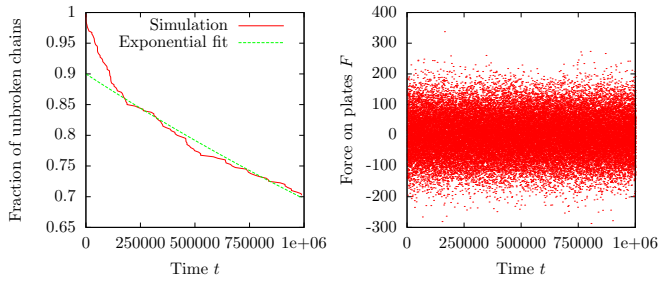

Figure 6.36: Fraction of intact bonds as a function of time t for strain-controlled conditions. The elongation is kept at $L = 100$.

7 Discussion

In this section we discuss and interpret the implications and validity of the results presented in Chapter 6. We follow roughly the same line as in the latter chapter, beginning with equilibrium considerations, discussing the model assumption with recombination, and the model without recombination. We then continue by discussing the validity of the scaling laws obtained, and the relation of the simulation features to the real world. Finally we discuss errors and inaccuracies involved in the present work.

7.1 Equilibrium considerations

It seems obvious that the breaking process described in this thesis is a prototypical example of a non-equilibrium process – at least when the applied force is large enough for the bundle to break within a finite time, or recombination is disallowed. We can regard the bundle as evolving stochastically away from the state where all the chains are uniformly distributed and intact, towards a state where the plates are completely separated from each other. However, in the limit of weak perturbation, i.e. low applied force, when the timescale of breaking the bundle is much larger than the thermal timescale, the process might still be so slow that we can regard the state of the system during most of the time as a perturbation of an equilibrium state, that however slowly evolves in time.

The data collapse demonstrated in Figure 6.5 between the quantities L/L_c and $\sigma_{\text{eff}} b/k_{\text{B}}T$ suggests that this is the case, for parameters in the range we are considering. In the equilibration stage, where no bonds are allowed to break, the equilibrium state is well defined. In this case, the bundle is stretched due to the applied force, and the monomers are thermalized, having statistically speaking the same velocity and kinetic energy distributions[1].

These considerations on the bundle is supported by the numerical investigations of the velocity and energy distributions of the individual beads of the bundle. It is seen that both before and under single simulations, these distributions are fitted by the Maxwell-Boltzmann distribution. From these we could also extract the temperature of each instant in the simulations. The Maxwell-Boltzmann distribution is the correct distribution in both the microcanonical ensemble (in the thermodynamic limit, which may be fair for our system of 40000 particles). Hence, when the mentioned distributions are well fitted, this indicates that the bundle is close to thermal equilibrium.

At equilibrium, in addition to velocity and energy, the positions of the beads should be distributed as at equilibrium. This is manifested through a measured stress-strain curve, which can be compared to theoretical expressions. By comparing the effective stress-strain curve of the bundles that are allowed to break chains, we observed in Section 6.1 that the curves fall on top of each other independently of the initial applied stress. This data collapse in the secondary regime indicates two major effects.

Firstly, it indicates that the mean-field estimate of the effective stress per chain is a fair approximation – the arithmetic average of the stress accounts for the entire evolution of the

[1] Disregarding the endpoints, which have effectively one less degree of freedom due to the confinement to the plates

bundle. This means that the fluctuations in the stress on the individual chains do not give rise to an unexpected evolution of the elongation of the bundle. Additionally, it implies that the presence of broken chains does not exert a large force on the confining plates in the stretch range considered – effectively eliminating the number of broken chains as a relevant variable in the equations, as long as the effective stress is introduced.

Secondly, the predictability of the strain as a function of applied effective stress suggests that the major part of the evolution happens close to an equilibrium state of the bundle. Herein, the remaining chains carry their share of the total load, and are close to their equilibrium length under this load. The breaking events are due to the stochastic fluctuations in the system, and rare compared to the thermal timescale and the timescale for load redistribution, and when a fair amount of chains are intact. A single breakage results in a small perturbation in the effective stress. Hence, the bundle has time to reach the local equilibrium distribution normally before another chain breaks.

7.2 The phase transition

The transition (or bifurcation) which was observed for the bundle with recombination, including the classification of sub- and supercritical loading, can be understood, at least qualitatively, in the context of the one-step model proposed in Section 3.2. However, the assumption of independent breaking events may be a spurious one, especially in the primary regime, where the system is out of equilibrium and the bundle undergoes excessive breaking. In the sense that it assumes independent breaking events, this model does not account for avalanches. However, when breakings are rare and the system is stable – e.g. in the metastable state during subcritical loading, it may be valid.

In the model, another fixed point is present at a lower fraction of intact fibers. This is an unstable fixed point, and constitutes the edge of the basin of attraction of the stable fixed point. This can be interpreted as a barrier – if the remaining fraction of fibers surpasses this barrier, the bundle evolves towards ultimate breakdown.

In the macroscopic model, the bundle will deterministically approach either complete breakdown or equilibrium, depending on which side of the unstable fixed point we start. However, due to the stochasticity involved – due to the finite size of the bundle – the bundle may "diffuse" over this barrier within a finite time. This means that the bundle will break down within a finite time even below the macroscopic "critical" force – which is the value of the force where the two fixed points overlap – the bifurcation point.

Moreover, during the initial stage the model is not directly applicable due to the fluctuations in the system – and the non-equilibrium behaviour. This is seen because the breaking rate actually decreases – the system is perturbed, and if the perturbation is large enough, the system is pushed over the barrier and evolves towards complete failure.

7.3 Breaking regimes

We now discuss and interpret the breaking regimes. To sum up the observations presented in section 6.4 for this case, the process can be divided into three distinct regimes:

1. Primary regime. This regime is characterized by a high breaking rate, which decays to an approximately constant rate. In this regime, the curve displaying broken chains as a

function of time is reminiscent of the *work-hardening* regime typical of creep processes. In this model, this observation corresponds to the fact that the chains when in the coiled-up configurations are more likely to break, and as they are more stretched, they are more able to withstand the force, becoming less likely to break. This is still the most mysterious regime.

2. Secondary regime. This regime is characterized by a low, seemingly constant breaking rate and strain rate. We argued that the bundle in this regime is close to thermal equilibrium.

3. Tertiary regime. This regime is characterized by a quickly increasing breaking rate and strain rate, leading ultimately to complete breakdown of the bundle.

In the following we interpret these characteristic regimes in terms of the mechanisms at work.

7.3.1 Interpretation of the breaking process

During the process of describing the failure of the bundle, we have identified four distinct important parameters that may change throughout the breaking process of the bundle under applied stress:

- Applied force. The initial tensile load that we initially apply to the bundle.
- Temperature. Although not unambiguosly defined in a system out of equilibrium or without thermal coupling, the instantaneous temperature tells us how much kinetic energy that is contained in the system, i.e. the magnitude of the microscopic fluctuations.
- Broken chains – or equivalently, the number of intact bonds. The former determines the mean load sharing, and the latter leads to dissipated energy.
- Elongation.

The data collapse shown in Figure 6.5 suggests the existence of an equation of state (which has not been identified, only approximated) relating these quantities to each other. In this sense, the bundle may be seen as mainly dependent on three quantities, which we may choose without loss of generality.

In the case of adiabatic stretching, starting out with equivalent initial states, the average evolution of the bundle is only dependent on the applied force, as in principle all the external factors are otherwise incorporated in the model and hence regarded as constant. However, the quantities above controlling the breaking process are changing in time. Considering chains in a state close to equilibrium, as was justified in the previous section, the relevant quantities are temperature, applied effective stress and number remaining intact chains. Considering the variables isolated, they affect the breaking rate as follows: An increased temperature increases the breaking rate, due to more fluctuations in the system. A high number of intact chains is associated with a higher probability of one of them breaking, simply due to more chains being available. An increased effective stress is also associated with higher breaking rate, as it lowers the effective energy barrier associated with the two-particle Kramers approach.

By considering now the evolution of these three quantities during a stretching-breaking process, we attempt to describe the energetic mechanisms behind the three regimes of supercritical loading under isolated conditions.

When a single chain snaps, the following changes to the system occur, for simplicity considered sequentially:

1. The number of remaining intact chains is reduced.
2. Energy is dissipated from the system into the broken bond, lowering the temperature.
3. The force is redistributed democratically on the remaining chains, yielding a new effective stress σ_{eff}.
4. The bundle is stretched adiabatically to the new length given by σ_{eff}, transferring energy to the system – increasing the temperature.

The first point has the effect that the breaking rate is reduced. This is so also for the second one. The third has the effect of increasing the breaking rate, and so has the fourth point.

This first effect may be particularly present in the initial stage of the process. At this stage there are many chains in the bundle, and the applied load per chain is low. Thus one would expect an exponential-like decay of the number of chains in the bundle.

However, as chains break the temperature is altered according to the balance between the dissipated energy per breaking, and the energy received upon small stretching. If the former is larger, the number of intact beads must decay slower than exponentially. However, as more an more chains break, the length of stretching per breaking increases, and so does the transferred energy. Simultaneously the effect of applied effective stress starts to influence and the breaking rate increases.

In the primary regime, i.e. at a high number of chains and a low effective applied stress, the former two effects dominate, leading to a decaying breaking rate. In the tertiary regime, the latter two effects dominate, i.e. at high effective applied stress and low number of chains. The intermediate region – the secondary regime of linear breaking can thus be interpreted as a transient regime, i.e. a crossover between the two extremes.

Qualitatively this is in agreement with [32], where the secondary regime of the stretching of a protein gel was attributed to the crossover between reversible stretching and microscopic crack growth. The equal-load sharing nature of the present molecular model can not directly account for local effects such as microscopic crack growth, but we still may interpret the regimes as due to two distinct mechanisms, each dominating at individual points in time, and the crossover between them.

Note that this is merely a sketch of an interpretation of the process. We are not expecting these considerations to account for the entire breaking process. The presence of oscillations in the beginning of the process may be crucial for the breaking, and should be further studied. The presence of unstable modes has been addressed in the literature [14], and the initial breaking may suppress these modes, leading to a lower breaking rate. To draw conclusions, more intensive experimental studies must be carried out.

7.4 Power law behaviour, scaling, and hints to universality

In Chapter 6, a few power laws were identified. First, in Subsection 6.4.2, we found the relation between the lifetime and the applied force to be a power law of the form

$$t_f \sim F^{-\gamma}, \quad \gamma = 4.0 \pm 0.1. \tag{7.1}$$

This relation, as is displayed in Figure 6.22, is reminiscent of the Basquin law of fatigue found for a range of materials under cyclic loading [29], recently also for a protein gel [32] comparable to the model system we are studying. However, the validity of the relation found may be limited.

Fitting a power law is a not a straightforward procedure [7], as a range of functions may be linear in a log–log plot over short ranges. In this case, the power-law behaviour was found over roughly half a decade, due to limitations in investigating loads of both larger (due to the onset time of the force) and lower (due to the bundle settling in a metastable state) magnitude. In this respect it must be said not to be a *robust* power law, at least not at the present stage. Moreover, the error bars provided by the least squares fit may be artificially low. The exponent found is, however, comparable to the one found in for the protein gel [32], which was found to be 5.45 ± 0.05 over roughly one decade.

Similarly as above, the same behaviour was observed in Subsection 6.4.3 for the model without recombination, shown in Figure 6.23. The simulations were still limited in the large F limit, but unlimited at low F, other than by the available computer resources. The exponent found in this case was in agreement with the value for γ in the assumption of allowing recombination over the same range as the latter was found. At lower forces, however, the lifetime as a function of applied load deviates from the curve, indicating a crossover to a lower exponent – or another functional dependence. This crossover is physically easy to acknowledge, as the lifetime if it was a power law would diverge, $t_f \to \infty$ as $F \to 0$. This would be unphysical, since a bundle where recombination is disallowed would eventually break down in a finite time due to thermal fluctuations – even in the absence of an applied load.

Furthermore, by inspecting Figure 6.30, the estimated standard deviations weakly resemble power law behaviour with exponents in the same range. However, these estimated standard deviations are not sufficiently robust at the present stage. With many more simulations, it would be interesting to see of such a behaviour is found, especially in the context of the simple model suggested in Section 3.2.

Finally, the remarkable data collapse for the elongation difference vs. normalized time seen in Figure 6.28 hints to universality in the creep process. This is a feature seen experimentally, e.g. in the protein gel experiment [32]. Moreover, the exponent found for the strain rate, i.e.

$$\dot{L} \sim \tau_{\mathrm{ttf}}^{-1}, \tag{7.2}$$

is consistent with experimental results for the shear rate $\dot{\Gamma}$ in the same article [32]. The logarithmic fit it holds valid over roughly one and a half decade, and it may thus be the most robust power law we have found. However, a source of error is related to the way the averaging procedure is applied in order to obtain the trajectories involved – we applied it because it was the simplest one. Spefically, this has experiment has to be repeated for larger systems in order to ensure its validity.

7.5 Relation to real systems

The model undoubtedly shows a great potential. Despite its complexity, it is extremely rich, reproducing many of the properties experimentally seen, e.g. creep ringing, stress relaxation, work hardening, steady creep, and tertiary creep. In addition to reproducing realistic behaviour, it is clear that this model provides a wealth of information regarding the microscopic conditions of such systems, which are virtually impossible to obtain in laboratory experiments. This concerns e.g. stress on individual bonds, chain elongation, etc., and illustrates the potential in the approach. In this thesis we have only reported on a few of these.

7.6 Errors and inaccuracies

There are several sources of errors and inaccuracies in the present work. Throughout the thesis, we have briefly discussed some of them, but in this section we do this more thoroughly.

The model

The molecular model we have proposed and adopted in molecular dynamics simulations is, as discussed, a significantly idealized model for a polymer bundle. The idealizations can be summed up as follows:

- Classical particles. We consider a coarse-grained system where the beads (monomers) interact classically through two-particle interaction potentials. This is a valid approximation as long as long as we consider particles that have sufficiently large mass [13].
- Only nearest-neighbour interaction. The monomers interact only with their nearest neighbours in the chain. They presence of all other monomers are felt only through these neighbours, and the plates. We argued that the physical situation this corresponds to was the theta point (ref. Section 2.8).
- Thermal insulation. The simulations carried out for a system which was thermally insulated, i.e. unable to transport heat out of the system. This means that the numerical simulations correspond to an experimental set-up in vacuum or at a very short timescale.
- Finite system size. This is a necessity due to numerical considerations. The system is thus both coarse grained and small compared to most real polymeric systems.
- Parameter tuning. The parameters involved in the model – that can not be retrieved through scaling – have been set in a way that does not actually correspond to a real physical system, but rather in a slightly heuristic manner so that *something happens* during the time of computation. This is related to the finite size of the system. Expectingly, chains of thousands of beads will break significantly easier at the same temperature as chains of a hundred beads.
- Recombination of broken bonds. The bonds that were broken were in a major part of the simulations allowed to recombine. The physical validity of this is not clear, as one would expect broken ends to rather recombine with particles in the surrounding fluid, rather than with itself. Thus, simulations were carried out for the case where such bonds were disallowed to reform. Moreover, in the model, the broken chains were only allowed to recombine with themselves, and not with other broken bonds. This is certainly not physically admissible, but was compensated by the addition of periodic boundary conditions, effectively introducing a characteristic distance between interacting chains. However, in the case of isovolumetric stretching [50], this does not provide the correct physics.

The combination of the messages in these points suggests that the actual physical systems the model may correspond to are limited. We may argue that the system may, given the correct scales, correspond physically to a fairly small system of fairly short polymers at the theta point under a small perturbation load, during a short time window. However, it is to be regarded as a coarse-grained model [1], and moreover, it is important, as it is a genuine, obvious model to investigate as a first approach to describing more realistic feature-rich models of polymeric

systems under tension. We point out, however, that simulations have been introduced primarily to interpret and understand the results of the FBM, and therefore a relevant comparison is also with the conditions underlying this model, that to some extent could be changed to match the simulation conditions.

Additionally, by studying such a finite-sized idealized system, much insight into the underlying physical processes may be gained, as it allows us to inspect the detailed microscopic mechanisms involved, such as the actual bond breaking events, monitoring at all times the number of broken bonds, the bead distribution, the force distribution etc. Such microscopic inspections are hard generally hard to do in experimental settings, due to the short timescales and small spatial scales involved. Moreover, many features of such complex systems are often independent of the details of the model. Hence, it is natural to inspect a model with as few details as possible in the search for universal behaviour. For example, the Basquin law-like behaviour we observed with a specific initial state may be an example of such behaviour, but we stress again that further simulations are required to conclude.

On other accounts, it should be noted that the finite system limits us to inspect important details of the system predicted by the model proposed in , such as the slowing down at the identified bifurcation.

The method

We have briefly discussed some of the problems or ambiguities associated with the method earlier in the thesis. As in the previous section, we sum it up hereby, and discuss it thoroughly.

- Molecular dynamics. The very definition of molecular dynamics is to solve Newton's equations of motion by means of numerical integration, and this is guaranteed to accumulate errors. Employing molecular dynamics therefore relies largely on belief. However, significant numerical evidence indicates that molecular dynamics actually works – even in non-equilibrium settings – and we consider this to be the least of our problems. Actually, the exponentially diverging trajectories associated with such simulations might actually not be a disadvantage at all, as it is the statistical properties of the stretching-breaking process we are seeking.

- Computational complexity and time consumption of the simulations. The velocity Verlet algorithm is fast, but still requires a lot of time to run a single simulation on moderately fast computers, especially when the breaking rate is low. The model was chosen to be simple as possible for this reason – for each particle in the model only one force evaluation is needed. However, for long simulations the code should be genuinely parallelized.

- Amount of data. Due to the above point, a large amount of time was required in order to run simulations. Statistical robustness would require a large amount of simulations to be run, and as we were limited in both computational resources and time, the amount of data in the final simulations were limited. This also concerns the exploration of the parameter space, where the limited amount of simulations would yield only a qualitative grasp of the effect of the parameters.

- Statistical methods. The averaging procedures we have employed are simple, and may be too crude to properly describe the process. However, they are natural as a first step as the amount of data is limited. For further development, extreme-order statistics [23] could be employed for a more extensive analysis of the breaking process.

Hence, to sum up, most of the errors and inaccuracies in the method relies on the fact that molecular dynamics simulations are time-consuming. With a reduction of the single-simulation runtime, the final amount of data would have been larger, yielding more statistically robust results.

8 Concluding remarks

The motivation for this thesis has been the need to bridge the gap between the macroscopic and microscopic scales of our understanding of fracture in polymeric materials. The former is manifested in the fiber bundle model – a top-down approach – and the latter is represented by the particle description of materials – a bottom-up approach. In this thesis, we have introduced a molecular model of an idealized polymeric bundle, that effectively allows us to relate these scales by solving Newton's equations of motion on the particle level. By means of molecular dynamics simulations, we have explored the model and specifically investigated the effect of applying a constant load, stretching and breaking the bundle.

Despite its simplicity, the proposed model suffices to capture many of the characteristic features that are associated with polymeric materials under tensile stress. This encompasses, e.g., a multistage creep, creep ringing and stress relaxation. At the same time, at variance from real-life experiments, the simulations gives us a wealth of information about the system at the most microscopic level, since it gives us position and velocity of every individual particle. This abundance of information might become a difficulty in itself, and, because of the complexity involved, we have had to identify the important parameters for the evolution of the system.

Our results suggest that the system evolves in a near-equilibrium state during almost the entire stretching and breaking process. This is reflected through an identified *effective stress–strain* curve, where the individual simulations, parametrized by time, are seen to evolve along the same trajectory in the space spanned by the elongation and the *effective stress* scaled by the instantaneous temperature. The preliminary analysis presented in the thesis thus suggests that the universality observed in our simulations reflects a condition of near-equilibrium in the simulated samples during the long creep stage leading to the final breakdown.

Two different varieties of the same basic model have been considered, one allowing and the other disallowing recombination of broken bonds. For sufficiently low forces, the former model was seen to undergo a phase transition, for which below a critical force F_c the bundle was seen to stabilize, rather than completely break. Above this threshold, the bundle proceeded to complete failure.

The simulations carried out for the model with recombination indicate a power-law dependence for the lifetime t_f upon the applied force, $t_f \sim F^{-\gamma}$, $\gamma = 4 \pm 0.1$. This is reminiscent of the Basquin law of fatigue [5] known for a range of materials, recently also for a protein gel [32]. In the latter, a the corresponding exponent was estimated to 5.45 ± 0.5, which is not too far from our results. However, our measurements were taken over only roughly half a decade in the force F, and is thus not robust at the present stage. Moreover, strictly speaking, Basquin law concerns cyclic loading, while our simulations considered only (nearly) static loading.

In the model without recombination, the average elongation difference as a function of *normalized time* was, for a range of forces, observed to be independent of the applied force. This remarkable data collapse is in agreement with recent experimental results concerning the creep and failure process of a similar system [32]. The strain rate (elongation per time) was found to grow as $\dot{L} \sim \tau_{\mathrm{ttf}}^{-1}$, where τ_{ttf} is the normalized time-to-failure, in the regime of imminent failure. This is in excellent agreement with recent experimental findings for a protein gel [32], where the *shear rate* was found to follow the same relation.

On the theoretical side, approaches were made to understand the breaking process of a

bundle of polymers. In particular, we proposed a simple continuous-time fiber bundle model, viewing the breaking of individual fibres as a one-step Markovian process, that could account for the bundle failing. The model may serve to explain the suggested phase transition that was observed for the simulation model that allowed for recombination. Moreover, we have inspected simple models for polymers in order to understand their behaviour under tensile stress.

The limitations of the results presented in this thesis are mainly related to two things: Time and computational resources. Molecular dynamics simulations are computationally demanding processes, which require millions of timesteps and perhaps billions of force evaluations, only for a single choice of the starting configuration and simulation conditions. Since a large number of simulations are required in order to provide reliable statistics – preferably for a large number of different physical conditions – this requires an increasingly vast amount of processor time. Moreover, in order to check the validity of the scaling laws – and the behaviour of the exponents found – more of the parameter space should be explored.

However, despite these limitations, we are content with the results provided by the simulations, primarily because this constitutes an important and promising first step towards a thorough understanding of the physics connecting the microscopic mechanisms to the macroscopic framework of failure processes of polymeric materials. This study provides a sound basis for extending the present investigations to a much larger scale, addressing a range of problems concerning scaling relations, universality and fluctuations in the FBM and in variants of the basic model. In particular, it provides a first anticipation of the results to be expected, as well as a preliminary assessment of the role of different model and simulation parameters. More importantly, the results allow us to estimate the effort required for the quantitative validation of the FBM relations and scaling exponents, that represents essential information to plan for the next upgraded stage of the present study.

A manuscript is in preparation based on the results, focusing on the relation with the experimental data for the fracture of protein gels [32].

8.1 Future prospects

The results presented in this thesis illustrates the potential in the model, and in general, the potential in connecting the microscopic description of failure processes of polymeric materials to the macroscopic framework provided by fiber bundle models. The work involved in the current thesis may be considered as a first step towards a larger research project aiming to unify the two spatial scales of failure processes. In the following, we propose an outline for such a research project.

Firstly, general simulations should be carried out using a system coupled to a thermal bath, preferably by a Langevin-type thermostat, as this has proven effective in similar settings [39]. The coupling strength could be varied (where to zero coupling limit agrees with our adiabatic simulations), to inspect the effect of thermalization on the breaking process. Simulations would then more closely resemble real-life and experimental settings, as heat may be dissipated, and the mathematical formalism from the canonical ensemble could be employed with validity.

As a first step in a thorough research project, quantitative measurements of single-chain polymers should be carried out. In this context, the most interesting property would be to inspect the lifetime as a function of temperature and applied force, or, in a strain-controlled setting, as a function of imposed strain. This has been done for similar systems [39], and would *in retrospect* seem as a natural starting point also for the work in this thesis. The result of this

would be a better prediction of the breaking rate, which again could be used to determine the validity and efficacy of the proposed one-step process fiber bundle model.

The next step concerns the computational extension of the project. Using national and international supercomputer resources (made available, for instance, by the PRACE partnership), extensive numerical simulations of the model presented in this thesis could be carried out. In this respect, in order to resemble more realistic systems, the number of chains and the number of beads per chains could be extended by orders of magnitude. As this would require many times the processor time, this would impose a genuine parallelization of the algorithms. Moreover, a systematic study of a multitude of temperatures and applied forces, and other parameters, should be undertaken. In particular, a computational extension would allow for a systematic inspection of the *primary creep* regime, which experimentally is seen to follow power-law behaviour in similar systems [32]. Due to the initial creep ringing at large forces, we were limited from quantitatively considering this regime, as this would require more robust data from the long-running simulations at low forces.

The third step consists of extending the model to include features of real systems. The first of these extensions could consist in including interactions between non-neighbouring beads. All beads in the same chain should interact, and beads also from different chains should interact, with a similar Morse-like interaction potential as was proposed in the basic model that was introduced. In the basic model, for a system of N particles, the runtime per timestep is of order $\mathcal{O}(N)$, since the number of force evaluations are $\sim N$ – i.e. the number of *bonds*. Since the interactions will still be limited to short range, the careful implementation of a list of interacting neighbours would still retain the order $\mathcal{O}(N)$ character of the computation, with a somewhat larger prefactor. Nevertheless, further investigations put requirements on extensive optimization and genuine parallelization of the simulation program.

An important aspect of introducing such chain-chain interactions is that it breaks the mean-field nature of the present molecular model. Now, the locality of the chains may influence the breaking process. Thus, there is reason to believe that load will not be shared equally among surviving chains, but rather locally between the nearby chains. This allows for the inspection of the spatial growth of local microcracks in the material, which has been experimentally observed to significantly influence the creep and failure process of polymeric materials [32]. In this framework, the Local Load Sharing versions of the fiber bundle model are highly relevant. By means of these simulations, physically correct load sharing exponents could be obtained for a range of materials [41]. The introduction of bead-bead interactions also yields the possibility of finding the existence of solid-like and fluid-like phases within the material under the stretching process, and would allow us to study the properties of the material around the tips of the microcracks. Moreover, it would allow us to study the effects of entanglements and knots, which are predicted to significantly influence the mechanical and rheological properties of polymers [4]. Also for this extended model, preliminary single-chain inspections could be useful.

On the theoretical side, the models proposed for the static and dynamic description of the polymers could be extended. To describe the static properties for systems with bead-bead interactions, more sophisticated polymer models may be employed, accounting for excluded volume, reptation, polymer melts, etc. This theory has proven efficient in describing a variety of polymeric systems. In order to describe the dynamic properties of such systems, the situation becomes more complex and more refined methods are generally needed. The proposed one-step model may still be applicable to such systems, but locality in breaking events must be introduced in order for it to apply, and it may thus prove too simple.

Finally, when sufficient large-scale simulations have been carried out with models and meth-

ods which can realistically resemble real systems, laboratory experiments should be carried out. Only upon comparing to results from the real world, our models, methods and simulations can be verified, and the link between the microscopic and macroscopic description of failure phenomena to be reliable.

We thus conclude this thesis by merely stating that the present work provides promising insight into the microscopic origin of failure phenomena. In fact, we remain with more unanswered questions than we started out with – which illustrates the richness and potential in the models proposed and the approach we have chosen.

Bibliography

[1] J. Armstrong, C. Chakravarty, and P. Ballone. Statistical mechanics of coarse graining: Estimating dynamical speedups from excess entropies. *The Journal of chemical physics*, 136(12):124503, 2012.

[2] S. Arrhenius. Xxxi. on the influence of carbonic acid in the air upon the temperature of the ground. *The London, Edinburgh, and Dublin Philosophical Magazine and Journal of Science*, 41(251):237–276, 1896.

[3] S. Y. Auyang. *Foundations of complex-system theories: in economics, evolutionary biology, and statistical physics*. Cambridge University Press, 1999.

[4] P. Ballone. Private communication.

[5] O. Basquin. The exponential law of endurance tests. In *Proc. ASTM*, volume 10, pages 625–630, 1910.

[6] G. G. Batrouni, A. Hansen, and J. Schmittbuhl. Heterogeneous interfacial failure between two elastic blocks. *Physical Review E*, 65(3):036126, 2002.

[7] A. Clauset, C. R. Shalizi, and M. E. Newman. Power-law distributions in empirical data. *SIAM review*, 51(4):661–703, 2009.

[8] P. De Gennes. Dynamics of entangled polymer solutions. I. The Rouse model. *Macromolecules*, 9(4):587–593, 1976.

[9] P.-G. de Gennes. *Scaling Concepts in Polymer Physics*. 1979.

[10] S. F. Edwards and M. Doi. *The Theory of Polymer Dynamics*. Oxford: Clarendon Press, 1986.

[11] P. J. Flory. *Statistical mechanics of chain molecules*. 1969.

[12] S. Frankland, V. Harik, G. Odegard, D. Brenner, and T. Gates. The stress–strain behavior of polymer–nanotube composites from molecular dynamics simulation. *Composites Science and Technology*, 63(11):1655–1661, 2003.

[13] D. Frenkel and B. Smit. *Understanding molecular simulation: from algorithms to applications*, volume 1. Academic press, 2001.

[14] A. Ghosh, D. Dimitrov, V. Rostiashvili, A. Milchev, and T. Vilgis. Thermal breakage and self-healing of a polymer chain under tensile stress. *The Journal of chemical physics*, 132(20):204902, 2010.

[15] R. E. Gillilan and K. R. Wilson. Shadowing, rare events, and rubber bands. a variational verlet algorithm for molecular dynamics. *The Journal of Chemical Physics*, 97(3):1757–1772, 1992.

[16] H. Goldstein. *Classical mechanics*. Addison-Wesley series in physics. Addison-Wesley Pub. Co., 1980.

[17] W. Grellmann, G. Heinrich, M. Kaliske, M. Klüppel, K. Schneider, and T. Vilgis. *Fracture Mechanics and Statistical Mechanics of Reinforced Elastomeric Blends*. Springer, 2013.

[18] N. Grønbech-Jensen and O. Farago. A simple and effective verlet-type algorithm for simulating langevin dynamics. *Molecular Physics*, 111(8):983–991, 2013.

[19] C. Hall. *Polymer Materials: An Introduction for Technologists and Scientists*. 1981.

[20] P. C. Hemmer and A. Hansen. The distribution of simultaneous fiber failures in fiber bundles. *Journal of applied mechanics*, 59(4):909–914, 1992.

[21] H. J. Herrmann and S. Roux. Statistical models for fracture in disordered media. 1990.

[22] W. G. Hoover. Canonical dynamics: Equilibrium phase-space distributions. *Phys. Rev. A*, 31:1695–1697, Mar 1985.

[23] J. P. III. Statistical inference using extreme order statistics. *The Annals of Statistics*, 3(1):pp. 119–131, 1975.

[24] A. Jaishankar, V. Sharma, and G. H. McKinley. Interfacial viscoelasticity, yielding and creep ringing of globular protein–surfactant mixtures. *Soft Matter*, 7(17):7623–7634, 2011.

[25] N. V. Kampen. *Stochastic Processes in Physics and Chemistry*. 1992.

[26] R. Koeller. Applications of fractional calculus to the theory of viscoelasticity. *Journal of Applied Mechanics*, 51(2):299–307, 1984.

[27] H. A. Kramers. Brownian motion in a field of force and the diffusion model of chemical reactions. *Physica*, 7(4):284–304, 1940.

[28] R. Kubo. The fluctuation-dissipation theorem. *Reports on Progress in Physics*, 29(1):255, 1966.

[29] F. Kun, H. Carmona, J. Andrade Jr, and H. Herrmann. Universality behind basquins law of fatigue. *Physical review letters*, 100(9):094301, 2008.

[30] F. Kun, R. C. Hidalgo, H. J. Herrmann, and K. F. Pál. Scaling laws of creep rupture of fiber bundles. *Physical Review E*, 67(6):061802, 2003.

[31] P. Langevin. Sur la théorie du mouvement brownien. *CR Acad. Sci. Paris*, 146(530-533), 1908.

[32] M. Leocmach, C. Perge, T. Divoux, and S. Manneville. Creep and brittle failure of a protein gel under stress. *arXiv preprint arXiv:1401.8234*, 2014.

[33] A. M. Lyapunov. The general problem of the stability of motion. *International Journal of Control*, 55(3):531–534, 1992.

[34] J. C. Mann and F. T. Peirce. 9the time factor in hair testing. *Journal of the Textile Institute Transactions*, 17(2):T82–T93, 1926.

[35] Y. Moreno, J. Gomez, and A. Pacheco. Fracture and second-order phase transitions. *Physical review letters*, 85(14):2865, 2000.

[36] S. Nosé. A unified formulation of the constant temperature molecular dynamics methods. *The Journal of Chemical Physics*, 81(1):511–519, 1984.

[37] F. A. Oliveira and P. L. Taylor. Breaking in polymer chains. ii. the lennard-jones chain. *J. Chem. Phys.*, 101, 1994.

[38] J. Paturej, A. Milchev, V. Rostiashvili, and T. Vilgis. Thermal degradation of unstrained single polymer chain: Non-linear effects at work. *The Journal of chemical physics*, 134(22):224901, 2011.

[39] J. Paturej, A. Milchev, V. G. Rostiashvili, and T. A. Vilgis. Polymer chain scission at constant tensionan example of force-induced collective behaviour. *EPL (Europhysics Letters)*, 94(4):48003, 2011.

[40] Y. Pomeau and P. Manneville. Intermittent transition to turbulence in dissipative dynamical systems. *Communications in Mathematical Physics*, 74(2):189–197, 1980.

[41] S. Pradhan, A. Hansen, and B. K. Chakrabarti. Failure processes in elastic fiber bundles. *Reviews of modern physics*, 82(1):499, 2010.

[42] S. Roux. Thermally activated breakdown in the fiber-bundle model. *Physical Review E*, 62(5):6164, 2000.

[43] M. Schulz. *Statistical physics and economics: concepts, tools and applications*, volume 184. Springer, 2003.

[44] S. B. Smith, L. Finzi, and C. Bustamante. Direct mechanical measurements of the elasticity of single DNA molecules by using magnetic beads. *Science*, 258(5085):1122–6, Nov. 1992.

[45] L. H. Sperling. *Introduction to Physical Polymer Science*. 2005.

[46] G. R. Strobl. *The Physics of Polymers: Concepts for Understanding Their Structures and Behavior*. 2007.

[47] S. Strogatz. *Nonlinear Dynamics And Chaos*. Studies in nonlinearity. Sarat Book House, 2007.

[48] W. C. Swope, H. C. Andersen, P. H. Berens, and K. R. Wilson. A computer simulation method for the calculation of equilibrium constants for the formation of physical clusters of molecules: Application to small water clusters. *The Journal of Chemical Physics*, 76(1), 1982.

[49] S. Turner. Creep of Polymeric Materials. *Oxford: Elsevier Science Ltd.*, pages 1813–1817, 2001.

[50] W. L. Vandoolaeghe. Polymer networks at surfaces. Master's thesis, 2003.

[51] L. Verlet. Computer "experiments" on classical fluids. i. thermodynamical properties of lennard-jones molecules. *Phys. Rev.*, 159:98–103, Jul 1967.

[52] R. C. Weast, M. J. Astle, and W. H. Beyer. *CRC handbook of chemistry and physics*, volume 69. CRC press Boca Raton, FL, 1988.

[53] F.-J. Wortmann and K. Schulz. Non-linear viscoelastic performance of nomex, kevlar and polypropylene fibres in a single-step stress relaxation test: 1. experimental data and principles of analysis. *Polymer*, 35(10):2108–2116, 1994.

A Derivations

A.1 Probability distribution of the end-to-end separation vector of the FJC

We defined the end-to-end separation vector by

$$\mathbf{R} = \mathbf{r}_n - \mathbf{r}_0 = \sum_{i=1}^{n} \mathbf{b}_i, \tag{A.1}$$

and the constraint on the bond vectors is $|\mathbf{b}_i| = b$. The probability of finding a specific bond in a certain infinitesimal volume $\mathrm{d}V_i = \mathrm{d}^3\mathbf{b}_i$ of space is

$$p(\mathbf{b}_i)\,\mathrm{d}^3\mathbf{b}_i = C\delta(b - |\mathbf{b}_i|)\,\mathrm{d}^3\mathbf{b}_i \tag{A.2}$$

where C is a normalization constant, determined by

$$1 = \int_{\mathbb{R}^3} p(\mathbf{b}_i)\,\mathrm{d}^3\mathbf{b}_i = C\int_{\mathbb{R}^3} \delta(b - |\mathbf{b}_i|)\,\mathrm{d}^3\mathbf{b}_i \tag{A.3}$$

$$= 4\pi C\int_0^\infty \delta(b - b_i)b_i^2\,\mathrm{d}b_i = 4\pi C b^2, \tag{A.4}$$

so $C = 1/4\pi b^2$. Hence,

$$p(\mathbf{b}_i) = \frac{1}{4\pi b^2}\delta(b - |\mathbf{b}_i|). \tag{A.5}$$

The corresponding characteristic function (Fourier transform) is found by

$$g(\mathbf{k}) = \int \mathrm{d}^3\mathbf{b}_i\, e^{i\mathbf{k}\cdot\mathbf{b}_i}\, p(\mathbf{b}_i) = 2\pi\int_0^\infty\int_0^\pi \mathrm{d}b_i\mathrm{d}\theta_i\, b_i^2 \sin\theta_i e^{ikb_i\cos\theta_i}\frac{1}{4\pi b^2}\delta(b - b_i) \tag{A.6}$$

$$= \frac{1}{2}\int_0^\pi \mathrm{d}\theta_i\, \sin\theta_i e^{ikb\cos\theta_i} = \frac{1}{2}\int_{-1}^{1} \mathrm{d}(\cos\theta_i)\, e^{ikb\cos\theta_i} = \frac{e^{ikb} - e^{-ikb}}{2ikb} \tag{A.7}$$

$$= \frac{\sin kb}{kb} \tag{A.8}$$

Since the beads are independently distributed, the joint probability distribution for all the n bond vectors is

$$p(\mathbf{b}_1, \ldots, \mathbf{b}_n) = \prod_{i=1}^{n} p(\mathbf{b}_i). \tag{A.9}$$

We wish now to determine the probability distribution of the end-to-end displacement vector $\mathbf{R} = \sum_{i=1}^{n} \mathbf{b}_i$. This is found by

$$p(\mathbf{R}) = \int \prod_{i=1}^{n} \mathrm{d}^3\mathbf{b}_i \, \delta^3(\mathbf{R} - \sum_{i=1}^{n} \mathbf{b}_i) p(\mathbf{b}_1, \ldots, \mathbf{b}_n) \tag{A.10}$$

$$= \int \prod_{i=1}^{n} \mathrm{d}^3\mathbf{b}_i \, p(\mathbf{b}_i) \delta^3(\mathbf{R} - \sum_{j=1}^{n} \mathbf{b}_j). \tag{A.11}$$

We find the corresponding characteristic function

$$G(\mathbf{k}) = \int \mathrm{d}^3\mathbf{R} \, e^{i\mathbf{k}\cdot\mathbf{R}} \, p(\mathbf{R}) \tag{A.12}$$

$$= \int \mathrm{d}^3\mathbf{R} \prod_{j=1}^{n} \mathrm{d}^3\mathbf{b}_j \, e^{i\mathbf{k}\cdot\mathbf{R}} \, p(\mathbf{b}_j) \delta^3(\mathbf{R} - \sum_{l=1}^{n} \mathbf{b}_l) \tag{A.13}$$

$$= \prod_{j=1}^{n} \int \mathrm{d}^3\mathbf{b}_j \, e^{i\mathbf{k}\cdot\mathbf{b}_j} p(\mathbf{b}_j) \tag{A.14}$$

$$= g(\mathbf{k})^n = \left(\frac{\sin kb}{kb} \right)^n. \tag{A.15}$$

The inverse Fourier transform yields the distribution function:

$$p(\mathbf{R}) = \frac{1}{(2\pi)^3} \int \mathrm{d}^3\mathbf{k} \, e^{-i\mathbf{k}\cdot\mathbf{R}} G(\mathbf{k}) \tag{A.16}$$

$$= \frac{1}{(2\pi)^3} \int \mathrm{d}^3\mathbf{k} \, e^{-i\mathbf{k}\cdot\mathbf{R}} \left(\frac{\sin kb}{kb} \right)^n. \tag{A.17}$$

From the characteristic function, we can find

$$\nabla_{\mathbf{k}}^l G(\mathbf{k}) = \int \mathrm{d}^3\mathbf{R} \, \left(\nabla_{\mathbf{k}}^l e^{i\mathbf{k}\cdot\mathbf{R}} \right) \, p(\mathbf{R}) \tag{A.18}$$

$$= i^l \int \mathrm{d}^3\mathbf{R} \, \mathbf{R}^l e^{i\mathbf{k}\cdot\mathbf{R}} \, p(\mathbf{R}), \tag{A.19}$$

so that

$$\langle \mathbf{R}^l \rangle = i^{-l} \nabla_{\mathbf{k}}^l G(\mathbf{k})|_{\mathbf{k}=\mathbf{0}} \tag{A.20}$$

$$= i^{-l} \nabla_{\mathbf{k}}^l \left(\frac{\sin kb}{kb} \right)^n |_{\mathbf{k}=\mathbf{0}} \tag{A.21}$$

It is evident that all odd moments vanish since $\mathbf{R}$ by necessity is real. Hence,

$$\langle \mathbf{R} \rangle = 0, \tag{A.22}$$

and

$$\langle \mathbf{R}^2 \rangle = i^{-2} \nabla_{\mathbf{k}}^2 \left(\frac{\sin kb}{kb} \right)^n |_{\mathbf{k}=\mathbf{0}} \tag{A.23}$$

$$= -\frac{1}{k^2} \frac{\partial}{\partial k} \left(k^2 \frac{\partial}{\partial k} \left(\left(\frac{\sin kb}{kb} \right)^n \right) \right) |_{k=0} \tag{A.24}$$

$$= nb^2, \tag{A.25}$$

for example. The latter shows the scaling law for the mean square displacement, namely

$$\sqrt{\langle \mathbf{R}^2 \rangle} \sim n^{1/2}. \tag{A.26}$$

In the limit of large n, we have that $[\sin kb/kb]$ will be sharply peaked around small values of kb. Thus, for sufficiently large n, we may approximate

$$\left(\frac{\sin kb}{kb}\right)^n = \left(1 - \frac{1}{3!}(kb)^2 + \mathcal{O}\left((kb)^4\right)\right)^n = \left(\exp\left(-\frac{1}{3!}(kb)^2\right) + \mathcal{O}\left((kb)^4\right)\right)^n \tag{A.27}$$

$$\simeq \exp\left(-\frac{n}{3!}(kb)^2\right) \tag{A.28}$$

so that

$$p(\mathbf{R}) \simeq \frac{1}{(2\pi)^3}\int \mathrm{d}^3\mathbf{k}\, \exp\left(-i\mathbf{k}\cdot\mathbf{R} - \frac{nb^2}{6}k^2\right) \tag{A.29}$$

$$= I(R_x)I(R_y)I(R_z), \tag{A.30}$$

where

$$I(R_j) = \frac{1}{2\pi}\int_{-\infty}^{\infty} \mathrm{d}k_j\, \exp\left(-ik_jR_j - \frac{nb^2}{6}k_j^2\right) \tag{A.31}$$

$$= \sqrt{\frac{3}{2\pi nb^2}}\exp\left(-\frac{3R_j^2}{2nb^2}\right), \tag{A.32}$$

and hence

$$p(\mathbf{R}) = \left(\frac{3}{2\pi nb^2}\right)^{3/2}\exp\left(-\frac{3R^2}{2nb^2}\right) \tag{A.33}$$

is the approximate probability distribution in the large n limit.

A.2 Elongation of the FJC under tension

We imagine attaching the two ends of the freely jointed chain to a micro-manipulation device exerting a force $\mathbf{F}$ upon it. This force acting on the endpoint of the chain corresponds to it being immersed in a linear potential, which gives an additional contribution to the Hamiltonian of $-\mathbf{F}\cdot\mathbf{R} = -\mathbf{F}\cdot\sum_{i=1}^n \mathbf{b}_i$. Hence, the partition function for the stretched chain can be written as

$$Z = \frac{1}{(4\pi b^2)^n}\int \prod_{i=1}^n \mathrm{d}^3\mathbf{b}_i \delta(b - |\mathbf{b}_i|)\exp(\beta\mathbf{F}\cdot\mathbf{b}_i) \tag{A.34}$$

$$= \left[\frac{1}{4\pi b^2}\int \mathrm{d}^3\mathbf{b}_i\delta(b-|\mathbf{b}_i|)\exp(\beta\mathbf{F}\cdot\mathbf{b}_i)\right]^n = Z_i^n, \tag{A.35}$$

where $\beta = 1/k_{\mathrm{B}}T$ and we have implicitly defined

$$Z_i = \frac{1}{4\pi b^2}\int \mathrm{d}^3\mathbf{b}_i\delta(b-|\mathbf{b}_i|)\exp(\beta\mathbf{F}\cdot\mathbf{b}_i), \tag{A.36}$$

which can be readily solved to yield

$$Z_i = \frac{1}{2b^2}\int_0^\infty \int_0^\pi \mathrm{d}b_i \mathrm{d}\theta_i b_i^2 \sin\theta_i \delta(b-b_i)\exp(\beta F b_i \cos\theta_i) \tag{A.37}$$

$$= \frac{1}{2}\int_0^\pi \mathrm{d}\theta_i \sin\theta_i \exp(\beta F b\cos\theta_i) = \frac{1}{2}\int_{-1}^1 \mathrm{d}u \exp(\beta F b u) \tag{A.38}$$

$$= \frac{\sinh(\beta F b)}{\beta F b}. \tag{A.39}$$

The expected total elongation of the chain in the direction $\hat{\mathbf{F}} = \mathbf{F}/F$ can be written as

$$L = \left\langle \mathbf{R}\cdot\hat{\mathbf{F}}\right\rangle = \left\langle \sum_{i=1}^n b_i\cos\theta_i \right\rangle = \sum_{i=1}^n \langle b_i\cos\theta_i\rangle = nb\langle\cos\theta_i\rangle \tag{A.40}$$

$$= \frac{nb}{2Z_i}\int_0^\pi \mathrm{d}\theta_i \sin\theta_i\cos\theta_i \exp(\beta F b\cos\theta_i) \tag{A.41}$$

$$= \frac{nb}{2Z_i}\frac{\partial}{\partial(\beta F b)}\int_0^\pi \mathrm{d}\theta_i \sin\theta_i \exp(\beta F b\cos\theta_i) \tag{A.42}$$

$$= \frac{nb}{Z_i}\frac{\partial Z_i}{\partial(\beta F b)} = nb\frac{\partial \ln Z_i}{\partial(\beta F b)} \tag{A.43}$$

$$= nb\frac{\partial}{\partial(\beta F b)}\left[\ln(\sinh(\beta F b)) - \ln(\beta F b)\right] \tag{A.44}$$

$$= nb\left[\coth(\beta F b) - \frac{1}{\beta F b}\right] = nb\mathcal{L}(\beta F b), \tag{A.45}$$

where $\mathcal{L}(x) = \coth x - x^{-1}$ is the Langevin function. The above expression yields the stress-strain curve of a single freely jointed chain.

A.3 Partition functions for the Gaussian chain

Following a similar procedure as in [50], we now consider a chain conformation to be specified by the set $S = \{\mathbf{r}_i\}$ where $\mathbf{r}_i$ is the position of bead i of the chain, for $i = 0, 1, \ldots, n$. Given that bead $i-1$ is localized at $\mathbf{r}_{i-1}$, this corresponds to the probability distribution

$$p(\mathbf{r}_i;\mathbf{r}_{i-1}) = \left(\frac{3}{2\pi b^2}\right)^{3/2}\exp\left(-\frac{3}{2b^2}(\mathbf{r}_i-\mathbf{r}_{i-1})^2\right), \tag{A.46}$$

for bead i. The probability distribution for a full chain of n bonds is thus

$$p(S) = \prod_{i=1}^n \psi(\mathbf{r}_i;\mathbf{r}_{i-1}) \tag{A.47}$$

$$= \mathcal{N}\exp\left(-\frac{3}{2b^2}\sum_{i=1}^n(\mathbf{r}_i-\mathbf{r}_{i-1})^2\right), \tag{A.48}$$

where $\mathcal{N}$ is a normalization constant. The partition function is found by integrating $p(S)$ over all possible conformations S. In the limit of large n, we may replace the discrete variable i with

the continuous variable s, so that $\mathbf{r}_i \to \mathbf{r}(s)$. In this case $\mathbf{r}_i - \mathbf{r}_{i-1}$ may be approximated by the functional derivative $\partial\mathbf{r}/\partial s$, and the sum in the exponential may be approximated by an integral. Hence, the probability distribution function for a chain with endpoints at $\mathbf{R}'$ and $\mathbf{R}$ is given by the *functional integral*

$$G(\mathbf{R},\mathbf{R}';n) = \mathcal{N}\int_{\mathbf{r}(0)=\mathbf{R}'}^{\mathbf{r}(n)=\mathbf{R}} \mathcal{D}\mathbf{r}\exp\left(-\frac{3}{2b^2}\int_0^n \mathrm{d}s\left(\frac{\partial\mathbf{r}}{\partial s}\right)^2\right), \tag{A.49}$$

where $\mathcal{D}\mathbf{r}$ indicates the integral over all possible paths $\mathbf{r}(s)$. This Green function [10] is the solution of the equation

$$\left[\frac{\partial}{\partial n} - \frac{b^2}{6}\nabla^2\right] G(\mathbf{R},\mathbf{R}';n) = \delta(\mathbf{R}-\mathbf{R}')\delta(n). \tag{A.50}$$

The boundary conditions are that G vanishes on and outside of the boundary.

A.3.1 The free chain

The distribution function for the unconfined Gaussian chain is given simply by the Gaussian function

$$G_0(\mathbf{R}-\mathbf{R}';n) = \left(\frac{3}{2\pi nb^2}\right)^{3/2}\exp\left(-\frac{3}{2nb^2}(\mathbf{R}-\mathbf{R}')^2\right), \tag{A.51}$$

which is easily seen to agree with the large n limit of the FJC as we fix $\mathbf{R}' = \mathbf{0}$:

$$G_0(\mathbf{R};n) = \left(\frac{3}{2\pi nb^2}\right)^{3/2}\exp\left(-\frac{3\mathbf{R}^2}{2nb^2}\right), \tag{A.52}$$

which moreover shows that the free Gaussian chain is invariant under the transformation $(n,b) \to (\lambda^{-2}n, \lambda b)$.

A.3.2 Confinement between two parallel plates

In the case of chain that is confined between two parallel plates, the situation is a bit more complicated. Without loss of generality, we fix the plates at $z = 0$ and $z = L$. We note that the Green function is separable:

$$G(\mathbf{R},\mathbf{R}';n) = g_x(x,x';n)g_y(y,y';n)g_z(z,z';n). \tag{A.53}$$

The boundary conditions may be stated as

$$g_z(z,z';n) = 0 \text{ when } z,z' = 0,L. \tag{A.54}$$

In the x cases, the solution is straightforward,

$$g_x(x,x';n) = \left(\frac{3}{2\pi nb^2}\right)^{1/2}\exp\left(-\frac{3}{2nb^2}(x-x')^2\right), \tag{A.55}$$

and correspondingly for g_y. In the z direction we use the eigenfunction expansion method, which yields

$$g_z(z,z';n) = \frac{2}{L}\sum_{k=1}^{\infty}\sin\frac{k\pi z}{L}\sin\frac{k\pi z'}{L}\exp\left(-\frac{b^2\pi^2k^2}{6L^2}n\right). \tag{A.56}$$

A.3.3 Attachment to one plate

We now consider the case where a chain is attached to one of the plates. Without loss of generality, we fix $\mathbf{R}' = (0, 0, \epsilon)$, and integrate over all $\mathbf{R}$ in the volume to obtain the associated partition function:

$$\mathcal{Z}_1(L; n) = \int_0^L \mathrm{d}z\, g_z(z, \epsilon; n) \tag{A.57}$$

$$= \frac{2}{L} \sum_{k=1}^{\infty} \int_0^L \mathrm{d}z\, \sin \frac{k\pi z}{L} \sin \frac{k\pi \epsilon}{L} \exp\left(-\frac{b^2\pi^2 k^2}{6L^2} n\right) \tag{A.58}$$

$$= \frac{2}{\pi} \sum_{k \text{ odd}} \frac{1}{k} \sin \frac{k\pi \epsilon}{L} \exp\left(-\frac{b^2\pi^2 k^2}{6L^2} n\right). \tag{A.59}$$

To the lowest order in ϵ,

$$\mathcal{Z}_1(L; n) = \frac{2\epsilon}{L} \sum_{k \text{ odd}} \exp\left(-\frac{b^2\pi^2 k^2}{6L^2} n\right). \tag{A.60}$$

This configuration may correspond to a chain that has been broken, which is still attached to one of the plates.

A.3.4 Attachment to two plates

For a Gaussian chain attached to two parallel plates at a separation L, the partition function is found similarly as above by fixing $\mathbf{R}' = (0, 0, \epsilon)$ and $z = L - \epsilon$, and integrate over all x, y. This yields

$$\mathcal{Z}_2(L; n) = \frac{2}{L} \sum_{k=1}^{\infty} (-1)^{k+1} \sin^2 \frac{k\pi \epsilon}{L} \exp\left(-\frac{b^2\pi^2 k^2}{6L^2} n\right) \tag{A.61}$$

$$= \frac{2\pi^2\epsilon^2}{L^3} \sum_{k=1}^{\infty} (-1)^{k+1} k^2 \exp\left(-\frac{b^2\pi^2 k^2}{6L^2} n\right) \tag{A.62}$$

to the lowest order in ϵ.

A.4 Expanding the master equation of the one-step FBM

In this section we expand the master equation of the process

$$\frac{\mathrm{d}p_n}{\mathrm{d}t} = -\left(b_n + r_n\right) p_n + b_{n+1} p_{n+1} + r_{n-1} p_{n-1}, \tag{A.63}$$

which in terms of the step operators $\mathbb{E}, \mathbb{E}^-$ can be written as

$$\frac{\mathrm{d}p_n}{\mathrm{d}t} = (\mathbb{E} - 1) b_n p_n + (\mathbb{E}^- - 1) r_n p_n. \tag{A.64}$$

We now follow the procedure outlined by Van Kampen [25] in order to expand the master equation. Firstly, we define b and r by

$$b_n/N = b(n/N) = n/Nf(\sigma N/n) \tag{A.65}$$
$$r_n/N = r(n/N) = (N-n)/Ng(\sigma N/n) \tag{A.66}$$

or

$$b(\phi) = \phi f(\sigma/\phi) \tag{A.67}$$
$$r(\phi) = (1-\phi)g(\sigma/\phi). \tag{A.68}$$

Expecting n to be sharply peaked around the macroscopic value $N\phi$, with a deviation of order $N^{1/2}$, we let

$$n = N\phi(t) + N^{1/2}\xi, \tag{A.69}$$

where ξ is a stochastic variable replacing n. Now,

$$\Pi(\xi, t) = p_n(t) \tag{A.70}$$

becomes the probability distribution in terms of ξ. Since $\mathbb{E}$ changes n to $n+1$, it should change ξ to $\xi + N^{1/2}$, so

$$\mathbb{E} = 1 + N^{-1/2}\frac{\partial}{\partial\xi} + \frac{1}{2}N^{-1}\frac{\partial^2}{\partial\xi^2} + \cdots, \tag{A.71}$$

and similarly

$$\mathbb{E}^- = 1 - N^{-1/2}\frac{\partial}{\partial\xi} + \frac{1}{2}N^{-1}\frac{\partial^2}{\partial\xi^2} - \cdots. \tag{A.72}$$

The time derivative in (A.64) is taken with constant n. Using (A.69),

$$0 = \frac{\mathrm{d}\phi}{\mathrm{d}t} - N^{-1/2}\frac{\mathrm{d}\xi}{\mathrm{d}t} \tag{A.73}$$

gives the corresponding direction in the (ξ, t) plane. Hence, the total derivative becomes

$$\frac{\mathrm{d}p_n}{\mathrm{d}t} = \frac{\partial\Pi}{\partial t} + \frac{\partial\Pi}{\partial\xi}\frac{\mathrm{d}\xi}{\mathrm{d}t} = \frac{\partial\Pi}{\partial t} - N^{1/2}\frac{\partial\Pi}{\partial\xi}\frac{\mathrm{d}\phi}{\mathrm{d}t}. \tag{A.74}$$

Moreover,

$$b_n = Nb(n/N) = Nb(\phi + N^{-1/2}\xi) \tag{A.75}$$
$$= N\left[b(\phi) + N^{-1/2}\xi b'(\phi) + \frac{1}{2}N^{-1}\xi^2 b''(\phi) + \cdots\right] \tag{A.76}$$

and

$$r_n = Nr(n/N) = Nr(\phi + N^{-1/2}\xi) \tag{A.77}$$
$$= N\left[r(\phi) + N^{-1/2}\xi r'(\phi) + \frac{1}{2}N^{-1}\xi^2 r''(\phi) + \cdots\right] \tag{A.78}$$

so (A.64) becomes

$$\begin{aligned}&\frac{\partial \Pi}{\partial t}\\&\quad - N^{1/2}\frac{\mathrm{d}\phi}{\mathrm{d}t}\frac{\partial \Pi}{\partial \xi} = \left(N^{1/2}\frac{\partial}{\partial \xi} + \frac{1}{2}\frac{\partial^2}{\partial \xi^2}\right)\left(b(\phi) + N^{-1/2}\xi b'(\phi) + \frac{1}{2}N^{-1}\xi^2 b''(\phi)\right)\Pi\\&\quad + \left(-N^{1/2}\frac{\partial}{\partial \xi} + \frac{1}{2}\frac{\partial^2}{\partial \xi^2}\right)\left(r(\phi) + N^{-1/2}\xi r'(\phi) + \frac{1}{2}N^{-1}\xi^2 r''(\phi)\right)\Pi + \mathcal{O}(N^{-1/2}).\end{aligned} \tag{A.79}$$

We find, to the leading order ($N^{1/2}$), factorizing out $\partial\Pi/\partial\xi$,

$$\frac{\mathrm{d}\phi}{\mathrm{d}t} = -b(\phi) + r(\phi), \tag{A.80}$$

which is the macroscopic equation for the system, from which we can obtain the average macroscopic behaviour of the system. The terms of second lowest order (N^0) are collected to yield

$$\frac{\partial \Pi}{\partial t} = \left[b'(\phi) - r'(\phi)\right]\frac{\partial \xi \Pi}{\partial \xi} + \frac{1}{2}\left[r(\phi) + b(\phi)\right]\frac{\partial^2 \Pi}{\partial \xi^2}. \tag{A.81}$$

This is a linear Fokker–Planck equation which can easily be solved to yield the quantities $\langle\xi\rangle$ and $\langle\xi^2\rangle$. This is the *linear noise approximation*. Note that this expansion is only valid sufficiently close to a stable fixed point of the macroscopic equation.

B Numerical extensions

B.1 Thermostats

A limitation of molecular dynamics as presented up to this point, is that it is limited to systems that are not allowed to exchange heat with the surroundings. At equilibrium this corresponds to the microcanonical ensemble, where the number of particles, energy and volume is conserved. Out of equilibrium, by performing work on the particles, the system is not a microcanonical ensemble (the energy may increase), but is still not allowed to exchange heat – and hence corresponds to adiabatic conditions. This corresponds physically only to real experiments carried out in vacuum, or on a very short timescale. These are in general hard to reproduce, and in most real life systems, even out of equilibrium, heat conduction is possible, and it is more feasible to carry out experiments with a fixed temperature.

Moreover, in applications, such as when considering properties of materials, temperature changes slowly and heat will be dissipated when one performs work on the system. The isothermal scenario corresponds in equilibrium to the canonical ensemble, and can be implemented in molecular dynamics by means of a thermostat. We present the outline of two distinct popular approaches in the following, firstly the Nosé-Hoover thermostat, and secondly thermal coupling by Langevin dynamics.

B.1.1 Nosé-Hoover thermostat

The Nosé-Hoover algorithm [22, 36] is a deterministic approach to isothermal conditions, and the idea behind it consists of extending the system with an additional artificial coordinate s, representing a coupling to a heat bath. Associated with s is an artificial mass Q. The variable s plays the role of a time-scaling parameter, i.e. the timescale in the extended system is stretched by the factor s. However, we don't go into detail in the physical basis here, both for clarity and as this is out of the scope of the thesis.

We consider herein rather the numerical consequences. Hoover realized that for the numerical implementation, fluctuating time-intervals was not just impractical, it was unnecessary. Using real (unscaled) coordinates, effectively replacing s with a thermodynamic friction coefficient ξ, the final equations of motion read

$$\frac{\mathrm{d}\mathbf{r}_i}{\mathrm{d}t} = \mathbf{v}_i, \tag{B.1}$$

$$\frac{\mathrm{d}\mathbf{v}_i}{\mathrm{d}t} = \frac{\mathbf{F}_i}{m} - \xi\mathbf{v}_i, \tag{B.2}$$

$$\frac{\mathrm{d}\xi}{\mathrm{d}t} = \left(\frac{K}{K_0} - 1\right)/\tau^2. \tag{B.3}$$

Effectively, the system of equations is merely extended by one equation. Herein, τ is a phenomenological relaxation time of, via the thermodynamic friction coefficient ξ, bring the kinetic energy K of the system to K_0 – the kinetic energy corresponding to the sought (isothermal)

temperature T_0. We note that in the limit of infinite relaxation time, $\tau \to \infty$, the equations reduce to the original ones.

Numerically, this poses additional difficulty, as the (total) force evaluation step (giving the acceleration $\mathbf{a} = \mathbf{F}/m - \xi\mathbf{v}$) now explicitly depends on the velocities of the involved particles, not just the positions. The first step is the same as before

$$\mathbf{r}(t + \Delta t) = \mathbf{r}(t) + \mathbf{v}(t)\Delta t + \mathbf{a}(t)\frac{\Delta t^2}{2}, \tag{B.4}$$

only with a modified expression for the acceleration. We can not yet directly compute $\mathbf{a}(t+\Delta t)$ as this requires knowledge of $\mathbf{v}(t+\Delta t)$ and $\xi(t+\Delta t)$. This can be solved by the use of predictor-corrector schemes, or iteratively, but at a significant expense: the solution is not time-reversible.

B.1.2 Langevin thermostat

The approach we discuss here is not deterministic in nature, being based on the seminal idea of Langevin [31] of describing a physical process by a stochastic differential equation. In this approach, we imagine the particles (or just some of them) as immersed in a liquid – the heat bath. The random collisions from the surrounding molecules account for the heat dissipation. Physically, this corresponds to the case where the MD particles are much larger than those in the solution, and hence, the movement of the beads much slower. The resulting equations of motion are obtained by adding the noise term $\mathbf{R}_i(t)$ to the classical Newton's equation of motion

$$m\frac{\mathrm{d}\mathbf{v}_i}{\mathrm{d}t} = -\gamma\mathbf{v}_i(t) + \mathbf{F}_i(t) + \mathbf{R}_i(t), \tag{B.5}$$

where γ is a friction coefficient controlling the coupling between the particles and the heat bath. The fluctuation-dissipation theorem [28] is satisfied via the relation

$$\langle R_{i,\alpha}(t)R_{j,\beta}(t')\rangle = 2\gamma k_\mathrm{B}T\delta_{ij}\delta_{\alpha\beta}\delta(t-t'). \tag{B.6}$$

In principle this constitutes all the ingredients in this approach. We note that the original equations are retrieved upon taking the limit $\gamma \to 0$.

Numerically, the method is implemented by, for each particle at each time step, pulling a random number per spatial direction from a Gaussian distribution with mean 0 and standard deviation $\sigma = \sqrt{2\gamma k_\mathrm{B}T}$. Representing a random kick from the bath, this enters into the velocity updating formulae, which can be readily implemented in Verlet-type integrators [18].

Langevin thermostats are generally not deterministic, due to the stochasticity in the random kicks, and hence breaks a fundamental postulate of classical mechanics and thus molecular dynamics. However, the advantages are many: the most prominent one being that we can run simulations with longer timestep than without thermal coupling, as the friction term tends to stabilize the system.